AWARD NUMBER: W81XWH-15-1-0297

TITLE: The Role of Cyclin D1 in the Chemoresistance of Mantle Cell Lymphoma

PRINCIPAL INVESTIGATOR: Vu Ngo

CONTRACTING ORGANIZATION: City Of Hope Beckman Research Institute
Durate, CA 91010

REPORT DATE: November 2018

TYPE OF REPORT: Final

PREPARED FOR: U.S. Army Medical Research and Materiel Command
Fort Detrick, Maryland 21702-5012

REPORT DOCUMENTATION PAGE

Form Approved
OMB No. 0704-0188

1. REPORT DATE	2. REPORT TYPE	3. DATES COVERED
Nov 2018	Final	1 Sep 2015 - 31 Aug 2018

4. TITLE AND SUBTITLE

The Role of Cyclin D1 in the Chemoresistance of Mantle Cell Lymphoma

5a. CONTRACT NUMBER
W81XWH-15-1-0297

5b. GRANT NUMBER

5c. PROGRAM ELEMENT NUMBER

6. AUTHOR(S)

Vu Ngo

E-Mail: vngo@coh.org

5d. PROJECT NUMBER

5e. TASK NUMBER

5f. WORK UNIT NUMBER

7. PERFORMING ORGANIZATION NAME(S) AND ADDRESS(ES)

City of Hope Beckman Research Institute
1500 East Duarte Road
Duarte, CA 91010-3000

8. PERFORMING ORGANIZATION REPORT NUMBER

9. SPONSORING / MONITORING AGENCY NAME(S) AND ADDRESS(ES)

U.S. Army Medical Research and Materiel Command
Fort Detrick, Maryland 21702-5012

10. SPONSOR/MONITOR'S ACRONYM(S)

11. SPONSOR/MONITOR'S REPORT NUMBER(S)

12. DISTRIBUTION / AVAILABILITY STATEMENT

Approved for Public Release; Distribution Unlimited

13. SUPPLEMENTARY NOTES

14. ABSTRACT

Mantle cell lymphoma (MCL) is an aggressive B-cell malignancy characterized by over-expression of the cell cycle regulatory protein cyclin D1 (CCND1). Increased CCND1 expression levels are strongly associated with shorter patient survival related to chemoresistance, but little is known about the contribution of CCND1 to the resistant nature of MCL. On the basis of our preliminary data, we *hypothesize* that cyclin D1 plays a genome protective role through regulating expression of *CDK5RAP3* (C53), which encodes a putative tumor suppressor known to antagonize the DNA checkpoint kinase CHEK1. We test this hypothesis by accomplishing the following *two goals*: 1) To determine whether CCND1 protects the genome integrity of MCL through its downstream target C53 and 2) to determine the mechanism by which CCND1 regulates C53 expression. We found that C53 is required for inducing DNA damage following CCND1 depletion. In addition, CCND1 was found to physically interact with HDAC1 and increase HDAC1 recruitment to the *C53* promoter. Furthermore, using a C53 reporter assay, we found that both CCND1 and HDAC1 can directly interact with and negatively regulate C53 promoter activity. Interestingly, co-expression of CCND1 and HDAC1 can enhance repression of C53 promoter activity, suggesting a potential cooperation of these molecules in the regulation of C53. Thus, our findings provide new insights into the oncogenic activity of CCND1 in MCL.

15. SUBJECT TERMS
Mantle cell lymphoma, cyclin D1, chemoresistance, CDK5RAP3

16. SECURITY CLASSIFICATION OF:			17. LIMITATION OF ABSTRACT	18. NUMBER OF PAGES	19a. NAME OF RESPONSIBLE PERSON
a. REPORT	b. ABSTRACT	c. THIS PAGE			19b. TELEPHONE NUMBER *(include area code)*
Unclassified	Unclassified	Unclassified	Unclassified	54	USAMRMC

Table of Contents

1 **INTRODUCTION:**

Mantle cell lymphoma (MCL) is an aggressive and difficult-to-treat B-cell malignancy that is frequently refractory and relapsed to conventional chemotherapy. MCL is characterized by over-expression of the cell cycle regulatory protein cyclin D1 (CCND1) due to the hallmark t(11;14) chromosomal translocation. Increased CCND1 expression levels are strongly associated with shorter patient survival related to chemoresistance, but little is known about the contribution of CCND1 to the resistant nature of MCL. In preliminary studies, we found that depletion of CCND1 increased DNA damage and sensitized MCL cells to chemotherapeutic agents. CCND1 depletion also caused an increase in the transcription of *CDK5RAP3,* a putative tumor suppressor gene known to antagonize the DNA checkpoint kinase CHEK1 (1). Interestingly, depletion of CDK5RAP3 rescued the toxicity of CCND1 knockdown in MCL cells. These findings led us to *hypothesize* that CCND1 protects the MCL genome integrity through regulating CDK5RAP3 expression. In this project, we have focused on the role of CDK5RAP3 as a potential downstream effector of CCND1 and elucidated the mechanism underlying CCND1-mediated CDK5RAP3 gene expression. Findings from this project have contributed to three publications from our group (2-4). In this final report, we summarize the results and accomplishments from the entire project period (2015-2018).

2 **KEYWORDS:** Mantle cell lymphoma, cyclin D1, chemoresistance, DNA damage, CDK5RAP3, CHEK1

3 **ACCOMPLISHMENTS:**

Major goals

The project has two major goals: 1) To determine whether CCND1 protects the genome integrity of MCL through its downstream target CDK5RAP3 (C53) and 2) to determine the mechanism by which CCND1 regulates C53 expression. To accomplish these goals, as described in the Statement Of Work, we have manipulated the expression levels of C53 in MCL cells by RNA interference (Task 1a) or by over-expression (Task 1b) and compared the effects of these manipulations with those produced by CCND1 knockdown. We also determined the transcriptional role of CCND1 in regulating C53 expression by examining its recruitment (Task 2a) and interactions with relevant transcription factors (Task 2b) at the C53 promoter. Our accomplishments towards these goals are summarized as follows.

Results

C53 depletion reduces DNA damage and restores ATR signaling in CCND1-depleted MCL cells.

We previously reported that depletion of CCND1 in MCL cell lines resulted in DNA double-strand breaks, reduced cell survival and increased sensitivity to DNA damaging agents (2). CCND1 knockdown (KD) also increased mRNA and protein levels of C53, a known negative regulator of CHEK1 (1). Remarkedly, we found that depletion of C53 rescued growth inhibition and apoptosis in CCND1-silenced cells, suggesting a potential role for C53 in mediating the cytotoxicity of CCND1 KD. To address this role of C53, we determined whether C53 depletion also rescue other phenotypes associated with CCND1 KD including DNA damage and defective ATR-CHEK1 signaling. Using the inducible CCND1 KD and CCND1/C53 double-KD (DKD) UPN-1 lines previously generated (Annual Report, 2016), we found that C53 depletion reduced gamma-H2AX levels in CCND1 KD cells after hydroxyurea (HU) exposure **(Figure 1A)**. Consistent with reduced gamma-H2AX levels, phosphorylation of the upstream kinases ATM and CHEK2 were also reduced in CCND1/C53 DKD cells under the same HU exposure condition (Annual Report, 2016).

We next determined whether depletion of C53 would restore defects in ATR signaling in CCND1-silenced cells. CCND1 KD and CCND1/C53 DKD UPN-1 cells were treated with etoposide overnight and ATR phosphorylation was assessed at differeent time points by immunoblot analysis. Under this condition, ATR phosphorylation in CCND1 KD cells was

increased at 4 h but then reduced by 8 h after etoposide removal **(Figure 1B)**. In contrast, ATR phosphorylat-ion remained high in CCND1/C53 DKD cells at 8 h after etoposide removal **(Figure 1B)**.

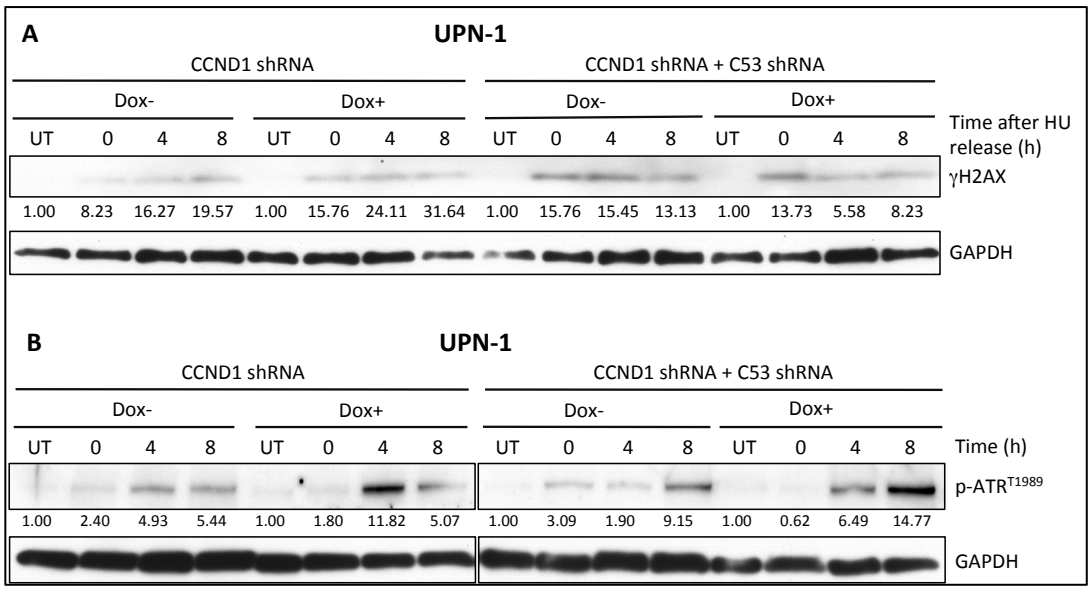

Figure 1. C53 depletion reduces DNA damage and restores ATR activity in CCND1 KD cells. A. UPN-1 cells transduced with CCND1 shRNA or both CCND1 shRNA and C53 shRNA were induced with doxycycline (Dox) for 3 days to induce shRNA expression. Cell were then treated with 1mM of hydroxyurea (HU) for 16 h followed by washing and incubation in normal growth medium. Cell lysates were prepared at indicated time after HU removal and immunoblotted with indicated antibodies. **B.** CCND1 KD and CCND1/C53 DKD UPN-1 cells as described in (A) were treated with 500 nM of etoposide for 16 h followed by washing and incubation in normal growth medium. Cell lysates were prepared at indicated time after etoposide removal and immunoblotted with indicated antibodies. Numbers below bands are relative densitometric values after normalization to GAPDH and untreated (UT) controls.

These data indicate that depletion of C53 restore ATR activity in CCND1 KD cells after etoposide exposure.

To further confirm the role C53 in mediating the defective ATR signaling in CCND1 KD cells, we examined whether depletion of C53 rescues premature mitotic entry caused by CCND1 depletion. CCND1 KD or CCND1/C53 DKD cells were treated with etoposide over night followed by incubation in normal growth medium and flow cytometric analysis of mitotic cells. Compared to untreated cells, etoposide-treated cells were arrested at the G2 phase up to 12 h after etoposide removal. However, in CCND1 KD cells, there was 2.5-fold increase in mitosis, as detected by phospho-Ser10 histone H3 **(Figure 2)**. However, increased mitotic entry in CCND1 KD cells was abrogated when C53 was depleted **(Figure 2)**. This finding further supports a role for C53 in regulating ATR signaling.

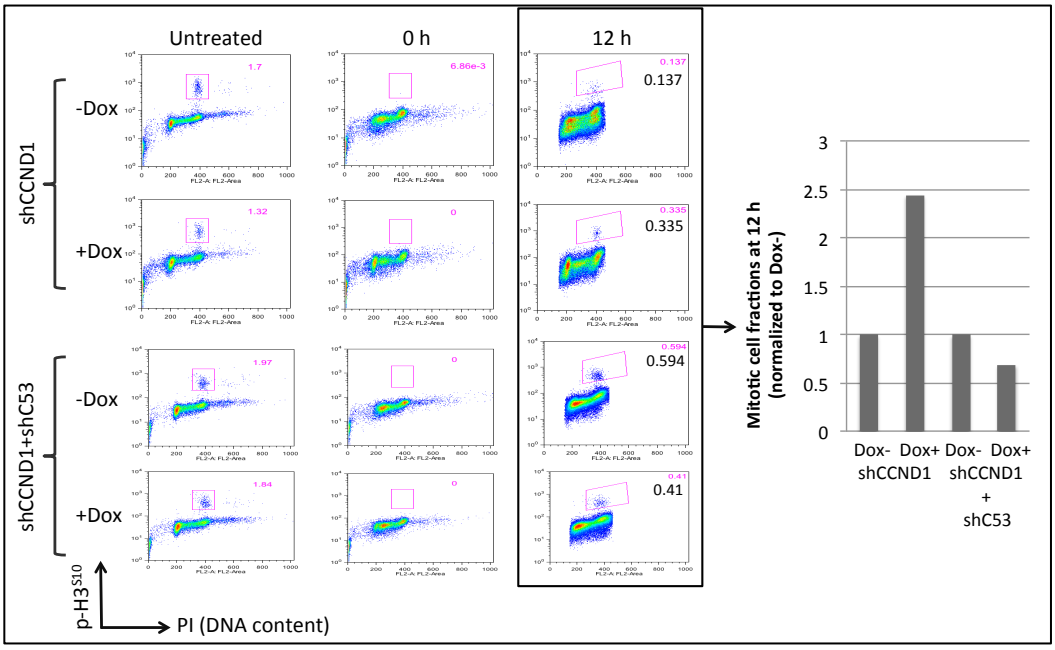

Figure 2. C53 depletion prevents premature mitotic entry in CCND1 KD cells. CCND1 KD and CCND1/C53 DKD UPN-1 cells were treated with 500 nM of etoposide for 16 h followed by incubating in normal growth medium. Cells at indicated times after etoposide removal were stained with p-histone H3 Ser10 antibody (detects mitotic cells) and propidium iodide (detects DNA content) and analyzed by flow cytometry. Gates drawn on p-H3 positive cells indicate mitotic cells. Bar graph on the right shows mitotic cell fractions after normalization to Dox- samples.

C53 overexpression did not phenocopy CCND1 KD.

In preliminary studies, we showed that depletion of CCND1 in MCL cells led to increased C53 expression, defective CHEK1 signaling and increased apoptosis. In addition, apoptotic cell death in CCND1 KD cells was rescued by depletion of C53. We also found that overexpression of specific C53 isoforms E or B in HEK-293T cells deregulated CHEK1 or CHEK2 signaling, respectively, following induced DNA damage. To further evaluate the role of C53 in MCL cells, we conditionally expressed the FLAG-tagged C53 isoform B or E in UPN-1 cells and determined the effects of C53 overexpression on cell growth and CHEK1 signaling. In contrast to our prediction, overexpression of either isoform B or E increased cell proliferation and had little effect on sensitivity of UPN-1 cells to DNA damaging agents (Annual Report, 2016). Further analysis revealed that neither forced expression of isoform E or D led to defective CHEK1 phosphorylation after recovering from HU exposure or under continuous HU exposure, respectively (Annual Report, 2016). These data indicate that overexpression of C53 alone is not sufficient to recapitulate the phenotype observed in CCND1 KD.

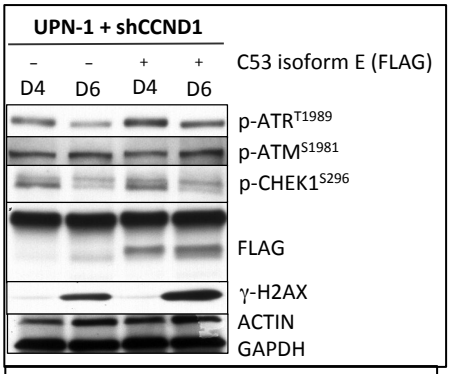

Figure 3. C53 overexpression increases DNA damage in CCND1 KD cells. shCCND1-expressing UPN-1 cells were transduced with a flag-tagged C53 isoform E and selected with puromycin. Immunoblot analysis was performed on day 4 and day 6 after selection with indicated antibodies.

C53 overexpression increases DNA damage in CCND1-depleted MCL cells.

Since overexpression of C53 alone is not sufficient to phenocopy the effect of CCND1 knockdown, we examined whether C53 overexpression in a CCND1-depleted background enhance the effects of CCND1 KD on the ATR signaling in MCL cells. **Figure 3** shows that overexpression of C53 in CCND1-depleted UPN-1 cells results in increased DNA damage as detected by upregulation of gamma-H2AX signals. However, we did not observe significant changes in phosphorylation activity of ATR and CHEK1. These data indicate that although increased C53 expression appears to enhance DNA damage in CCND1-depleted MCL cells, it is insufficient to affect ATR and CHEK1 phosphorylation.

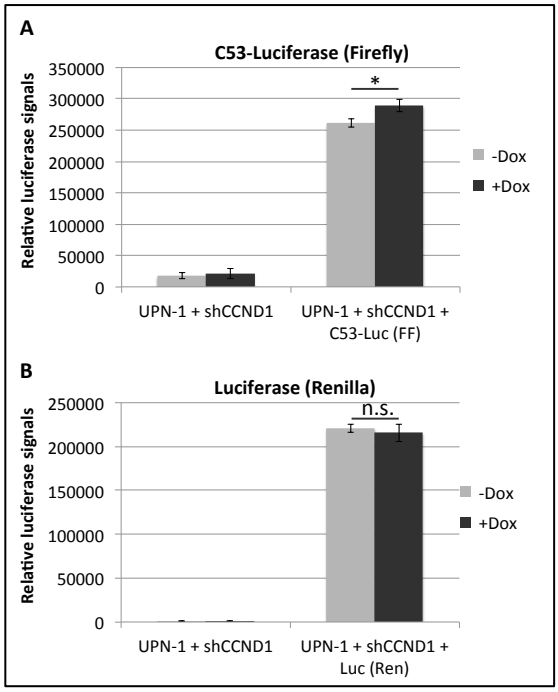

Figure 4. CCND1 depletion increases C53 promoter activity. shCCND1-expressing UPN-1 cells were transduced with C53 promoter-luciferase (Firefly, FF) (A) or with Renilla luciferase (Ren) (B). A luminescence assay was performed on day 2 after shCCND1 induction by doxycycline. Bar graphs are means of 3 technical repeats. Error bars, S.D. * $p < 0.05$ by a 2-tailed student t-test. n.s. not significant.

CCND1 negatively regulates C53 promoter activity.

In order to evaluate effects of CCND1 on C53 transcription, we cloned a *firefly* luciferase gene downstream of the C53 promoter isolated from the genomic DNA of Z-138 cells using PCR. We also

cloned a *Renilla* luciferase gene downstream of a retroviral LTR promoter as a negative control. These constructs were sequence verified to confirm the presence of inserts. To assess the effect of CCND1 on C53 promoter activity, we first transduce the C53-luciferase reporter or *Renilla* luciferase control into UPN-1 cells that express an inducible CCND1 shRNA. After induction of CCND1 shRNA by doxycycline, luciferase activity was measured by a luminescence assay. **Figure 4A** shows that after doxycycline addition, the C53 promoter activity is increased at a modest level, but significantly. In contrast, CCND1 depletion does not affect *Renilla* luciferase activity, which is not under control by the C53 promoter **(Figure 4B)**.

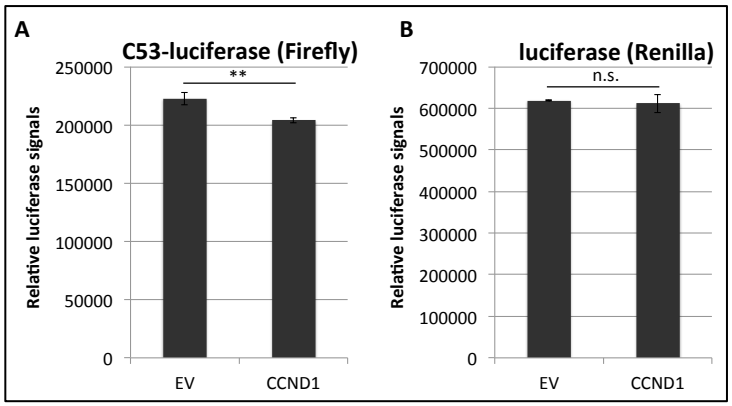

Figure 5. CCND1 overexpression decreases C53 promoter activity. HEK-293T cells were co-transfected with 1 ug of empty vector (EV) or CCND1-expressing vector and 0.5 ug of C53 promoter-luciferase (Firefly, FF) (A) or Renilla luciferase (Ren) (B). A luminescence assay was performed on day 2 after transfection. Bar graphs are means of 3 technical repeats. Error bars, S.D. ** $p < 0.01$ by a 2-tailed student t-test. n.s. not

To further confirm the effect of CCND1 on C53 promoter activity, we co-expressed CCND1 with C53-luciferase or *Renilla* luciferase construct in HEK-293T cells and compared luciferase activity with those from an empty vector control. We found that overexpression of CCND1 decreased C53 promoter activity **(Figure 5A)** without affecting those from the *Renilla* luciferase control **(Figure 5B)**. Altogether, these results indicate that CCND1 can directly interact with and negatively regulate the C53 promoter.

CCND1 interacts with HDAC1.

To determine what transcription factors were associated with CCND1 and recruited at the *C53* promoter, we first examined the recruitment of the transcriptional repressors HDAC1 and HP1, which were previously reported to interact with CCND1(5). Using the publicly available ENCODE data, we found that, unlike HP1, HDAC1 is highly recruited to the 5' end of *C53* in the myeloid leukemic cell line K562, suggesting its role in the regulation of *C53* activity. In addition, CCND1 was found to interact with HDAC1 in the MCL cell line GRANTA-519 by a mass spectrometer-based proteomics approach (6). Based on these observations, we hypothesize that CCND1 reppresses *C53* transcription in MCL cells through recruitment of HDAC1. To test this hypothesis, we first examined whether CCND1 physically associates with HDAC1 by co-expressing HDAC1 and CCND1 in HEK-293T cells and analyzed potential interactions using co-immunoprecipitation. **Figure 6A** shows that CCND1 strongly interacts with HDAC1 in HEK-293T cells (4). Validation of this interaction in Z-138 cells or in primary MCL samples by immunoprecipitation with CCND1 or HDAC1 antibody also showed CCND1 in the complex with HDAC1 and HDAC2 **(Figure 6B)** (4). Together, these results indicate that CCND1 physically interacts with HDAC1 (and HDAC2) in MCL cells.

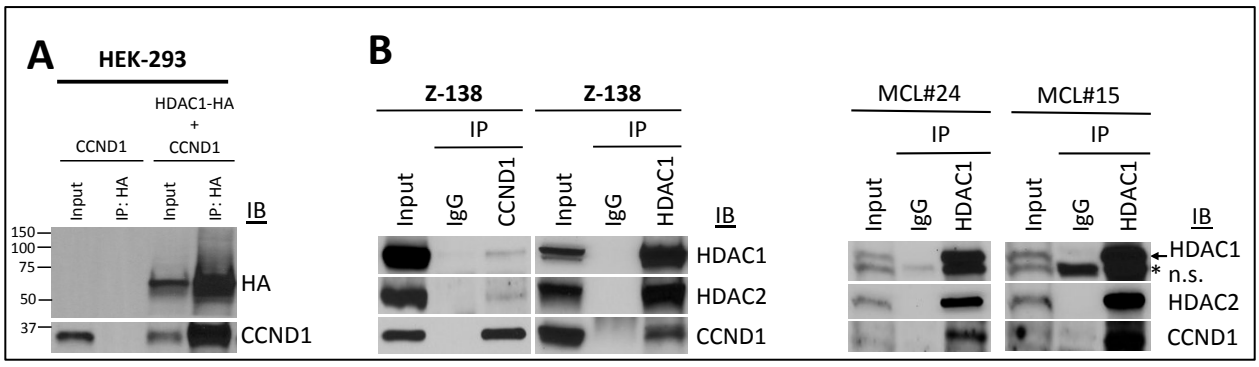

Figure 6. CCND1 interacts with HDAC1 and HDAC2. A. HEK-293T cells were transiently co-transfected with untagged CCND1 and HA-tagged HDAC1 and immunoprecipitated with HA antibody followed by immunoblotting with indicated antibodies. Lysates before immunoprecipitation were used as input samples. **B.** Z-138 cells or primary MCL samples were immunoprecipitated with isotype control IgG, CCND1 or HDAC1 antibody and immunoblotted with indicated antibodies. Lysates before immunoprecipitation were used as input samples. Arrow, specific HDAC1 staining. * non-specific bands.

HDAC1 is recruited to the C53 promoter.

To determine whether HDAC1 is recruited to the *C53* gene, we used an anti-HDAC1 antibody to perform chromatin immunoprecipitation in the MCL line Z-138 and sequenced the pulled-down DNA using high-throughput sequencing (ChIP-Seq). To determine the effect of CCND1 overexpression on the recruitment of HDAC1 at the *C53* gene, we also performed the ChIP-Seq experiments for Z-138 cells that ectopically expressed CCND1. Compared to IgG antibody control, HDAC1 pull-down exhibits two distinct peaks at the 5' end of the *C53* gene in Z-138 cells that express an empty vector control or CCND1-expressing vector **(Figure 7)**. Interestingly, more HDAC1 recruitment to the *C53* promoter was observed in CCND1-overexpressing Z-138 cells than those in empty vector control **(Figure 7)**. These results indicate that HDAC1 is recruited to the *C53* promoter and overexpression of CCND1 may enhance this recruitment.

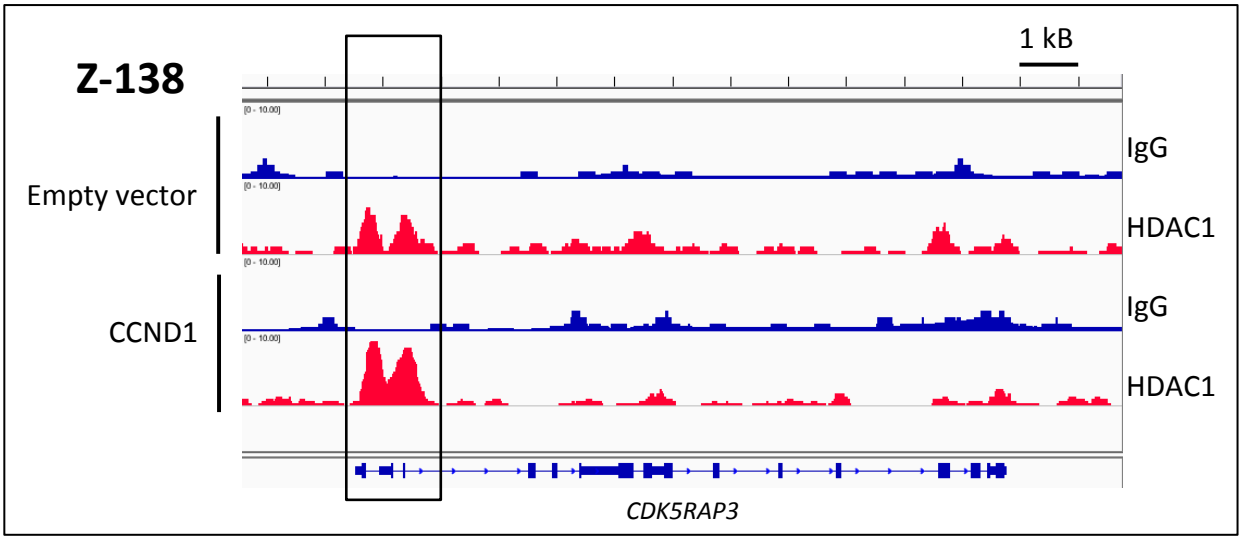

Figure 7. HDAC1 is recruited to the C53 gene locus. Z-138 cells were stably transduced with an empty vector or CCND1-expressing lentivirus and HDAC1 was immunoprecipitated with an isotype IgG control antibody or anti-HDAC1 antibody followed high-throughput sequencing (ChIP-Seq). The ChIP-Seq signals for HDAC1 (red) and IgG control (blue) were determined by peak-finding programs and shown by the Integrative Genomics Viewer at the *C53* (*CDK5RAP3*) genomic locus. The signals highlighted by the rectangular box are statistically significant ($p < 0.0001$).

CCND1 cooperates with HDAC1 to repress C53 expression.

Our findings of HDAC1 recruitment to the *C53* locus prompted us to examine whether HDAC1 represses *C53* expression. Using a C53 reporter system as described in **Figure 8A**, we co-transfected the reporter constructs with an empty vector, HDAC1, CCND1 or both HDAC1 and CCND1 in HEK-293T cells. While we consistently observed reduced C53 reporter activity upon CCND1 overexpression, as shown in our previous progress report, we found that HDAC1 overexpression also repressed *C53* promoter activity **(Figure 8B)**. Interestingly, when both HDAC1 and CCND1 were co-expressed, repression of the *C53* promoter activity was further enhanced **(Figure 8B)**. These results indicate that CCND1 may cooperate with HDAC1 to regulate *C53* expression.

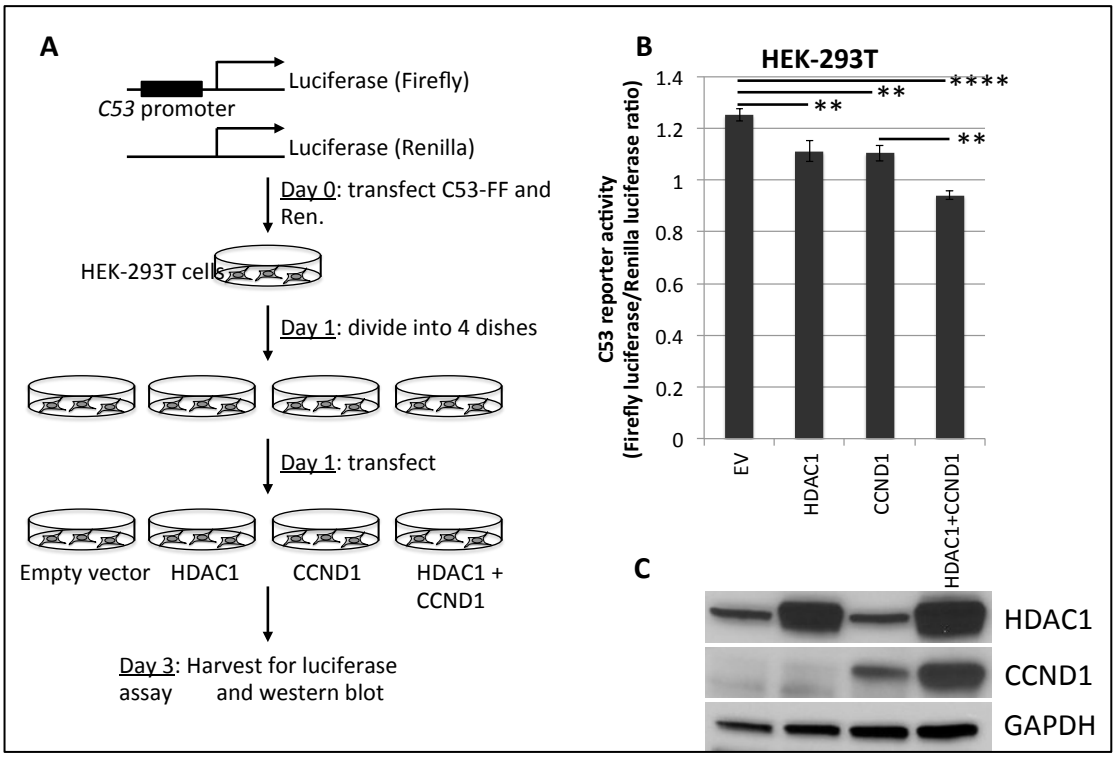

Figure 8. CCND1 cooperates with HDAC1 to regulate *C53* expression. A. An experiment scheme to examine effects of HDAC1 and CCND1 on the C53 promoter activity in HEK-293T cells. **B.** C53 promoter activity after HDAC1 or CCND1 overexpression. *C53* reporter activity of samples as described in (A) are shown as the ratio between the Firefly luciferase activity and the Renilla luciferase activity determined by the Dual-Luciferase Reporter Assay System (Promega). Bar graphs are means of three independent luciferase assays. Error bars, standard deviation. ** P< 0.01, **** P< 0.0001 by a 2-sided Student t-test. **C.** Immunoblots of samples depicted in (A) shows expression of indicated proteins.

In summary, we have shown that C53 depletion reduces DNA damage and restores ATR signaling in CCND1-depleted MCL cells. These results are consistent with the rescue of CCND1/C53 DKD cells from apoptosis and suggest a role for C53 in mediating cytotoxicity of CCND1 KD. However, overexpression of C53 isoforms in the MCL cell line UPN-1 did not recapitulate CCND1 KD phenotypes such as increased apoptosis, DNA damage and sensitivity to DNA damaging agents. This suggests that overexpression of C53 alone is insufficient to phenocopy CCND1 KD and that other downstream targets of CCND1 likely contribute to MCL survival. In addition, using chromatin immunoprecipitation, ChIP-Seq and C53 reporter assays, we have found that CCND1 physically interacts with HDAC1 and this interaction may result in the recruitment of HDAC1 to the C53 promoter, leading to repression of C53 expression. These findings uncovered a previously unrecognized role of CCND1 in the regulation of C53 expression. Our results provide further insights into the abnormal oncogenic signaling of CCND1 and thus have a potential for future development of more effective treatment strategies for MCL.

References

1. Jiang, H., Wu, J., He, C., Yang, W., and Li, H. 2009. Tumor suppressor protein C53 antagonizes checkpoint kinases to promote cyclin-dependent kinase 1 activation. *Cell Res* 19:458-468.
2. Mohanty, S., Mohanty, A., Sandoval, N., Tran, T., Bedell, V., Wu, J., Scuto, A., Murata-Collins, J., Weisenburger, D.D., and Ngo, V.N. 2017. Cyclin D1 depletion induces DNA damage in mantle cell lymphoma lines. *Leuk Lymphoma* 58:676-688.

3. Mohanty, A., Sandoval, N., Das, M., Pillai, R., Chen, L., Chen, R.W., Amin, H.M., Wang, M., Marcucci, G., Weisenburger, D.D., et al. 2016. CCND1 mutations increase protein stability and promote ibrutinib resistance in mantle cell lymphoma. *Oncotarget* 7:73558-73572.
4. Mohanty, A., Sandoval, N., Phan, A., Nguyen, T.V., Chen, R.W., Budde, E., Mei, M., Popplewell, L., Pham, L.V., Kwak, L.W., et al. 2018. Regulation of SOX11 expression through CCND1 and STAT3 in mantle cell lymphoma. *Blood*.
5. Fu, M., Rao, M., Bouras, T., Wang, C., Wu, K., Zhang, X., Li, Z., Yao, T.P., and Pestell, R.G. 2005. Cyclin D1 inhibits peroxisome proliferator-activated receptor gamma-mediated adipogenesis through histone deacetylase recruitment. *J Biol Chem* 280:16934-16941.
6. Jirawatnotai, S., Hu, Y., Michowski, W., Elias, J.E., Becks, L., Bienvenu, F., Zagozdzon, A., Goswami, T., Wang, Y.E., Clark, A.B., et al. 2011. A function for cyclin D1 in DNA repair uncovered by protein interactome analyses in human cancers. *Nature* 474:230-234.

What opportunities for training and professional development has the project provided?
The PI, Vu Ngo, has attended the following workshops and conferences to present research finding related to the project:

Gabrielle's Angel Foundation for Cancer Research Annual Symposium. 2015 Miami, Florida. Presentation title: The role of cyclin D1 in genomic stability and therapeutic implications in mantle cell lymphoma.

Lymphoma Research Foundation Workshop on Mantle Cell Lymphoma. 2016 Atlanta, Georgia. Presentation title: The role of cyclin D1 mutations in mantle cell lymphoma.

International Lymphoma Study Group (ILSG). 2016 Arcadia, California. Presentation title: Cyclin D1 mutations and ibrutinib resistance in mantle cell lymphoma.

ASH Meeting on Lymphoma Biology 2016, Colorado Springs, Colorado. Presentation title: Mechanisms of Ibrutinib Insensitivity in Mantle Cell Lymphoma.

The PI, Vu Ngo, has participated in the following professional development activities:

Member by invitation, The Mantle Cell Lymphoma Consortium, Lymphoma Research Foundation (2017).

Giving lectures "B cell receptor signaling in normal and malignant B cell development" at the *AstraZeneca Hematology Learning Event.* Duarte, California. (5/22/2017 and 9/13/2017).

How were the results disseminated to communities of interest?
Relevant results from this project have been reported in three peer-review publications as listed under PRODUCTS

What do you plan to do during the next reporting period to accomplish the goals?
Although this is our final report, we will perform follow-up studies and prepare a manuscript for publication of results obtained from this project. Specifically, we will determine whether depletion or inhibition of HDAC1 would affect C53 expression. We will also investigate the mechanism of de-repression of C53 expression as a potential therapeutic stragegy targeting the CCND1-C53-CHEK1 pathway.

4 **IMPACT:**

What was the impact on the development of the principal discipline(s) of the project?
Cyclin D1 overexpression as a result of chromosomal translocation is the founding lesion in MCL. We showed that experimentally targeting of cyclin D1 in MCL resulted in cell death and increased sensitivity to chemotherapeutic agents. These findings suggest that cyclin D1 is a valid drug target in MCL. However, there is currently no small molecule inhibitors for cyclin D1, which does not have an enzymatic activity and thus a drug binding pocket as most enzymatic drug targets do. To overcome this undruggability of cyclin D1, a better understanding of its cancer-causing pathways will likely uncover signaling components that can be targeted by pharmacological inhibitors. In this regard, our data have revealed that cyclin D1 regulates a

novel tumor suppressor CDK5RAP3 (C53), which is important for abnormal proliferation in MCL. Our findings therefore provide insights into the complex cancer-causing activity of cyclin D1, which would ultimately reveal actionable drug targets for MCL.

What was the impact on other disciplines?
In addition to MCL, cyclin D1 is also overexpressed in many other cancers including glioblastoma, breast, lung, prostate and ovarian cancer. A better understanding of the abnormal signaling caused by cyclin D1 overexpression and its downstream events including C53 regulation will also have relevant impact on these cancers.

What was the impact on technology transfer?
Nothing to Report.
What was the impact on society beyond science and technology?
Nothing to Report.

5 **CHANGES/PROBLEMS:**

Changes in approach and reasons for change
Experiments in the original Specific Aim 1c (Task 1c in SOW) were replaced with new experiments to "*determine whether C53 overexpression phenocopies CCND1 KD using alternative approaches*," as described in the Annual Report, 2016. This change was necessary because we needed to determine why C53 depletion could rescue cytotoxicity of CCND1 KD but C53 overexpression did not phenocopy CCND1 KD. Answers to this question would clarify the role of C53 in mediating CCND1 KD phenotypes. In addition, we chose to remove experiments in the original Specific Aim 1c because these experiments were mainly to confirm the effects of C53 on CHEK1 and CHEK2 activities in MCL cells, which have been previously described in HeLa cells by the Li's group (Jiang et al. *Cell Res.* 2009 19:458).

Actual or anticipated problems or delays and actions or plans to resolve them: N/A

Changes that had a significant impact on expenditures: N/A

Significant changes in use or care of human subjects, vertebrate animals, biohazards, and/or select agents: N/A

6 **PRODUCTS:**
Publications
1. Mohanty A, Sandoval N, Das M, Pillai R, Chen L, Chen RW, Amin HM, Wang M, Marcucci G, Weisenburger DD, Rosen ST, Pham LV, **Ngo VN.** CCND1 mutations increase protein stability and promote ibrutinib resistance in mantle cell lymphoma. *Oncotarget*. 2016; 7(45):73558-73572. PMID: 27713153
Acknowledgement of federal support: Yes.

2. Mohanty S, Mohanty A, Sandoval N, Tran T, Bedell V, Wu J, Scuto A, Murata-Collins J, Weisenburger DD, **Ngo VN.** Cyclin D1 depletion induces DNA damage in mantle cell lymphoma lines. *Leukemia & lymphoma*. 2017; 58(3):676-688. PMID: 27338091
Acknowledgement of federal support: Yes.

3. Mohanty A, Sandoval N, Phan A, Nguyen TV, Chen RW, Budde E, Mei M, Popplewell L, Pham LV, Kwak LW, Weisenburger DD, Rosen ST, Chan WC, Müschen M, **Ngo VN**. Regulation of SOX11 expression through CCND1 and STAT3 in mantle cell lymphoma. *Blood.* 2019; 133(4):306-318. PMID: 30530749
Acknowledgement of federal support: Yes.

Conference papers
The role of cyclin D1 mutations in mantle cell lymphoma. *Lymphoma Research Foundation Workshop on Mantle Cell Lymphoma.* Atlanta, Georgia, 2016.

Atish Mohanty, Natalie Sandoval, Manasi Das, Hesham M. Amin, Guido Marcucci, Raju Pillai, Dennis D. Weisenburger, Steven T. Rosen, Lan V. Pham and **Vu N. Ngo**. CCND1 mutations increase protein stability and promote ibrutinib resistance in Mantle Cell Lymphoma. *Blood* (ASH Annual Meeting Abstracts), 2016; 128: 4094.

Presentations
Mechanisms of Ibrutinib Insensitivity in Mantle Cell Lymphoma. ASH Meeting on Lymphoma Biology 2016, Colorado Springs, CO.

Cyclin D1 mutations and ibrutinib resistance in mantle cell lymphoma. *International Lymphoma Study Group (ILSG).* Arcadia, California, 2016.

Atish Mohanty, Natalie Sandoval, Manasi Das, Hesham M. Amin, Guido Marcucci, Raju Pillai, Dennis D. Weisenburger, Steven T. Rosen, Lan V. Pham and **Vu N. Ngo**. CCND1 mutations increase protein stability and promote ibrutinib resistance in Mantle Cell Lymphoma. *Blood* (ASH Annual Meeting Abstracts), 2016; 128: 4094.

Website(s) or other Internet site(s)
N/A
Technologies or techniques
N/A
Inventions, patent applications, and/or licenses
N/A
Other Products
N/A

7 PARTICIPANTS & OTHER COLLABORATING ORGANIZATIONS

What individuals have worked on the project?

Name:	*Vu Ngo*
Project Role:	*PI*
Researcher Identifier (e.g. ORCID ID):	
Nearest person month worked:	*4*
Contribution to Project:	*No change*

Name:	*Atish Mohanty*
Project Role:	*Postdoctoral Fellow*
Researcher Identifier (e.g. ORCID ID):	
Nearest person month worked:	*12*
Contribution to Project:	*No change*

Name:	*Natalie Sandoval and Andy Phan*
Project Role:	*Research Associate*
Researcher Identifier (e.g. ORCID ID):	

Nearest person month worked:	*3*
Contribution to Project:	*No change*

Has there been a change in the active other support of the PD/PI(s) or senior/key personnel since the last reporting period?
Nothing to Report.
What other organizations were involved as partners?
Nothing to Report.

8 **SPECIAL REPORTING REQUIREMENTS**
COLLABORATIVE AWARDS: *N/A*
QUAD CHARTS: *N/A*

9 **APPENDICES:**
Reprints of manuscripts

1. Mohanty A, Sandoval N, Das M, Pillai R, Chen L, Chen RW, Amin HM, Wang M, Marcucci G, Weisenburger DD, Rosen ST, Pham LV, **Ngo VN.** CCND1 mutations increase protein stability and promote ibrutinib resistance in mantle cell lymphoma. *Oncotarget*. 2016; 7(45):73558-73572. PMID: 27713153

2. Mohanty S, Mohanty A, Sandoval N, Tran T, Bedell V, Wu J, Scuto A, Murata-Collins J, Weisenburger DD, **Ngo VN.** Cyclin D1 depletion induces DNA damage in mantle cell lymphoma lines. *Leukemia & lymphoma*. 2017; 58(3):676-688. PMID: 27338091

3. Mohanty A, Sandoval N, Phan A, Nguyen TV, Chen RW, Budde E, Mei M, Popplewell L, Pham LV, Kwak LW, Weisenburger DD, Rosen ST, Chan WC, Müschen M, **Ngo VN**. Regulation of SOX11 expression through CCND1 and STAT3 in mantle cell lymphoma. *Blood.* 2019; 133(4):306-318. PMID: 30530749

Research Paper

CCND1 mutations increase protein stability and promote ibrutinib resistance in mantle cell lymphoma

Atish Mohanty[1], Natalie Sandoval[1], Manasi Das[1], Raju Pillai[3], Lu Chen[4], Robert W. Chen[5], Hesham M. Amin[6], Michael Wang[7], Guido Marcucci[1], Dennis D. Weisenburger[3], Steven T. Rosen[5], Lan V. Pham[6], Vu N. Ngo[1,2]

[1]Division of Hematopoietic Stem Cell and Leukemia Research, Gehr Leukemia Center, Beckman Research Institute of City of Hope, Duarte, CA 91010, USA

[2]Toni Stephenson Lymphoma Center, Beckman Research Institute of City of Hope, Duarte, CA 91010, USA

[3]Department of Pathology, Beckman Research Institute of City of Hope, Duarte, CA 91010, USA

[4]Department of Information Sciences, Beckman Research Institute of City of Hope, Duarte, CA 91010, USA

[5]Department of Hematology and Hematopoietic Cell Transplantation, Comprehensive Cancer Center, Beckman Research Institute of City of Hope, Duarte, CA 91010, USA

[6]Department of Hematopathology, The University of Texas MD Anderson Cancer Center, Houston, TX 77030, USA

[7]Department of Lymphoma/Myeloma, The University of Texas MD Anderson Cancer Center, Houston, TX 77030, USA

Correspondence to: Vu N. Ngo, **email:** vngo@coh.org

Keywords: *cyclin D1, somatic mutations, ibrutinib resistance, mantle cell lymphoma*

Received: *April 29, 2016* ***Accepted:*** *September 24, 2016* ***Published:*** *October 04, 2016*

ABSTRACT

Mantle cell lymphoma (MCL) is characterized by the t(11;14) translocation, which leads to deregulated expression of the cell cycle regulatory protein cyclin D1 (CCND1). Genomic studies of MCL have also identified recurrent mutations in the coding region of *CCND1*. However, the functional consequence of these mutations is not known. Here, we showed that, compared to wild type (WT), single E36K, Y44D or C47S *CCND1* mutations increased CCND1 protein levels in MCL cell lines. Mechanistically, these mutations stabilized CCND1 protein through attenuation of threonine-286 phosphorylation, which is important for proteolysis through the ubiquitin-proteasome pathway. In addition, the mutant proteins preferentially localized to the nucleus. Interestingly, forced expression of WT or mutant CCND1 increased resistance of MCL cell lines to ibrutinib, an FDA-approved Bruton tyrosine kinase inhibitor for MCL treatment. The Y44D mutant sustained the resistance to ibrutinib even at supraphysiologic concentrations (5–10 μM). Furthermore, primary MCL tumors with *CCND1* mutations also expressed stable CCND1 protein and were resistant to ibrutinib. These findings uncover a new mechanism that is critical for the regulation of CCND1 protein levels, and is directly relevant to primary ibrutinib resistance in MCL.

INTRODUCTION

CCND1 is an important cell cycle regulator in many cell types. CCND1 binds and activates cyclin-dependent kinase (CDK) 4, which in turn phosphorylates and inactivates retinoblastoma (Rb) protein, leading to G1/S cell cycle progression [1, 2]. CCND1 accumulates in the nucleus during the G1 phase and translocates to the cytoplasm for degradation by the ubiquitin-proteasome system when cells enter the S phase [3, 4]. Cell cycle-dependent proteolysis of CCND1 requires phosphorylation of threonine-286 (T286) residue, which is predominantly mediated by glycogen synthase kinase 3 beta (GSK3B) [5]. Other kinases including DYRK1B and p38 MAPK are also known to phosphorylate T286, also leading to ubiquitin-dependent degradation of CCND1 [6, 7].

Deregulated expression of CCND1 in cancer can be caused by several mechanisms. In mantle cell lymphoma (MCL), the *CCND1* gene located on chromosome 11 is usually rearranged to a strong enhancer in the immunoglobulin heavy-chain (*IGH*) locus on chromosome 14, leading to increased *CCND1* transcription and CCND1

protein levels [8, 9]. Increased CCND1 levels also occur due to genomic deletions or point mutations in the 3′ UTR, which results in shorter, more stable transcripts [10, 11]. Experimental models that expressed a non-degradable CCND1 variant, in which T286 was substituted by alanine, or expression of an alternatively spliced CCND1b isoform, which lacks T286, have resulted in predominantly nuclear CCND1 expression and cellular transformation [12, 13]. In addition, aberrant activation of AKT and mTOR signaling results in down-regulation of GSK3B, also leading to reduced phosphorylation-dependent proteolysis and increased CCND1 protein levels [14].

Mantle cell lymphoma (MCL) is an incurable B-cell malignancy that frequently develops resistance to conventional chemotherapy and has a prognosis with a median overall survival of approximately 1–2 years after relapse [15, 16]. Recent treatment advances using the FDA-approved drug ibrutinib, which targets the B-cell antigen receptor (BCR) signaling molecule Bruton's tyrosine kinase (BTK), have produced durable responses in MCL [17]. However, one-third of MCL patients are ibrutinib-resistant, and even ibrutinib-sensitive patients eventually acquire resistance to the drug [17, 18]. The mechanisms underlying primary resistance to ibrutinib are not well understood. Recent studies have begun to provide some clues about potential mechanisms of primary ibrutinib resistance, including activation of the alternative NF-kB [19], ERK1/2 or AKT signaling pathways [20]. Mechanisms of acquired resistance to ibrutinib in patients who initially responded to the drug but then relapsed have also been reported, including recurrent mutations of the enzyme active site in BTK (C481S) or its substrate phospholipase C gamma 2 (PLCG2) [18, 21, 22]. These studies suggest that multiple mechanisms likely contribute to ibrutinib resistance in MCL.

Recent large-scale genomic studies of MCL have identified a hotspot for recurring somatic mutations in exon 1 of *CCND1* in 18–35% of the cases, likely arising through somatic hypermutation [23–25]. However, little is known about the functional role of these mutations in MCL. This study investigated the functional consequences of *CCND1* mutation on protein stability and sensitivity of MCL cells to ibrutinib therapy. The three most frequent *CCND1* mutations (E36K, Y44D and C47S) were cloned and expressed in MCL cell lines or HEK-293T cells. CCND1 protein stability and interaction with GSK3B were evaluated by cyclohexamide treatment and immunoprecipitation, respectively. Subcellular localization of the mutant CCND1 protein was determined by cell fractionation and immunofluorescence. In addition, primary MCL tumors with *CCND1* mutations were examined for CCND1 protein stability and sensitivity to ibrutinib. These studies have uncovered an important role for *CCND1* mutations in deregulating protein turnover, and a potential role in resistance to ibrutinib in some MCL tumors.

RESULTS

CCND1 mutations increased CCND1 protein levels through defective proteolysis

To study the role of *CCND1* somatic mutations, the *CCND1* exon 1 of eight MCL cell lines was sequenced and found to have the germ-line sequence (data not shown). Therefore, site-directed mutagenesis was used to generate the three most frequent mutations, E36K, Y44D and C47S, as previously reported (Figure 1A) [19, 23–25]. Hemagglutinin (HA)-tagged wild type (WT) or mutant *CCND1* cDNA was cloned into a retroviral vector and expressed in the MCL cell lines UPN-1, Z-138 and JEKO-1. An empty vector was used as a negative control. After establishing stably transduced cells by hygromycin selection, equal numbers of cells from each culture were harvested and mRNA and total protein lysates were prepared. Anti-HA antibody was used to assess exogenous CCND1 protein expression by immunoblot analysis. All three mutants showed increased protein expression compared to the WT counterparts in all three MCL cell lines (Figure 1B, Supplementary Figure S1A). In Supplementary Figure S1A, JEKO-1 cells that expressed the non-degradable T286A *CCND1* mutant [5] were also included for comparison. Compared to WT, mutant CCND1 proteins did not affect the kinase function of CDK4, as determined by phosphorylation of the CDK4 substrate Rb in JEKO-1 cells (Supplementary Figure S1B). To determine whether increased protein expression was due to increased transcription, mRNA expressed from WT and mutant *CCND1* was compared by real-time quantitative PCR (qPCR) using primers specific for the exogenous *CCND1-HA* mRNA (Figure 1C). There was no significant increase in mutant mRNA levels compared to that of WT samples in both UPN-1 and Z-138 cells (Figure 1C). Next, we determined whether increased protein levels were due to deregulated protein turnover. We treated WT or mutant *CCND1*-expressing cells with cyclohexamide (CHX) to inhibit *de novo* protein synthesis, and CCND1 proteolysis was examined by immunoblot analysis. In both UPN-1 and Z-138 cells, while more than 50% of WT CCND1 was degraded as early as 90 min after CHX, little reduction in Y44D CCND1 levels was observed during the same period (Figure 1D, 1E). Similar stability was also observed the C47S mutant in UPN-1 cells under the same experimental conditions (Supplementary Figure S2). Taken together, we concluded that *CCND1* mutations increased protein, but not mRNA, levels, and this was likely due to defective proteolysis.

CCND1 mutations interfere with T286 phosphorylation

Since phosphorylation of T286 is required for proteasome-mediated CCND1 turnover [5], we next

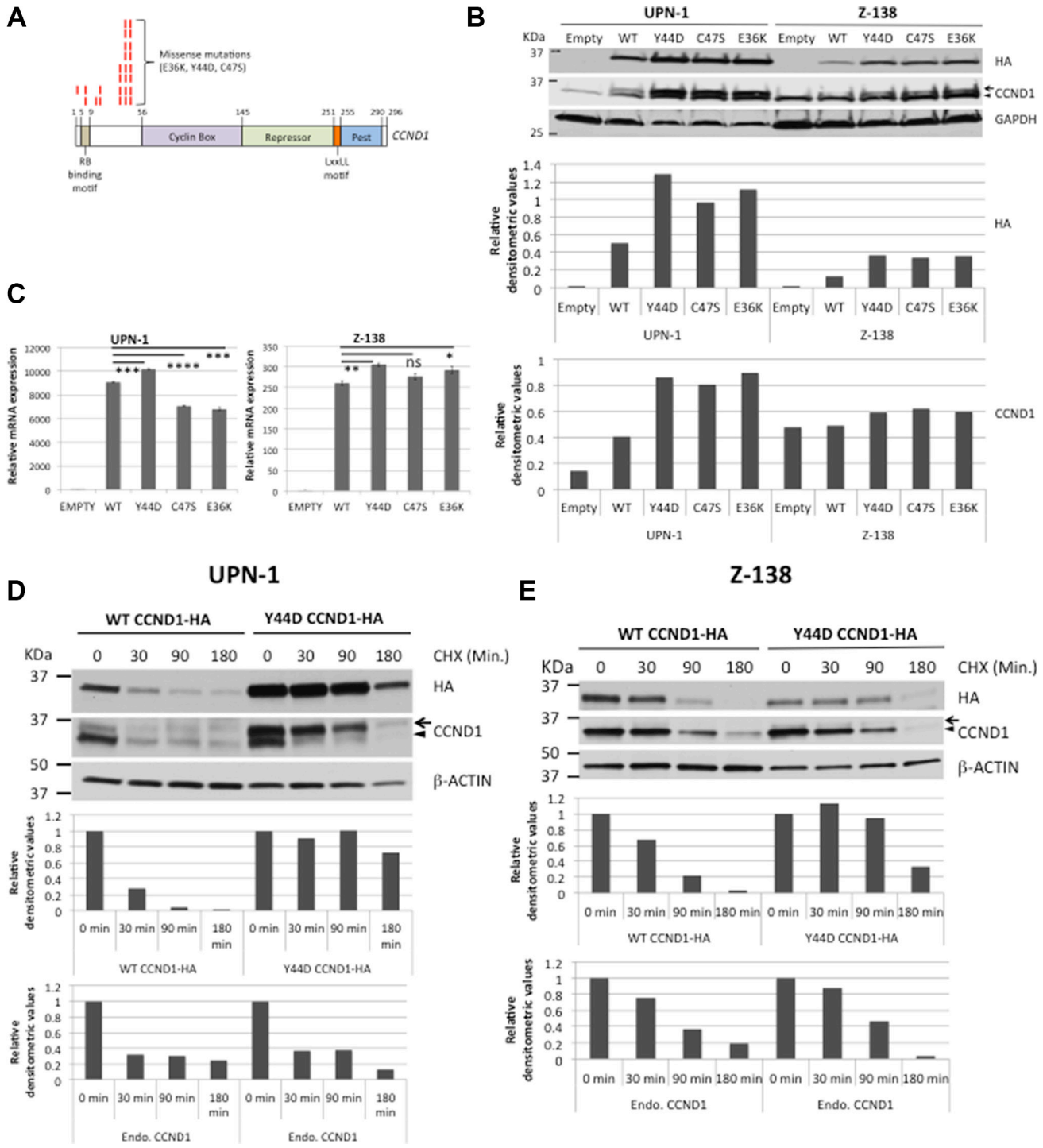

Figure 1: *CCND1* mutations increase protein levels. (**A**) Diagram shows recurring point mutations (red bars) in the N-terminus of CCND1 protein. (**B**) Immunoblot analysis of WT and mutant CCND1 expression. UPN-1 or Z-138 cells were transduced with WT or mutant CCND1-HA and selected for stable expression by hygromycin. Cell lysates (10 μg per lane) were separated by SDS-PAGE gel and immunoblotted with indicated antibodies. Arrow indicates a mobility shift of the CCND1-HA protein. Arrowhead indicates endogenous CCND1. Bar graphs below the immunoblot show relative densitometric values of indicated bands after normalization to GAPDH loading controls. (**C**) Quantitative PCR analysis of mRNA expression of WT and mutant *CCND1*. Cell lines generated as described in (B) and mRNAs were harvested for quantitative PCR analysis of CCND1-HA mRNA expression. Shown are the means of mRNA expression levels after normalization to GAPDH signals from four independent amplification experiments. Error bars, SD. ****$P < 0.0001$; ***$P < 0.001$; **$P < 0.01$; *$P < 0.05$ by a two-tailed Student's *T*-test. (**D**, **E**) UPN-1 or Z138 cells expressing WT or Y44D CCND1-HA were treated with 10 μM of cyclohexamide (CHX) for indicated times and 10 μg of cell lysates per lane were prepared for immunoblot analysis with indicated antibodies. Arrow, CCND1-HA protein. Arrowhead, endogenous CCND1. Bar graphs below immunoblots in (D, E) show relative densitometric values of indicated bands from the blots after normalization to time zero control samples.

examined the effect of CCND1 mutations on this phosphorylation. Immunoblot analysis of T286 phosphorylation levels taken directly from on-going cell cultures was, however, confounded by the higher steady-state levels of mutant CCND1 proteins (Supplementary Figure S1C). As an alternative approach, we evaluated T286 phosphorylation in cells that were treated with CHX over night to allow complete degradation of CCND1, and then returned back to normal growth conditions for renewed protein synthesis. Under this experimental condition, T286 phosphorylation of newly synthesized Y44D CCND1 was markedly reduced in both UPN-1 and Z-138 cells as compared to phosphorylation of WT CCND1 (Figure 2A, 2B). Reduced T286 phosphorylation of Y44D CCND1 was not due to decreased protein levels, as the mutant protein levels accumulated faster than WT protein over the same time period after CHX treatment and release (Figure 2A, 2B). Because of the low expression levels of CCND1-HA in Z-138 cells (Figure 1B and Figure 2B), to enhance detection of T286 phosphorylation, CCND1-HA was immunoprecipitated with the HA-specific antibody followed by immunoblotting with the phospho-T286 CCND1 antibody. T286 phosphorylation levels were markedly reduced in both Y44D and C47S CCND1 immunoprecipitates, as compared to phospho-T286 signals on WT CCND1 (Figure 2C). These data indicate that these N-terminal *CCND1* mutations interfere with T286 phosphorylation at the C-terminus of CCND1.

Reduced T286 phosphorylation on mutant CCND1 prompted us to evaluate the interaction of the T286 phosphorylating enzyme GSK3B with WT and mutant CCND1 using the co-immunoprecipitation (co-IP) method. Using anti-HA antibody to immunoprecipitate CCND1-HA proteins in JEKO-1 cells, we detected little difference between WT and mutant proteins on binding with known interacting partners such as CDK4 (Figure 2D). In contrast, GSK3B was found to co-precipitate more with WT than with Y44D or C47S mutants (Figure 2D). Surprisingly, GSK3B was not detectable in T286A CCND1-HA pull-down despite the fact that this mutant had WT sequence at the N-terminus (Figure 2D). To confirm differential binding of WT and mutant CCND1 to GSK3B, we performed a reverse co-IP experiment using an anti-GSK3B antibody. Figure 2E shows that all three mutants co-migrated with GSK3B without reduced binding, which is inconsistent with the results observed in the HA pull-down experiments. Despite the apparent discrepancy between the forward and reverse IP experiments, which could reflect the accessibility of the C-terminally tagged HA epitope (see Discussion), our data appear to indicate little effect of Y44D and C47S mutations on CCND1-GSK3B interaction.

Because T286 phosphorylation increases the ubiquitination of CCND1 protein [5], we next determined whether *CCND1* mutations affected protein ubiquitination. UPN-1 cells that stably express empty vector, WT or Y44D CCND1-HA were briefly treated with 5 nM of the proteasome inhibitor PS-341 (bortezomib) for two hours to enhance detection of ubiquitination. Treated cells were lysed in 2% SDS and heated at 95°C for five minutes to disrupt potential interactions of ubiquitin (Ub)-conjugated proteins that might co-precipitate with CCND1-HA. These lysates were subsequently immunoprecipitated with HA antibodies and Ub conjugates on CCND1 were examined by immunoblot analysis with anti-Ub antibody. As expected, WT CCND1 (both endogenous and exogenous protein) levels in the input accumulated after two hours of bortezomib treatment (Figure 2F). In contrast, little accumulation of mutant CCND1-HA was detected under the same treatment conditions (Figure 2F), consistent with deregulated proteolysis of mutant CCND1 as shown above. In the immunoprecipitates, more Y44D than WT CCND1 protein levels were detected, consistent with their respective CCND1-HA levels in the inputs (Figure 2F). However, Ub conjugate signals on Y44D CCND1 were less than that on WT CCND1 (Figure 2F). These results indicate that the Y44D mutation increases CCND1 protein stability through disruption of the Ub-proteasome pathway.

Y44D and C47S mutants preferentially localize to the nucleus

The T286A mutant protein was found predominantly in the nucleus because this mutation disrupted nuclear export of CCND1 [4]. To determine the cellular localization of CCND1 with N-terminal mutations, which also interfere with T286 phosphorylation, we performed cell fractionation experiments and compared WT and Y44D CCND1-HA protein levels in the nuclear extracts of UPN-1 cells. Cytosolic and nuclear fractions were confirmed by immunoblotting with the cytosolic markers β-ACTIN or GAPDH and nuclear marker histone H3. While WT and Y44D CCND1-HA proteins were detected in both the cytosolic and nuclear fractions, Y44D CCND1 protein levels were consistently higher than that of WT CCND1 in both fractions (Figure 3A). As an alternative approach, we used immunofluorescence to evaluate the subcellular distribution of WT and mutant CCND1-HA proteins expressed in HEK-293T cells, which were chosen for their large cytoplasmic surface area to facilitate data analysis. Using fluorescently labeled anti-HA antibody, we demonstrated that the Y44D and C47S mutant proteins preferentially localized to the nucleus as compared to WT CCND1 protein (Figure 3B). The T286A mutant was found predominantly in the nucleus, as expected from previous studies [4]. Together, we conclude that the Y44D and C47S *CCND1* mutation interferes with T286 phosphorylation and deregulates CCND1 nuclear export.

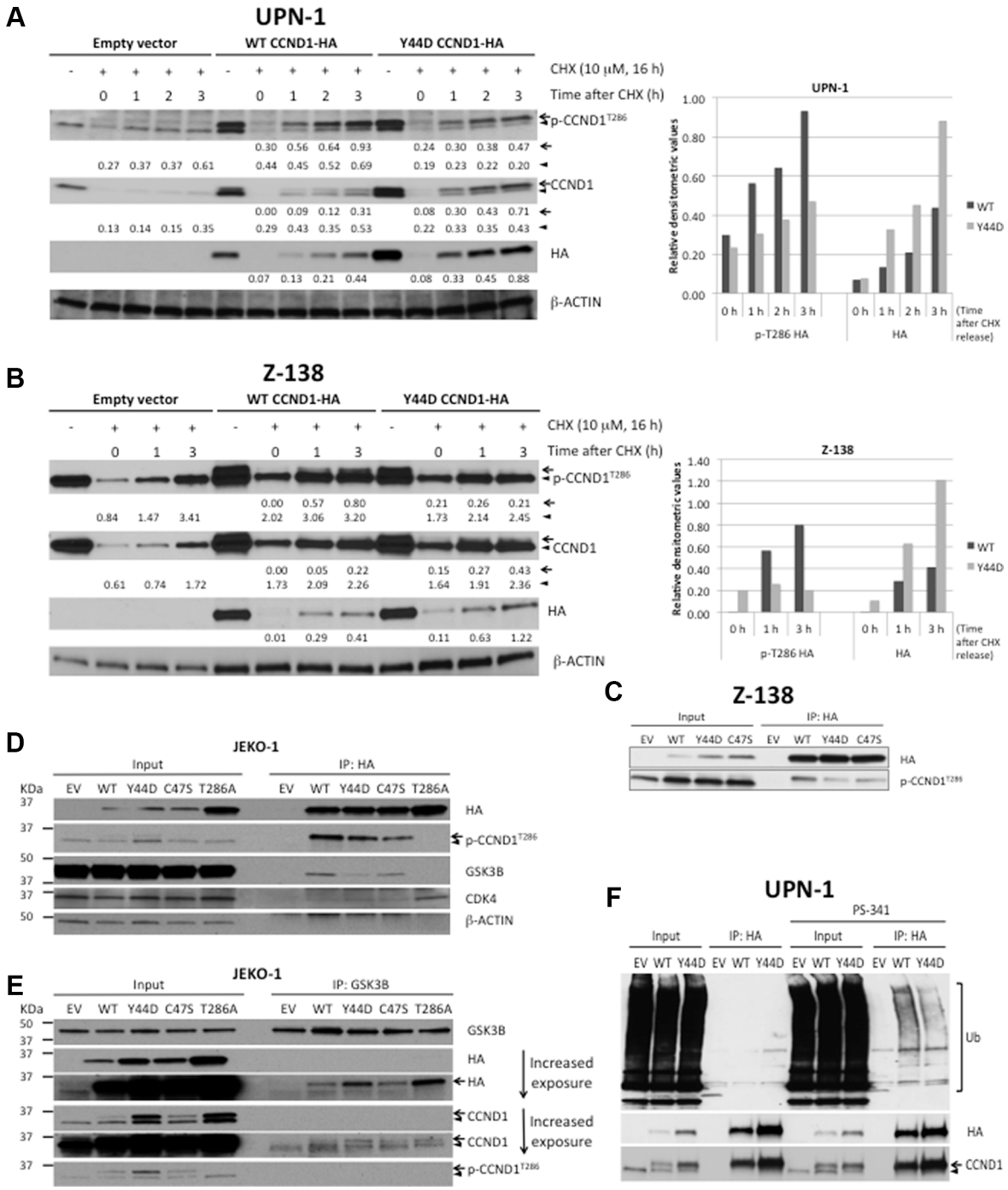

Figure 2: *CCND1* mutations interfere with T286 phosphorylation and protein ubiquitination. (**A**, **B**) UPN-1 or Z138 cells expressing WT, Y44D CCND1-HA, or an empty vector control were treated with 10 μM of cyclohexamide (CHX) for 16 hours and released to normal growth medium for indicated times. Cell lysates (10 μg per lane) were prepared for immunoblot analysis with indicated antibodies. Arrow, CCND1-HA protein. Arrowhead, endogenous CCND1. Numbers below the blots are relative densitometric values of corresponding bands after normalization to β-ACTIN loading controls. Graphical representation of selected densitometric values was shown in the bar graphs on the right. (**C**) Z-138 cells expressing an empty vector (EV), WT, or mutant CCND1-HA were immunoprecipitated with HA antibody and immunoblotted with indicated antibodies. Lysates before immunoprecipitation were used as input samples. (**D**, **E**) Analysis of mutant CCND1 interaction with GSK3B. (D) JEKO-1 cells expressing an empty vector (EV), WT, or mutant CCND1-HA were immunoprecipitated with HA antibody and immunoblotted with indicated antibodies. (E) JEKO-1 cell lines described in (D) were immunoprecipitated with GSK3B antibody and immunoblotted with indicated antibodies. Arrow, CCND1-HA protein. Arrowhead, endogenous CCND1. (**F**) Y44D *CCND1* mutation affects ubiquitin (Ub)-dependent degradation. UPN-1 cells that stably expressed an empty vector (EV) control, WT or Y44D CCND1-HA were treated with 5 nM of the proteasome inhibitor PS-341 for 2 h. Treated cells were lysed in 2% SDS and heated at 95°C for 5 min. Lysates were subsequently immunoprecipitated with HA antibodies and Ub conjugates on CCND1 were examined by immunoblot analysis with anti-Ub antibody.

CCND1 mutations promote resistance to ibrutinib

Previous studies showed that CCND1 was essential for MCL survival [26, 27], and that ibrutinib treatment decreased CCND1 protein levels in sensitive, but not in resistant, MCL cell lines [20]. These findings prompted us to determine a potential correlation between CCND1 levels and ibrutinib sensitivity. Ibrutinib-sensitive JEKO-1 cells [19, 20], which stably expressed WT or mutant CCND1 (Supplementary Figure S1A), were treated with a single dose of increasing concentrations of ibrutinib for four days and analyzed for cell growth and apoptosis using flow cytometry. Ibrutinib significantly inhibited cell growth and induced apoptosis in a dose-dependent manner in control cells transduced with an empty vector. In contrast, WT and

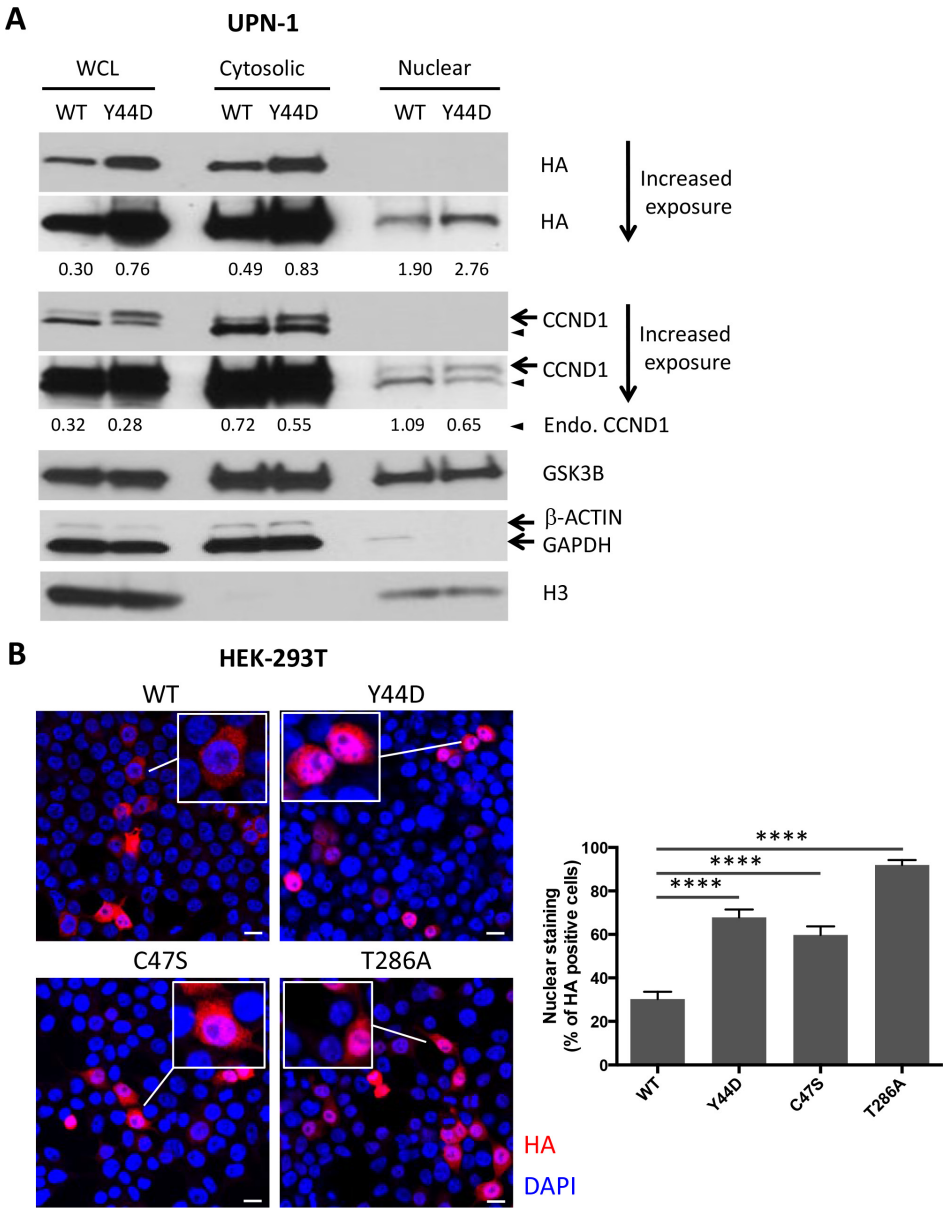

Figure 3: Subcellular localization of CCND1 mutants. (**A**) Cytosolic and nuclear extracts were prepared as described in Materials and Methods from UPN-1 cells that stably expressed WT or Y44D CCND1. The extracts (30 μg per lane) were immunoblotted with indicated antibodies. β-ACTIN or GAPDH and histone H3 were used to confirm cytosolic and nuclear fractions, respectively. Numbers below the blots are relative densitometric values of corresponding bands after normalization to β-ACTIN (for WCL and Cytosolic) or histone H3 (for Nuclear) loading controls. WCL, whole cell lysates; Endo., endogenous. (**B**) Subcellular distribution of WT and mutant CCND1-HA proteins, which were transiently expressed in HEK-293T cells, was evaluated by immunofluorescence. Shown are representative confocal immunofluorescence images of WT and mutant CCND1-expressing cells stained with anti-HA antibody (red) followed by nuclear staining with DAPI (blue). Scale bars, 20 μm. Bar graphs show the percentages of HA positive cells that have HA staining in the nucleus from two separate experiments. Error bars, SEM; ****$P < 0.0001$ by a two-tailed Student's *T*-test. Approximately 150 HA positive cells from each group were counted.

mutant CCND1-expressing cells were more resistant up to 5 μM of ibrutinib. At 10 μM, ibrutinib was toxic to WT, E36K and C47S mutants, but less so to Y44D and T286A mutants (Figure 4A, 4B). To confirm that the rescue effect of exogenously expressed CCND1 protein was specific to loss of BTK activity, we used a short-hairpin RNA (shRNA) to deplete BTK in JEKO-1 cells that expressed CCND1 variants (Supplementary Figure S3A). As expected, BTK depletion was toxic in JEKO-1 cells that expressed an empty vector (Supplementary Figure S3B). However, BTK shRNA-mediated toxicity in JEKO-1 cells was rescued by exogenous WT or mutant CCND1 (Supplementary Figure S3B), consistent with results shown in Figure 4A, 4B.

We next examined the effect of ibrutinib on expression of CCND1 protein levels. JEKO-1 cells expressing WT or mutant CCND1 were treated with 10 μM of ibrutinib for up to six hours and CCND1 levels were determined by immunoblot analysis. In a time-dependent manner, ibrutinib decreased the protein levels of WT and C47S mutant but not of Y44D mutant (Figure 4C), which appeared to correlate with the resistance of the Y44D mutant at high doses of the drug. These data indicate that increased CCND1 levels promote ibrutinib resistance and certain *CCND1* mutations can provide sustained protection from high doses of ibrutinib.

Defective T286 phosphorylation-dependent degradation of the Y44D CCND1 mutant and its protection of JEKO-1 cells against ibrutinib suggests a role for GSK3B in ibrutinib toxicity. To test this hypothesis, we used immunoblot analysis to evaluate GSK3B activity in JEKO-1 cells treated with ibrutinib. In a time-dependent manner, ibrutinib reduced the inhibitory serine-9 phosphorylation of GSK3B [28, 29], resulting in increased activity of this kinase (Figure 5A). Consistent with this finding, the activity of AKT, which phosphorylates GSK3B on serine-9 [30], was also reduced (Figure 5A). These results indicate that ibrutinib antagonizes the regulatory role of AKT, leading to re-activation of GSK3B which, in turn, mediates CCND1 degradation. To confirm that ibrutinib toxicity was GSK3B dependent, JEKO-1 cells were treated with increasing doses of ibrutinib in the presence of the GSK3B inhibitor SB-216763 [31]. Compared to DMSO-treated controls, addition of SB-216763 at both 0.5 and 1 μM partially rescued the cells from ibrutinib-mediated growth inhibition and apoptosis (Figure 5B, 5C). Treatment with the inorganic salt LiCl, which inhibits GSK3B [32], also rescued JEKO-1 cells from ibrutinib toxicity (Supplementary Figure S4). Thus, GSK3B kinase activity contributes to the cytotoxic effect of ibrutinib in JEKO-1 cells.

To further confirm the role of CCND1 mutations in interference with GSK3B-mediated T286 phosphorylation, we next investigated whether these mutations rescue cells from pharmacological agents that target the AKT-GSK3B pathway such as the PI3K inhibitor CAL-101 (idelalisib) [33] and the mTOR kinase inhibitor PP242 [34]. As expected, these drugs reduced AKT activity, re-activated GSK3B by decreasing serine-9 phosphorylation, and down-regulated CCND1 levels (Figure 5A). Similar to ibrutinib, both CAL-101 and PP242 demonstrated dose-dependent toxicity in control or WT CCND1-HA expressing JEKO-1 cells. However, overexpression of Y44D, C47S or T286A CCND1 was sufficient to rescue the cells from growth inhibition and apoptosis induced by increasing concentrations of CAL-101 or PP242 (Figure 5D–5G). Altogether, these data indicate that *CCND1* mutations promote resistance to GSK3B activating agents such as ibrutinib, CAL-101 or PP242.

Analysis of *CCND1* mutations in primary MCL tumors

To investigate the role of *CCND1* mutations in primary MCL tumors, the sequence of *CCND1* exon 1 was determined by Sanger sequencing in 16 primary tumors. The tumor content in these samples was confirmed to have greater than 90% CD19+, CD5+ lymphoma cells by flow cytometry (data not shown). Three samples from patients who did not received ibrutinib therapy at the time of sample collection were found to carry single C47S or C47R heterozygous mutations (Figure 6A). Immunoblot analysis of seven samples with sufficient tumor materials showed that MCL tumors with *CCND1* mutations expressed more CCND1 protein than WT samples, except for sample MCL 13 (Figure 6B). To examine whether increased CCND1 protein levels in these mutant cases was due to the presence of more stable, 3′ UTR-truncated transcripts, we used a previously-described RT-PCR assay [10] to compare full-length and 3′ UTR-truncated mRNA levels in these samples. While Z-138 cells were confirmed to predominantly express 3′ UTR-truncated *CCND1* mRNA as previously reported [10], all three *CCND1* mutated samples expressed the full-length mRNA, as did control HEK-293T cells (Figure 6C). One sample (MCL 2) with WT *CCND1* exon 1 was found to express UTR-truncated transcripts (Figure 6C). Therefore, we conclude that increased CCND1 protein accumulation in the mutant cases was not due to expression of stable UTR-truncated *CCND1* mRNAs.

To examine whether the increased protein level in MCL tumors with *CCND1* mutations was due to deregulated protein turnover, MCL cells were treated with CHX and the rate of CCND1 proteolysis was evaluated by immunoblot analysis. In contrast to WT CCND1 samples examined (MCL 10, 13 and 15), which showed CCND1 degradation after three hours in CHX, two of three *CCND1* mutant samples (MCL 11 and 47) had a prolonged half-life (Figure 6D). Interestingly, sample MCL 2, which expressed WT CCND1, also showed less CCND1 degradation (Figure 6D), likely due to unknown mutations that deregulate CCND1 proteolysis. Thus,

CCND1 mutations may affect protein stability in some primary MCL tumors and correlate with increased protein levels in these samples.

We next compared the sensitivity of MCL tumors that express WT or mutant *CCND1* to ibrutinib. In a dose-dependent manner, ibrutinib reduced cell viability in all three WT *CCND1* MCL samples (MCL 10, 13, and 15) after 72 hours (Figure 6E). In contrast, two of the three mutated samples (MCL 11 and 47) were more resistant to ibrutinib. Interestingly, MCL 2 was also resistant to the drug, which appeared to correlate with increased CCND1 protein stability observed in this sample. The difference in ibrutinib response between WT and mutated samples was not statistically significant, likely due to the small

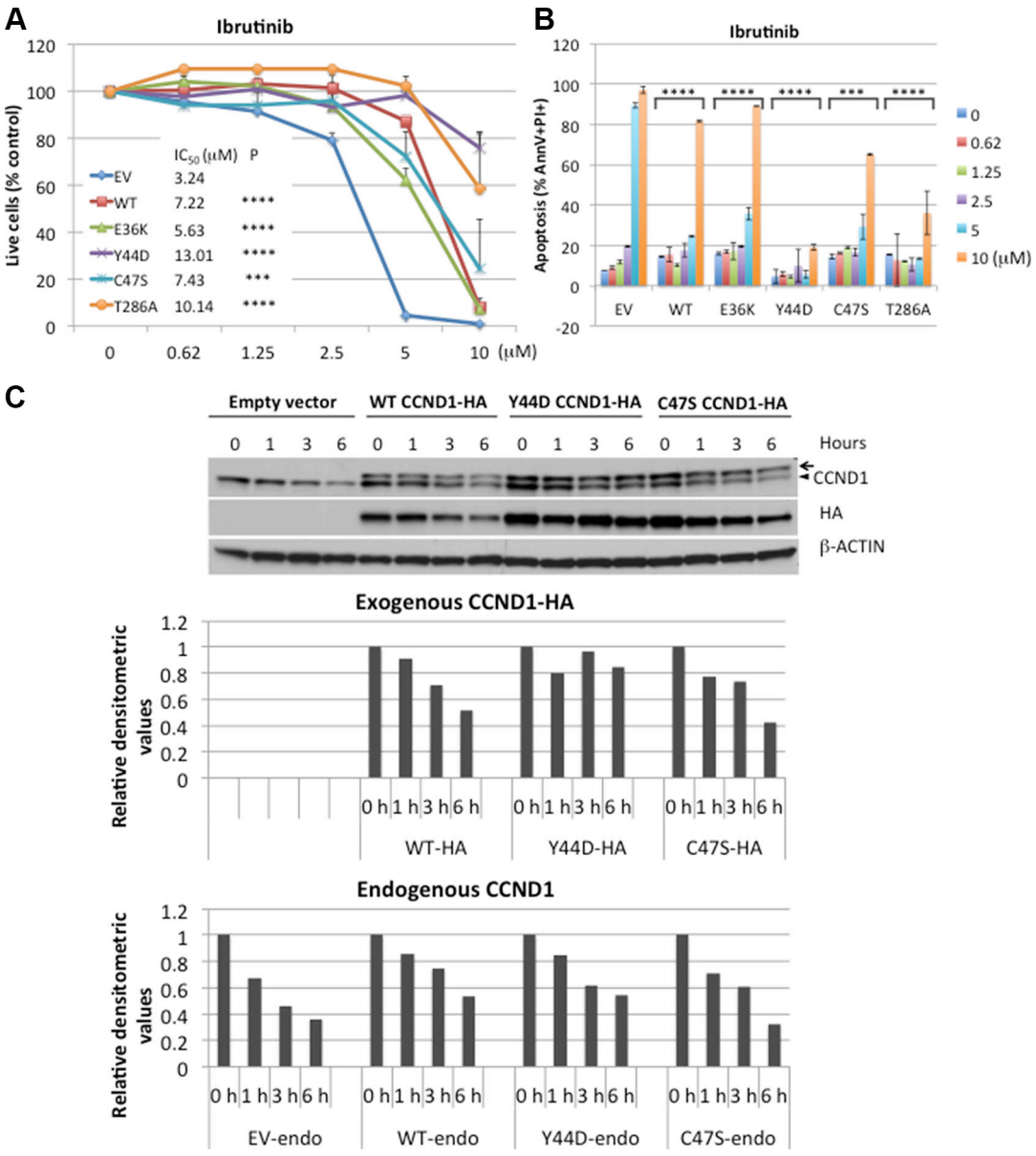

Figure 4:*CCND1* mutations promote resistance to ibrutinib. (**A**) JEKO-1 cells expressing an empty vector (EV), WT, or mutant CCND1-HA were treated with indicated doses of ibrutinib for four days and propidium iodide (PI)-negative (viable) cells were assessed by flow cytometry. Shown are PI negative fractions normalized to control untreated samples. Fifty percent inhibition concentration (IC_{50}) values were calculated by GraphPad Prism 7 software (GraphPad). (**B**) Apoptosis of JEKO-1 cells in the same experiment as described in A were assessed by Annexin V/PI staining on day 4. Shown are percentages of Annexin V+/PI+ cells. Line graphs or bar graphs show means of three independent experiments. Error bars, SD. Error bars where not visible fall within the points. ****$P < 0.0001$, ***$P < 0.001$ (two-way ANOVA). *P* values indicate significance levels for the effect of WT or mutants on ibrutinib sensitivity compared to empty vector (EV) control. (**C**) JEKO-1 cells expressing an empty vector (EV), WT, or mutant CCND1-HA were treated with 10 μM of ibrutinib for indicated times and 10 μg of cell lysates per lane were prepared for immunoblotting with indicated antibodies. Arrow, CCND1-HA protein. Arrowhead, endogenous CCND1. Bar graphs below the blot show relative densitometric values of indicated bands after normalization to time zero control samples.

sample size. However, there was a significant difference in response to ibrutinib between samples with different CCND1 protein stability. These results indicate that *CCND1* mutations or other mechanisms that increase CCND1 protein stability and/or levels contribute to the resistance of MCL tumors to ibrutinib.

DISCUSSION

High-throughput sequencing of the MCL genome has consistently revealed *CCND1* as the second most frequently mutated gene after the ataxia telangiectasia mutated (ATM) gene [23–25]. We found that these

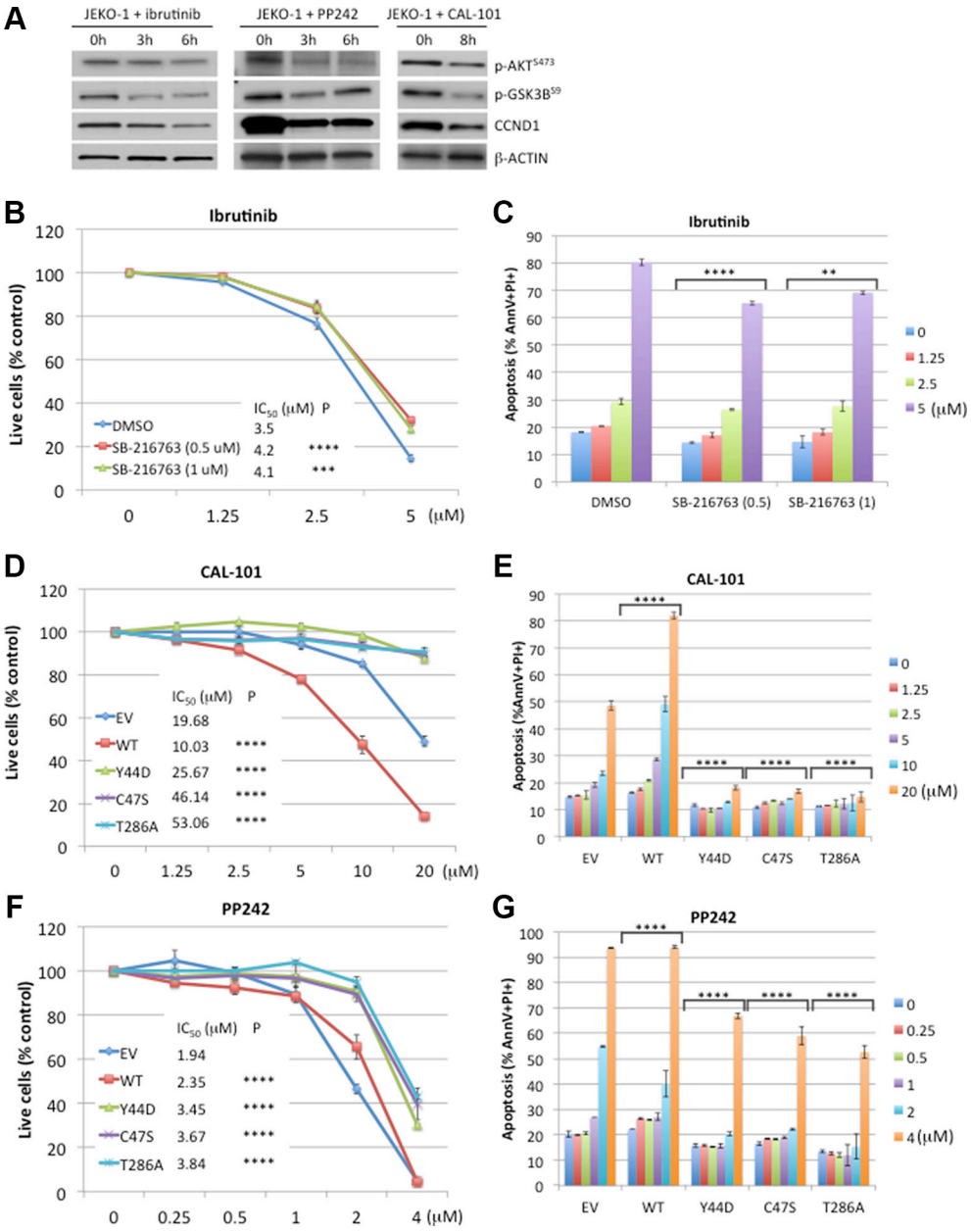

Figure 5: *CCND1* mutations promote resistance to CAL-101 and PP242. (**A**) Immunoblot analysis of JEKO-1 cells treated with ibrutinib (10 μM), PP242 (4 μM) or CAL-101 (10 μM) for indicated times and immunoblotted (30 μg of lysate per lane) with indicated antibodies. (**B**, **C**). SB-216763 rescues ibrutinib toxicity. JEKO-1 cells were co-treated with indicated doses of ibrutinib and 0.5 μM or 1 μM of SB-216763. Viable, PI-negative cells (B) or apoptotic cells (C) were assessed by flow cytometry on day 4. (**D**–**G**) JEKO-1 cells expressing an empty vector (EV), WT, or mutant CCND1-HA were treated with indicated doses of CAL-101 (D, E) or PP242 (F, G) and live cells (D, F) or apoptotic cells (E, G) were analyzed by flow cytometry on day 4. Shown in line graphs are PI negative fractions normalized to control untreated samples. Line graphs or bar graphs show means of three independent experiments. Error bars, SD. Error bars where not visible fall within the points. ****$P < 0.0001$, ***$P < 0.001$, **$P < 0.01$ (two-way ANOVA). *P* values indicate significance levels for the effect of SB-216763 (B, C), compared to DMSO, or of WT and mutants (D–G), compared to empty vector (EV) control, on sensitivity to increasing concentrations of the indicated drugs.

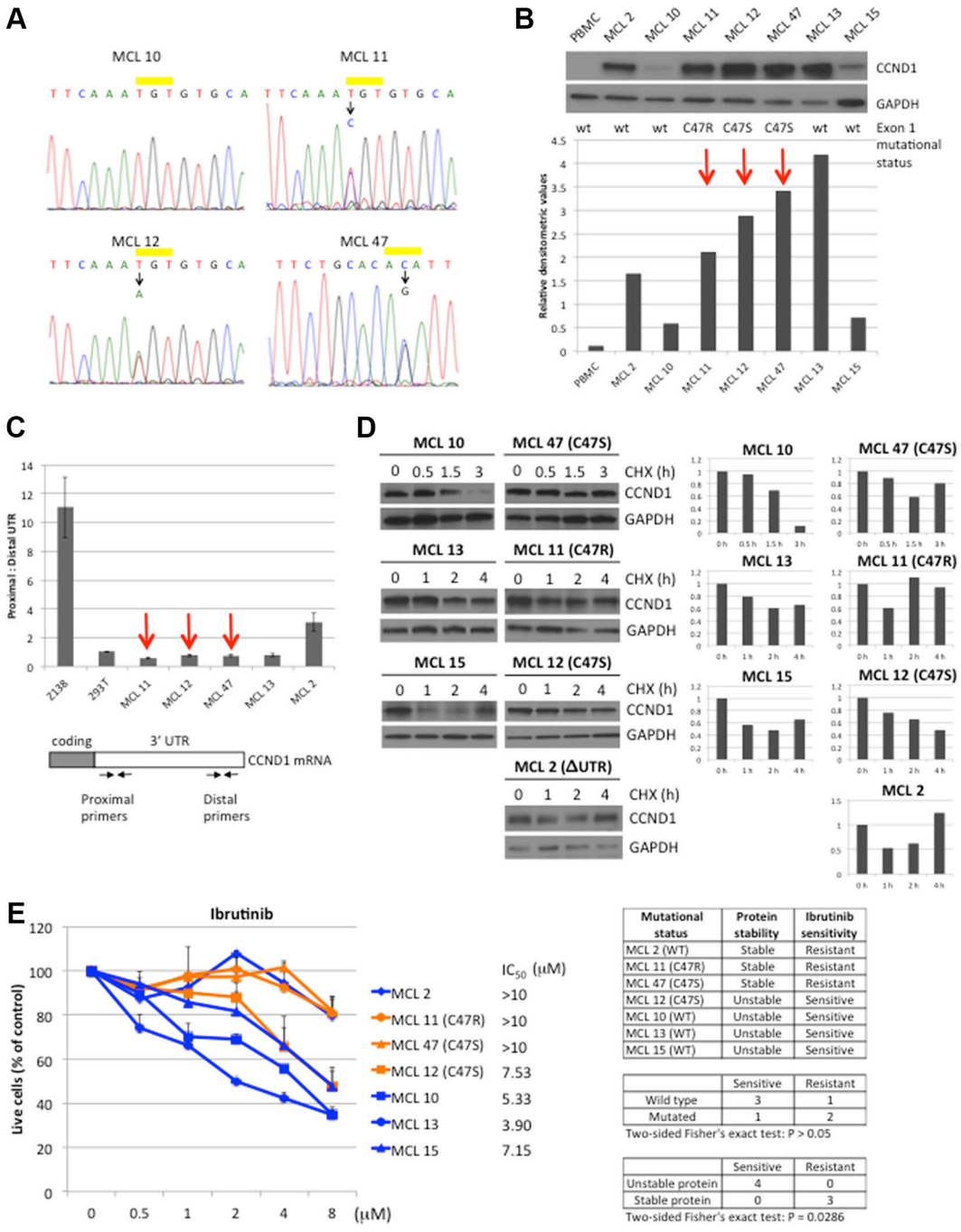

Mutational status	Protein stability	Ibrutinib sensitivity
MCL 2 (WT)	Stable	Resistant
MCL 11 (C47R)	Stable	Resistant
MCL 47 (C47S)	Stable	Resistant
MCL 12 (C47S)	Unstable	Sensitive
MCL 10 (WT)	Unstable	Sensitive
MCL 13 (WT)	Unstable	Sensitive
MCL 15 (WT)	Unstable	Sensitive

	Sensitive	Resistant
Wild type	3	1
Mutated	1	2

Two-sided Fisher's exact test: P > 0.05

	Sensitive	Resistant
Unstable protein	4	0
Stable protein	0	3

Two-sided Fisher's exact test: P = 0.0286

Figure 6: *CCND1* mutations in primary MCL. (**A**) Sequencing chromatograms of CCND1 point mutations in MCL samples. WT and mutated CCND1 alleles on residue cysteine-47 (yellow bar) from MCL tumors 10, 11, 12 and 47 are shown. For MCL 47, complementary sequence from the reverse primer is shown. (**B**) CCND1 expression in MCL tumors. Lysates (10 μg per lane) from indicated MCL tumors were immunoblotted with indicated antibodies. Peripheral blood mononuclear cells (PBMC) were used as negative control for CCND1 expression. Bar graphs show relative densitometric values of CCND1 expression from the immunoblot after normalization to GAPDH loading control. Red arrows highlight the *CCND1* mutated samples. (**C**) Analysis of *CCND1* truncated 3′UTR transcript in MCL tumors. The relative abundance between the full-length and truncated 3′UTR was determined by using proximal and distal primers (see primer locations in the diagram of the *CCND1* mRNA transcript). (**D**) CCND1 stability in MCL tumors. Indicated MCL tumors were treated with 10 μM of cyclohexamide (CHX) for indicated times and 10 μg of cell lysates were prepared for immunoblot analysis with indicated antibodies. Bar graphs show relative densitometric values of CCND1 expression from corresponding blots after normalization to GAPDH. (**E**) Sensitivity of MCL tumors to ibrutinib. Indicated MCL tumors were treated with indicated doses of ibrutinib for three days and metabolically active cells were assessed by CellTiter-Glo Luminescent assay (Promega). Shown are fractions of luminescence signals from metabolically active cells normalized to untreated samples. Line graphs show mean values from three independent experiments. Error bars, S.E.M. IC_{50} values were calculated by GraphPad Prism 7 software. The table summarizes the ibrutinib response with respect to *CCND1* mutation status or protein stability. Correlation of either mutation status or protein stability with ibrutinib sensitivity was analyzed by the two-sided Fisher's exact test.

recurrent mutations, which are located in the N-terminus of CCND1, interfere with T286 phosphorylation, leading to deregulated CCND1 turnover and increased protein levels. In addition, these mutations increased the resistance of MCL to ibrutinib, highlighting their relevance to this emerging therapy.

Many lines of evidence suggest that CCND1 translocation alone is not sufficient and additional genetic lesions are required for MCL development. For example, the Emu-CCND1 transgenic mouse, which mimics the t(11;14) translocation, developed lymphoma only after crossing with transgenic mice that expressed an established oncogene such as *MYC* [35, 36]. Alternatively, B-cell lymphoma also developed when crossing the Emu-CCND1 mouse with transgenic mice that had other genetic aberrations observed in MCL, such as BIM-deficient [37] or ATM-deficient mice [38]. Interestingly, the Emu-T286A CCND1 transgenic mice, which constitutively expressed nuclear mutant CCND1, developed lymphoma without introducing a second genetic hit [13]. Although the B-cell lymphomas that developed in these mice had a mature B-cell phenotype like human MCL, the T286A mutation has been observed only rarely in MCL and whether this mouse model recapitulates human MCL remains uncertain. Our data demonstrate that N-terminal *CCND1* mutations interfere with T286 phosphorylation and promote CCND1 nuclear localization, which are reminiscent of the T286A CCND1 mutant phenotype. The frequent occurrence of these N-terminal *CCND1* mutations indicates that defective T286 phosphorylation may be more common in MCL than previously thought. Our findings thus support the oncogenic role of defective T286 phosphorylation, as postulated by Diehl and colleagues [39].

How do N-terminal CCND1 mutations affect the C-terminal T286 phosphorylation? Our initial hypothesis was that these mutations may affect docking of GSK3B and, thus, subsequent phosphorylation. Although co-IP experiments using an anti-HA antibody showed less binding of GSK3B to Y44D and C47S mutants, reverse co-IP experiments using anti-GSK3B antibody did not confirm this result. In contrast, GSK3B pull-down showed little effect of Y44D or C47S mutants on interaction with GSK3B. An important clue from this apparent discrepancy between the forward and reverse IP experiments was the absence of GSK3B signals in the T286A-HA pull-down (Figure 2D). However, T286A-HA signals were readily detectable in the immunoprecipitates of GSK3B pull-down, which confirmed GSK3B-T286-HA interaction (Figure 2E). These observations indicate that, unlike in the WT CCND1-HA pull-down, the anti-HA antibody did not recognize the C-terminally tagged HA epitope of the T286A mutant in the complex with GSK3B. Therefore, we speculate that reduced GSK3B signals in the immunoprecipitates of Y44D or C47S pull-down, as compared to WT, may be due to reduced binding of the anti-HA antibody to the C-terminally tagged HA epitope in these mutants. Re-cloning of CCND1 constructs with N-terminally tagged HA is, therefore, necessary to test this possibility and to clarify whether CCND1 mutations affect GSK3B docking.

Despite the efficacy of ibrutinib in MCL, one-third of the patients do not respond to this therapy and acquired resistance to this drug is almost universal [17, 40]. A better understanding of why some patients respond well, but others do not, is needed. Sustained PI3K/AKT signaling or increased activation of the alternative NF-kB pathway have been proposed as potential mechanisms that may compensate for the BCR—BTK—NF-kB axis, which is targeted by ibrutinib [19, 20]. Similar to agents that target AKT signaling (such as CAL-101 and PP242), ibrutinib can also inhibit AKT activity, leading to activation of GSK3B and increased phosphorylation-dependent proteolysis of CCND1. The N-terminal CCND1 mutations that increase protein stability by evading GSK3B-mediated phosphorylation provide another distinct mechanism of resistance to such therapies.

Two out of three MCL tumors with mutated *CCND1* were resistant to ibrutinib. However, sample MCL 12, which also carried the C47S mutation, was sensitive to this drug. The mutant CCND1 protein in this sample appeared less stable than CCND1 with the same mutation from sample MCL 47, as revealed by the CHX experiments (Figure 6D). In addition, although *in vitro* overexpression of C47S CCND1 was sufficient to confer ibrutinib resistance in JEKO-1 cells, protection from ibrutinib toxicity was less robust than the Y44D mutation. These observations suggest that *CCND1* mutations may provide different levels of protection from ibrutinib toxicity, depending on the cellular context and tumor heterogeneity. Conversely, sample MCL 2 had WT *CCND1* but was resistant to ibrutinib. Interestingly, this sample displayed more stable CCND1 protein, suggesting other mechanisms that may contribute to CCND1 stability in addition to the N-terminus point mutations. Because of the small sample size in the present study, further validation of our findings in more MCL tumors will be required to confirm the correlation between *CCND1* mutations and ibrutinib resistance.

In summary, these findings uncovered residues previously not known to play a role in the regulation of CCND1 turnover. Our data demonstrate that single N-terminal CCND1 mutations stabilize and increase protein levels, which contributes to ibrutinib resistance. This study suggests that *CCND1* mutations may be a useful biomarker for ibrutinib insensitivity. Further studies using a larger sample size are needed to evaluate this potential clinical utility.

MATERIALS AND METHODS

Cell lines and culture conditions

Human MCL lines UPN-1, Z-138 and JEKO-1 were kindly provided by Dr. Louis Staudt. UPN-1 cells were

confirmed to carry the cyclinD1/IGH fusion gene and other chromosomal rearrangements, as previously described [41], by metaphase fluorescence *in situ* hybridization (FISH) analysis (data not shown). Z-138 cells were confirmed to express truncated CCND1 3′UTR transcripts as described [10] (Figure 6C). JEKO-1 cells were not authenticated. Cells were cultured in RPMI-1640 medium (Life Technologies, Grand Island, NY) supplemented with 10% fetal bovine serum and penicillin/streptomycin and maintained in a humidified, 5% CO2 incubator at 37°C.

Primary MCL preparation

Viably cryo-preserved MCL cells were obtained from the tumor bank of the Pathology Department of City of Hope as de-identified samples after approval by the Institutional Review Board. Frozen cells were briefly thawed in 37°C water bath, washed in RPMI-1640 medium and cultured in RPMI-1640 medium supplemented with 20% fetal bovine serum and 200 Kunits/ml of DNAse I (Sigma, St. Louis, MO) for 15 minutes in 37°C CO2 incubator followed by washing. Cells were recovered overnight in CO2 incubator before experiments.

Antibodies and chemicals

The following antibodies were used: HA (C29F4), Histone H3, pCCND1-T286 (D29B3), GSK3B (D5C5Z), pS9-GSK3B and p-AKT S473 (Cell Signaling Technology, Danvers, MA), CDK4, CCND1(M20), ACTIN, GAPDH, (Santa Cruz, Dallas, TX), The following chemicals were used: cyclohexamide, Lithium chloride (LiCl) (Sigma, St. Louis, MO) SB-216763, CAL-101, PP242, PS-341 (Selleck Chemicals, Houston, TX). Ibrutinib was obtained from commercial sources (Selleck Chemicals or MedKoo Biosciences, Inc. Chapel Hill, NC) or from Craig Thomas (NCI, Bethesda, MD) as a gift. Ibrutinib from these sources was confirmed to have similar killing activity on JEKO-1 cells (data not shown).

Expression vectors

The retroviral expression vector pBMN-CCND1-HA-IRES-Hygro, encoding carboxy-terminus HA-tagged CCND1, was constructed by ligation of PCR-generated CCND1-HA products from the plasmid pRc/CMV-Cyclin D1 HA (Addgene plasmid # 8948, a gift from Philip Hinds) into the pBMN-IRES-Hygro vector (a gift from Gary Nolan) at XhoI and NotI restriction sites. CCND1-HA PCR products were generated using the following primer pairs: 5′ TAGTAGctcgagGCCG CCACCATGGAACACCAGCTCCTGTGC and 5′ CT ACTAGCGGCCGCTCAGATATCGGCGTAGTC. E36K, Y44D and C47S *CCND1* mutations were generated by the Quickchange Site-directed mutagenesis kit (Stratagene, La Jolla, CA) using the plasmid template pBMN-CCND1-HA-IRES-Hygro and primers as follows. E36K forward: 5′ P-ATGCTGAAGGCGGAGAAGACC TGCGCGCCCT, E36K reverse: 5′ P-GGCCCGCAGCAC CCGGTCGT, Y44D forward: 5′ P-GCGCCCTCGGTGT CCGACTTCAAATGTGTGC, Y44D reverse: 5′ P-GCA GGTCTCCTCCGCCTTCAGCAT, C47S forward: 5′ P-G TGTCCTACTTCAAATCTGTGCAGAAGGAGGT, C47S reverse: 5′ P-CGAGGGCGCGCAGGTCTCCTCCG. Mutations were confirmed by DNA sequencing. T286 *CCND1* mutation was derived from the plasmid pcDNA cyclin D1 HA T286A (Addgene plasmid #11182, a gift from Bruce Zetter) and subcloned into the pBMN-IRES-Hygro vector as described above.

DNA transfection and retroviral transduction

DNA transfection was performed by mixing DNA with Lipofectamine2000 (Life Technologies, Grand Island, NY) and following the manufacturer's instructions. For retroviral transduction, a retroviral vector and a mixture of helper plasmids for viral envelope and *gag*/*pol* were transfected into HEK293T cells using Lipofectamine 2000. Retroviral supernatants were harvested 48 hours after transfection and were used to transduce ecotropic receptor-expressing target cells by centrifugation at 1200 × g for one hour in 4 μg/ml polybrene.

Quantitative real-time PCR

SYBR® Green-based quantitative real-time PCR was performed using RT² SYBRÒ Green qPCR Mastermix (Qiagen, Valencia, CA) and a StepOnePlus Real-time PCR system (Life Technologies, Grand Island, NY). The following probes were used: CCND1 forward primer: 5′ CGAGGAGGAGGAAGAGGAG. HA reverse primer: 5′ GTAGTCCGGGACGTCGTA. GAPDH forward primer: 5′ AAGGGCTCATGACCACAGTC. GAPDH reverse primer: 5′ GGATGACCTTGCCCACAG. Relative mRNA expression was normalized to GAPDH signals and calculated using the ddCt method. Proximal and distal CCND1 UTR primers have been described previously [10]. BTK gene knockdown experiments using a previously validated shRNA sequence [42] (GCACAAACTCTCCTACTATGA) were analyzed by the StepOnePlus Real-time PCR system using the Applied Biosystems probe BTK (Hs00975865_m1) and GAPDH (Hs02758991_g1).

Immunoblot and immunoprecipitation analyses

Cells were lysed in the presence of protease inhibitor cocktail (Sigma, St. Louis, MO) and Halt phosphatase inhibitor cocktail (Pierce Biotechnology, Rockford, IL) for 30 min. Lysates were cleared by centrifugation and protein concentrations were determined by BCA protein assay (Pierce Biotechnology, Rockford, IL).

Ten or 30 µg of lysates per lane were separated by 4–15% SDS-PAGE and immobilized on the nitrocellulose membranes (ThermoFisher, Waltham, MA) for immunoblotting. Immunoblot signals were developed by a chemiluminescent detection method (Pierce Biotechnology, Rockford, IL) and captured by standard autoradiographic films. Signal intensities were quantitated using the NIH Image J software (imagej.nih.gov).

For immunoprecipitation, cells were lysed at 4×10^7 cells/ml in IP buffer from Pierce Biotechnology (25 mM Tris•HCl pH 7.4, 150 mM NaCl, 1% NP-40, 1 mM EDTA, 5% glycerol), in presence of 1 mM PMSF, 10 mM glycerophosphate, 1× concentration of Protease and Halt Phosphatase cocktail inhibitors for 30 min on ice. Lysates were cleared by centrifuging for 15 minutes at 14,000 × g at 4°C. Five µg of IgG1 isotype control was mixed with 50 µl of 1:1 slurry of PBS and protein A agarose beads and the mixture was added to 1 ml of lysate followed by one-hour incubation on a rotating mixer at 4°C. Lysates were cleared again by centrifugation for one minute at 2400 × g at 4°C. Supernatants were quantified for protein concentrations using the BCA protein assay. Approximately, 1.5 mg of lysate from each sample was incubated with 40 µl of 1:1 slurry of PBS and HA antibody (IgG1)-conjugated agarose beads (Sigma, St. Louis, MO) overnight on a rotating mixer at 4°C. Agarose beads were washed 4 times in 1 ml of PBS containing 0.5% NP40 for 10 min each and pelleted by centrifugation at 2400 × g for 5 min. After discarding the supernatant, washed agarose beads were suspended in 100 µl of 1× sample buffer containing 5 µl of beta-mercaptoethanol and heat denatured for 5 min at 95°C. Samples were separated on 10% polyacrylamide gels and transferred to nitrocellulose membranes for western blot analysis.

For IP of Ub-conjugated CCND1, cells were harvested, washed twice with cold PBS, and lysed in 2% sodium dodecyl sulfate (SDS), 150 mM NaCl, 10 mM Tris-HCl pH 8.0, and protease inhibitors at 95°C for 5 min then kept on ice for 10 min, as previously described [43]. The lysate was then diluted in IP buffer containing protease and phosphatase inhibitors at ratio 1:10 and incubated on ice for 30 min. Lysates were cleared by centrifuging for 15 min at 14,000 × g at 4°C and used for immunoprecipitation as described above.

Cell fractionation

Nine million cells were harvested and divided into two parts: 1 million cells were used for whole cell lysate and 8 million cells were used for fractionation. Cells were washed twice in PBS and treated with 250 µl of the Harvest buffer (10 mM HEPES pH 7.9, 50 mM NaCI, 0.5 M sucrose, 0.1 mM EDTA, 0.5% Triton X-100, with freshly added 1 mM DTT, protease and phosphatase inhibitors) for 5 min on ice. Lysates were cleared by centrifugation at 720 × g for 10 min in swinging bucket rotor at 4°C. Supernatants were transferred to new tubes, cleared by centrifugation at 14,000 × g for 15 min at 4°C and used as cytoplasmic fractions. The pellets from Harvest Buffer treatment were washed 2 to 3 times in 500 µl of Buffer A (10 mM HEPES pH 7.9, 10 mM KCI, 0.1 mM EDTA, 0.1 mM EGTA, and freshly added 1 mM DTT, protease and phosphatase inhibitors). Final pellets were lysed for 15 min at 4°C in Buffer B (10 mM HEPES pH 7.9, 500 mM NaCI, 0.1 mM EDTA, 0.1 mM EGTA, 0.1% NP-40, and freshly added 1 mM DTT, protease and phosphatase inhibitors). Pellets were sonicated and centrifuged for 15 min at 14,000 × g. Supernatants were used as nuclear fractions.

Immunofluorescence

HEK-293T cells expressing WT or mutant CCND1-HA proteins were seeded at a density of 0.5×10^6 cells/ml on a glass bottom 35 mm dish for 2 days. Cells were washed with PBS twice and fixed with 4% paraformaldehyde for 30 min at RT. Fixed cells were blocked with 5% BSA and 0.5% TritonX-100 in phosphate buffered saline (PBS) for 30 min at RT. Cells were then stained with anti-HA antibody for overnight at 4°C in a humidified chamber, followed by staining with fluorescently labeled secondary antibodies and nuclear staining with 4′,6-diamidino-2-phenylindole (DAPI) (Life Technologies, Grand Island, NY). Cells were observed using a confocal microscope (Inverted LSM510 Meta 2-Photon Microscope, Zeiss) with a 63X objective. Images were captured and analyzed using Zen Imaging Software (ZEISS USA, Dublin CA).

Viability and apoptosis measurements

Cell viability was assessed either by using the CellTiter-Glo Luminescent assay (Promega, Madison, WI) following instructions by the manufacturer or by flow cytometric analysis for propidium iodide negative population. Apoptosis was measured by Annexin V-based methods using Annexin V Apoptosis Detection Kit (eBioscience, Inc., San Diego, CA).

Sanger sequencing

Analysis of *CCND1* exon 1 by Sanger sequencing was performed using the CCND1 primers and method as described [23].

ACKNOWLEDGMENTS

We thank Drs. John Chan for helpful discussion and Craig Thomas for research reagents.

CONFLICTS OF INTEREST

No potential conflicts of interest were disclosed by all authors.

GRANT SUPPORT

This work was supported in part by the National Cancer Institute of the National Institutes of Health under grant number P30CA033572. D.D.W is supported by NIH/NCI grant 5U01CA62505-19. V.N.N. is supported by the American Hematology Society and the Gabrielle's Angel Foundation for Cancer Research.

REFERENCES

1. Matsushime H, Roussel MF, Ashmun RA, Sherr CJ. Colony-stimulating factor 1 regulates novel cyclins during the G1 phase of the cell cycle. Cell. 1991; 65:701–713.
2. Kato J, Matsushime H, Hiebert SW, Ewen ME, Sherr CJ. Direct binding of cyclin D to the retinoblastoma gene product (pRb) and pRb phosphorylation by the cyclin D-dependent kinase CDK4. Genes Dev. 1993; 7:331–342.
3. Lukas J, Pagano M, Staskova Z, Draetta G, Bartek J. Cyclin D1 protein oscillates and is essential for cell cycle progression in human tumour cell lines. Oncogene. 1994; 9:707–718.
4. Diehl JA, Cheng M, Roussel MF, Sherr CJ. Glycogen synthase kinase-3beta regulates cyclin D1 proteolysis and subcellular localization. Genes Dev. 1998; 12:3499–3511.
5. Diehl JA, Zindy F, Sherr CJ. Inhibition of cyclin D1 phosphorylation on threonine-286 prevents its rapid degradation via the ubiquitin-proteasome pathway. Genes Dev. 1997; 11:957–972.
6. Zou Y, Ewton DZ, Deng X, Mercer SE, Friedman E. Mirk/dyrk1B kinase destabilizes cyclin D1 by phosphorylation at threonine 288. J Biol Chem. 2004; 279:27790–27798.
7. Casanovas O, Miro F, Estanyol JM, Itarte E, Agell N, Bachs O. Osmotic stress regulates the stability of cyclin D1 in a p38SAPK2-dependent manner. J Biol Chem. 2000; 275:35091–35097.
8. Williams ME, Meeker TC, Swerdlow SH. Rearrangement of the chromosome 11 bcl-1 locus in centrocytic lymphoma: analysis with multiple breakpoint probes. Blood. 1991; 78:493–498.
9. Raffeld M, Jaffe ES. bcl-1, t(11;14), and mantle cell-derived lymphomas. Blood. 1991; 78:259–263.
10. Wiestner A, Tehrani M, Chiorazzi M, Wright G, Gibellini F, Nakayama K, Liu H, Rosenwald A, Muller-Hermelink HK, Ott G, Chan WC, Greiner TC, Weisenburger DD, et al. Point mutations and genomic deletions in CCND1 create stable truncated cyclin D1 mRNAs that are associated with increased proliferation rate and shorter survival. Blood. 2007; 109:4599–4606.
11. Deshpande A, Pastore A, Deshpande AJ, Zimmermann Y, Hutter G, Weinkauf M, Buske C, Hiddemann W, Dreyling M. 3′UTR mediated regulation of the cyclin D1 proto-oncogene. Cell Cycle. 2009; 8:3584–3592.
12. Lu F, Gladden AB, Diehl JA. An alternatively spliced cyclin D1 isoform, cyclin D1b, is a nuclear oncogene. Cancer Res. 2003; 63:7056–7061.
13. Gladden AB, Woolery R, Aggarwal P, Wasik MA, Diehl JA. Expression of constitutively nuclear cyclin D1 in murine lymphocytes induces B-cell lymphoma. Oncogene. 2006; 25:998–1007.
14. Dal Col J, Zancai P, Terrin L, Guidoboni M, Ponzoni M, Pavan A, Spina M, Bergamin S, Rizzo S, Tirelli U, De Rossi A, Doglioni C, Dolcetti R. Distinct functional significance of Akt and mTOR constitutive activation in mantle cell lymphoma. Blood. 2008; 111:5142–5151.
15. Jares P, Colomer D, Campo E. Genetic and molecular pathogenesis of mantle cell lymphoma: perspectives for new targeted therapeutics. Nat Rev Cancer. 2007; 7:750–762.
16. Perez-Galan P, Dreyling M, Wiestner A. Mantle cell lymphoma: biology, pathogenesis, and the molecular basis of treatment in the genomic era. Blood. 2011; 117:26–38.
17. Wang ML, Rule S, Martin P, Goy A, Auer R, Kahl BS, Jurczak W, Advani RH, Romaguera JE, Williams ME, Barrientos JC, Chmielowska E, Radford J, et al. Targeting BTK with ibrutinib in relapsed or refractory mantle-cell lymphoma. N Engl J Med. 2013; 369:507–516.
18. Chiron D, Di Liberto M, Martin P, Huang X, Sharman J, Blecua P, Mathew S, Vijay P, Eng K, Ali S, Johnson A, Chang B, Ely S, et al. Cell-cycle reprogramming for PI3K inhibition overrides a relapse-specific C481S BTK mutation revealed by longitudinal functional genomics in mantle cell lymphoma. Cancer discovery. 2014; 4:1022–1035.
19. Rahal R, Frick M, Romero R, Korn JM, Kridel R, Chan FC, Meissner B, Bhang HE, Ruddy D, Kauffmann A, Farsidjani A, Derti A, Rakiec D, et al. Pharmacological and genomic profiling identifies NF-kappaB-targeted treatment strategies for mantle cell lymphoma. Nature medicine. 2014; 20:87–92.
20. Ma J, Lu P, Guo A, Cheng S, Zong H, Martin P, Coleman M, Wang YL. Characterization of ibrutinib-sensitive and -resistant mantle lymphoma cells. Br J Haematol. 2014; 166:849–861.
21. Furman RR, Cheng S, Lu P, Setty M, Perez AR, Guo A, Racchumi J, Xu G, Wu H, Ma J, Steggerda SM, Coleman M, Leslie C, et al. Ibrutinib resistance in chronic lymphocytic leukemia. N Engl J Med. 2014; 370:2352–2354.
22. Woyach JA, Furman RR, Liu TM, Ozer HG, Zapatka M, Ruppert AS, Xue L, Li DH, Steggerda SM, Versele M, Dave SS, Zhang J, Yilmaz AS, et al. Resistance mechanisms for the Bruton's tyrosine kinase inhibitor ibrutinib. N Engl J Med. 2014; 370:2286–2294.
23. Kridel R, Meissner B, Rogic S, Boyle M, Telenius A, Woolcock B, Gunawardana J, Jenkins C, Cochrane C,

Ben-Neriah S, Tan K, Morin RD, Opat S, et al. Whole transcriptome sequencing reveals recurrent NOTCH1 mutations in mantle cell lymphoma. Blood. 2012; 119:1963–1971.

24. Bea S, Valdes-Mas R, Navarro A, Salaverria I, Martin-Garcia D, Jares P, Gine E, Pinyol M, Royo C, Nadeu F, Conde L, Juan M, Clot G, et al. Landscape of somatic mutations and clonal evolution in mantle cell lymphoma. Proc Natl Acad Sci U S A. 2013; 110:18250–18255.
25. Zhang J, Jima D, Moffitt AB, Liu Q, Czader M, Hsi ED, Fedoriw Y, Dunphy CH, Richards KL, Gill JI, Sun Z, Love C, Scotland P, et al. The genomic landscape of mantle cell lymphoma is related to the epigenetically determined chromatin state of normal B cells. Blood. 2014; 123:2988–2996.
26. Weinstein S, Emmanuel R, Jacobi AM, Abraham A, Behlke MA, Sprague AG, Novobrantseva TI, Nagler A, Peer D. RNA inhibition highlights cyclin D1 as a potential therapeutic target for mantle cell lymphoma. PLoS One. 2012; 7:e43343.
27. Mohanty S, Mohanty A, Sandoval N, Tran T, Bedell V, Wu J, Scuto A, Murata-Collins J, Weisenburger DD, Ngo VN. Cyclin D1 depletion induces DNA damage in mantle cell lymphoma lines. Leuk Lymphoma. 2016:1–13.
28. Sutherland C, Leighton IA, Cohen P. Inactivation of glycogen synthase kinase-3 beta by phosphorylation: new kinase connections in insulin and growth-factor signalling. The Biochemical journal. 1993; 296 (Pt 1):15–19.
29. Stambolic V, Woodgett JR. Mitogen inactivation of glycogen synthase kinase-3 beta in intact cells via serine 9 phosphorylation. The Biochemical journal. 1994; 303:701–704.
30. Cross DA, Alessi DR, Cohen P, Andjelkovich M, Hemmings BA. Inhibition of glycogen synthase kinase-3 by insulin mediated by protein kinase B. Nature. 1995; 378:785–789.
31. Coghlan MP, Culbert AA, Cross DA, Corcoran SL, Yates JW, Pearce NJ, Rausch OL, Murphy GJ, Carter PS, Roxbee Cox L, Mills D, Brown MJ, Haigh D, et al. Selective small molecule inhibitors of glycogen synthase kinase-3 modulate glycogen metabolism and gene transcription. Chemistry & biology. 2000; 7:793–803.
32. Stambolic V, Ruel L, Woodgett JR. Lithium inhibits glycogen synthase kinase-3 activity and mimics wingless signalling in intact cells. Current biology. 1996; 6:1664–1668.
33. Lannutti BJ, Meadows SA, Herman SE, Kashishian A, Steiner B, Johnson AJ, Byrd JC, Tyner JW, Loriaux MM, Deininger M, Druker BJ, Puri KD, Ulrich RG, et al. CAL-101, a p110delta selective phosphatidylinositol-3-kinase inhibitor for the treatment of B-cell malignancies, inhibits PI3K signaling and cellular viability. Blood. 2011; 117:591–594.
34. Zeng Z, Shi YX, Tsao T, Qiu Y, Kornblau SM, Baggerly KA, Liu W, Jessen K, Liu Y, Kantarjian H, Rommel C, Fruman DA, Andreeff M, et al. Targeting of mTORC1/2 by the mTOR kinase inhibitor PP242 induces apoptosis in AML cells under conditions mimicking the bone marrow microenvironment. Blood. 2012; 120:2679–2689.
35. Bodrug SE, Warner BJ, Bath ML, Lindeman GJ, Harris AW, Adams JM. Cyclin D1 transgene impedes lymphocyte maturation and collaborates in lymphomagenesis with the myc gene. EMBO J. 1994; 13:2124–2130.
36. Lovec H, Grzeschiczek A, Kowalski MB, Moroy T. Cyclin D1/bcl-1 cooperates with myc genes in the generation of B-cell lymphoma in transgenic mice. EMBO J. 1994; 13:3487–3495.
37. Katz SG, Labelle JL, Meng H, Valeriano RP, Fisher JK, Sun H, Rodig SJ, Kleinstein SH, Walensky LD. Mantle cell lymphoma in cyclin D1 transgenic mice with Bim-deficient B cells. Blood. 2014; 123:884–893.
38. Yamamoto K, Lee BJ, Li C, Dubois RL, Hobeika E, Bhagat G, Zha S. Early B-cell-specific inactivation of ATM synergizes with ectopic CyclinD1 expression to promote pre-germinal center B-cell lymphomas in mice. Leukemia. 2015; 29:1414–1424.
39. Alt JR, Cleveland JL, Hannink M, Diehl JA. Phosphorylation-dependent regulation of cyclin D1 nuclear export and cyclin D1-dependent cellular transformation. Genes Dev. 2000; 14:3102–3114.
40. Martin P, Maddocks K, Leonard JP, Ruan J, Goy A, Wagner-Johnston N, Rule S, Advani R, Iberri D, Phillips T, Spurgeon S, Kozin E, Noto K, et al. Postibrutinib outcomes in patients with mantle cell lymphoma. Blood. 2016; 127:1559–1563.
41. M'Kacher R, Farace F, Bennaceur-Griscelli A, Violot D, Clausse B, Dossou J, Valent A, Parmentier C, Ribrag V, Bosq J, Carde P, Turhan AG, Bernheim A. Blastoid mantle cell lymphoma: evidence for nonrandom cytogenetic abnormalities additional to t(11;14) and generation of a mouse model. Cancer genetics and cytogenetics. 2003; 143:32–38.
42. Davis RE, Ngo VN, Lenz G, Tolar P, Young RM, Romesser PB, Kohlhammer H, Lamy L, Zhao H, Yang Y, Xu W, Shaffer AL, Wright G, et al. Chronic active B-cell-receptor signalling in diffuse large B-cell lymphoma. Nature. 2010; 463:88–92.
43. Choo YS, Zhang Z. Detection of protein ubiquitination. Journal of visualized experiments. 2009.

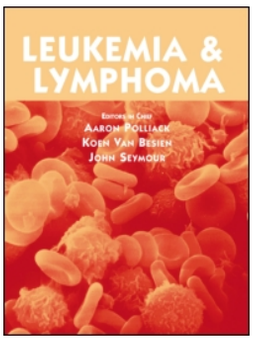

Leukemia & Lymphoma

ISSN: 1042-8194 (Print) 1029-2403 (Online) Journal homepage: http://www.tandfonline.com/loi/ilal20

Cyclin D1 depletion induces DNA damage in mantle cell lymphoma lines

Suchismita Mohanty, Atish Mohanty, Natalie Sandoval, Thai Tran, Victoria Bedell, Jun Wu, Anna Scuto, Joyce Murata-Collins, Dennis D. Weisenburger & Vu N. Ngo

To cite this article: Suchismita Mohanty, Atish Mohanty, Natalie Sandoval, Thai Tran, Victoria Bedell, Jun Wu, Anna Scuto, Joyce Murata-Collins, Dennis D. Weisenburger & Vu N. Ngo (2017) Cyclin D1 depletion induces DNA damage in mantle cell lymphoma lines, Leukemia & Lymphoma, 58:3, 676-688, DOI: 10.1080/10428194.2016.1198958

To link to this article: https://doi.org/10.1080/10428194.2016.1198958

LEUKEMIA & LYMPHOMA, 2017
VOL. 58, NO. 3, 676–688
http://dx.doi.org/10.1080/10428194.2016.1198958

Taylor & Francis
Taylor & Francis Group

ORIGINAL ARTICLE: RESEARCH

Cyclin D1 depletion induces DNA damage in mantle cell lymphoma lines

Suchismita Mohanty[a*], Atish Mohanty[a*], Natalie Sandoval[a], Thai Tran[b], Victoria Bedell[c], Jun Wu[d], Anna Scuto[c], Joyce Murata-Collins[c], Dennis D. Weisenburger[c] and Vu N. Ngo[a]

[a]Division of Hematopoietic Stem Cell and Leukemia Research, Beckman Research Institute, Duarte, CA, USA; [b]Irell & Manella Graduate School of Biological Sciences, Duarte, CA, USA; [c]Department of Pathology, City of Hope National Medical Center, Duarte, CA, USA; [d]Animal Resource Center, Beckman Research Institute of City of Hope, Duarte, CA, USA

ABSTRACT

Elevated cyclin D1 (CCND1) expression levels in mantle cell lymphoma (MCL) are associated with aggressive clinical manifestations related to chemoresistance, but little is known about how this important proto-oncogene contributes to the resistance of MCL. Here, we showed that RNA interference-mediated depletion of CCND1 increased caspase-3 activities and induced apoptosis in the human MCL lines UPN-1 and JEKO-1. *In vitro* and xenotransplant studies revealed that the toxic effect of CCND1 depletion in MCL cells was likely due to increase in histone H2AX phosphorylation, a DNA damage marker. DNA fiber analysis suggested deregulated replication initiation after CCND1 depletion as a potential cause of DNA damage. Finally, in contrast to depletion or inhibition of cyclin-dependent kinase 4, CCND1 depletion increased chemosensitivity of MCL cells to replication inhibitors hydroxyurea and cytarabine. Our findings have an important implication for CCND1 as a potential therapeutic target in MCL patients who are refractory to standard chemotherapy.

ARTICLE HISTORY
Received 21 March 2016
Revised 13 May 2016
Accepted 30 May 2016

KEYWORDS
Chemoresistance; cyclin D1; DNA damage; mantle cell lymphoma; replication stress

Introduction

Mantle cell lymphoma (MCL) is an incurable B-cell malignancy that accounts for 6–8% of all non-Hodgkin lymphomas. Most MCL patients respond initially to conventional chemotherapy, but then quickly develop resistance, leading to a median survival of 3–5 years.[1,2] MCL is characterized by the recurrent t(11;14) chromosomal translocation,[3] resulting in CCND1 overexpression. CCND1 binds and activates cyclin-dependent kinase (CDK) 4 or CDK6 to mediate phosphorylation-dependent degradation of the major G1 checkpoint protein retinoblastoma protein (RB) and promote S-phase entry.[4–6] Other D-type cyclins, cyclin D2 (CCND2) and cyclin D3 (CCND3), which also associate with CDK4 and CDK6,[7] are less common in MCL, and their expression are more associated with CCND1 negative cases.[8,9] Salaverria et al.[9] has reported 55% of MCL cases that lacked CCND1 expression had chromosomal rearrangement at the *CCND2* locus. Translocation at the *CCND3* locus has been reported only in one CCND1 negative case [8] and this translocation appear more common in other B-cell lymphomas.[10] While the CDK4/RB-dependent function of CCND1 is important for MCL development, targeting this pathway by inactivating CDK4/6 kinase causes G1 arrest with little cytotoxicity in the lymphoma cells.[11–15]

Overexpression of CCND1 has been shown to correlate with increased chemoresistance and poor survival in many cancers.[16–19] In MCL, Rosenwald et al.[20] demonstrated that elevated CCND1 expression levels are associated with high tumor cell proliferation and aggressive clinical manifestations, likely related to chemoresistance. In another study by Tiemann et al.,[21] the authors showed that depletion of CCND1 using siRNA increased the sensitivity of MCL cell lines to etoposide or doxorubicin. These reports suggest an important role of CCND1 in protecting MCL cells against conventional chemotherapeutic agents, but the mechanisms underlying this function are largely unknown. In this study, we address this question by hypothesizing that CCND1 is essential for genomic stability in MCL tumors. We tested the hypothesis by determining the effects of CCND1 depletion on DNA stability and cellular response to the DNA damaging agents hydroxyurea (HU) or cytarabine in MCL lines

CONTACT Vu N. Ngo vngo@coh.org Division of Hematopoietic Stem Cell and Leukemia Research, Beckman Research Institute, City of Hope, Beckman Center, Room 2312, 1500 E. Duarte Road, Duarte, CA 91010, USA
*These authors contributed equally to this work.

Supplemental data for this article can be accessed here.

and primary MCL cells *in vitro* and in a xenotransplant model.

Materials and methods

Cell lines and culture conditions

Human MCL lines UPN-1 and JEKO-1 were kindly provided by Dr Louis Staudt. The UPN-1 cell line was confirmed to carry the cyclinD1/IGH fusion gene or t(11;14) translocation and other chromosomal rearrangements, as previously described,[22] by metaphase fluorescence *in situ* hybridization (FISH) analysis (Supplementary Figure S1). JEKO-1 cells were previously reported to carry the t(11;14) translocation.[23] Cells were cultured in RPMI-1640 medium (Life Technologies, Grand Island, NY) supplemented with 10% fetal bovine serum and penicillin/streptomycin and maintained in a humidified, 5% CO_2 incubator at 37 °C.

Primary MCL preparation

Viably cryo-preserved MCL cells were obtained from the tumor bank of the Pathology Department of City of Hope as de-identified samples after approval by the Institutional Review Board. Cells were briefly thawed in 37 °C water bath, washed in RPMI-1640 medium and subsequently cultured in RPMI-1640 medium supplemented with 20% fetal bovine serum.

Antibodies and chemicals

The following antibodies were used: pRB-S807/811 (Cell Signaling Technology, Danvers, MA), pRBL2-S672, RBL2 (Abgent, Inc., San Diego, CA), CCND1, CDK4, CDK6, GAPDH, β-ACTIN (Santa Cruz, Dallas, TX), RB (BD Biosciences, San Jose, CA), and γH2AX (Millipore, Billerica, MA). The following chemicals were used: PD-0332991 (Selleck Chemicals, Houston, TX), hydroxyurea, cytarabine, and aphidicolin (Sigma, St. Louis, MO).

RNA interference reagents and siRNA transfection

All shRNA constructs and sequences were obtained from a previously generated shRNA library [24] and listed in Supplementary Table S1. SMARTpool ON-TARGETplus siRNA targeting CCND1 or CDK4 was purchased together with scramble control siRNA from Dharmacon (Dharmacon, Lafayette, CO). Two rounds of siRNA transfection were performed on days 0 and 2 as recommended by the manufacturer.

Western blotting

Cells were lysed in the presence of protease inhibitors (Roche, Basel, Switzerland) and phosphatase inhibitors (Sigma, St. Louis, MO) for 30 min. Lysates were cleared by centrifugation and protein concentrations were determined by BCA protein assay (Life Technologies, Grand Island, NY). About 30–80 μg of lysates were separated by 4–15% SDS–PAGE and immobilized on the nitrocellulose membranes for immunoblotting.

Viability and apoptosis measurements

Cell viability was performed either by using the TC20 Automated Cell Counter (Biorad, Hercules, CA), based on the trypan blue exclusion method, or by a Celltiter-Glo assay (Promega, Madison, WI) following instructions by the manufacturer. To measure apoptosis, cells were stained with anti-active Caspase-3 and anti-cleaved PARP antibodies (BD Biosciences, San Jose, CA) or analyzed by Annexin V-based methods using Annexin V Apoptosis Detection Kit (eBioscience, Inc., San Diego, CA).

Retroviral transduction

A retroviral vector and a mixture of helper plasmids for viral envelope and *gag/pol* were transfected into HEK293T cells using Lipofectamine2000 (Life Technologies, Grand Island, NY). Retroviral supernatants were harvested 48 h after transfection and were used to transduce ecotropic receptor-expressing target cells by centrifugation at 1360*g* for 1 h in 4 μg/ml polybrene (Sigma, St. Louis, MO).

Rescue of shRNA toxicity by cDNA complementation

Complementation studies were performed in the UPN-1 cell line. Briefly, cells were transduced with retroviral vectors that express a 3′-UTR-directed CCND1 shRNA. CCND1 shRNA-transduced cells were subsequently infected with retroviruses co-expressing a wild-type CCND1 cDNA and hygromycin resistant gene. Hygromycin-selected cells were induced with doxycycline to induce shRNA expression and apoptosis was monitored over time by active caspase-3/cleaved PARP staining.

Immunofluorescence

Cells were fixed with 2% paraformaldehyde and permeabilized with 0.5% Triton X-100, followed by

blocking with 2% BSA and 0.05% Tween-20 in phosphate buffered saline. Cells were stained with primary antibodies and then with fluorescently labeled secondary antibodies, followed by nuclear staining with 4′,6-diamidino-2-phenylindole (DAPI) (Life Technologies, Grand Island, NY).

Xenograft study

Mouse care and experimental procedures were performed in accordance with established institutional guidelines and approved protocols from the Institutional Animal Care and Use Committee of the City of Hope. Five millions of CCND1 shRNA-transduced UPN-1 cells were subcutaneously injected into dorsal skin area of 7- to 8-week-old immunodeficient NOD/SCID/IL2R-Gamma (NSG) mice (Jackson Laboratories, Bar Harbor, ME). After tumors reached average size of ~5 mm, sucrose or doxycycline (Sigma, St. Louis, MO) was added to mouse drinking water and tumor growth was monitored every other day by caliper measurements.

DNA combing assay

Exponentially growing cells were pulse-labeled with 50 μM iododeoxyuridine (IdU) followed by 100 μM chlorodeoxyuridine (CIdU) for 20 and 40 min each. Labeled cells were harvested and DNA fiber spreads were processed as described.[25]

Cell cycle analysis

Cells were cultured with bromodeoxyuridine (BrdU) for 30 min, washed in PBS, and fixed overnight in 70% ethanol. Labeled cells were permeabilized in Perm/Wash buffer (BD-Biosciences) and treated with 4N hydrochloric acid and 1% Triton X-100. Acid was neutralized by sodium tetraborate (pH 8.5). Cells were incubated with an anti-BrdU antibody (BD-Biosciences) followed by washing and resuspending in RNAse/PI-staining solution (Life Technologies). Flow cytometric analysis was performed on a FACSCalibur (BD-Biosciences).

Statistical analyses

A two-tailed Student's *t*-test was used for normally distributed values. For non-normally distributed values, a two-tailed Mann–Whitney test was used. A chi-squared test or a two-sided Fisher's exact test was used for categorical data. All tests were analyzed using Prism Version 6.0b (GraphPad Software, Inc.). $p < 0.05$ was considered significant. Complete methods are available in Supplementary Methods.

Results

CCND1 is required for the survival of MCL cells

To examine CCND1 function in the proliferation and survival of MCL, we depleted this protein in the human MCL lines UPN-1 and JEKO-1 using short-interfering (si)RNA. To distinguish other roles of CCND1 from those of its well-characterized pathway through CDK4 or CDK6, we also depleted CDK4 in parallel experiments, as the cell lines we chose do not express CDK6 (Figure 1A). Protein knockdown were confirmed by immunoblot analysis (Figure 1B). Depletion of CCND1 or CDK4 after 7 days decreased cell proliferation in both cell lines (Figure 1C). To determine whether the growth inhibition observed in these cells was due to cytotoxic effects of gene silencing, the apoptotic marker active caspase 3 was evaluated by flow cytometry. Compared to controls, CCND1 depletion induced apoptosis in UPN-1 and JEKO-1 cells more than CDK4 depletion (Figure 1D and E). As an alternative method to evaluate cell death, Annexin V and propidium iodide (PI) positive cells were analyzed by flow cytometry on day 5 after siRNA transfection. Consistent with the results shown in Figure 1D and E, depletion of CCND1 but not CDK4 significantly increased Annexin V and PI staining in UPN-1 and JEKO-1 cells (see DMSO-treated samples in Figures 5A and B).

To determine that little toxicity in UPN-1 and JEKO-1 cells was not due to partial CDK4 knockdown, cells were treated with the CDK4/6-specific inhibitor PD-0332991.[13] The effectiveness of this drug was verified by its ability to block the phosphorylation on RB, a known target of CDK4/6. Since UPN-1 cells do not express RB,[26] the alternative CDK4/6 target protein RB-like 2 (RBL2) was evaluated. In a dose-dependent manner, PD-0332991 effectively blocked the phosphorylation of RB or RBL2, leading to decreased cell proliferation in both cell lines (Figure 1F and G). However, compared to DMSO-treated controls, PD-0332991 only modestly induced apoptosis in UPN-1 and JEKO-1 cells (Figure 1H and I). These results were similar to the effects of siRNA-mediated CDK4 depletion shown in Figure 1D and E.

We next used shRNA as an alternative gene knockdown method to confirm the effects of CCND1 depletion. UPN-1 and JEKO-1 cells were transduced with retroviral vectors that co-expressed control or CCND1 shRNA and enhanced green fluorescence protein (eGFP). The proliferation and/or survival of transduced

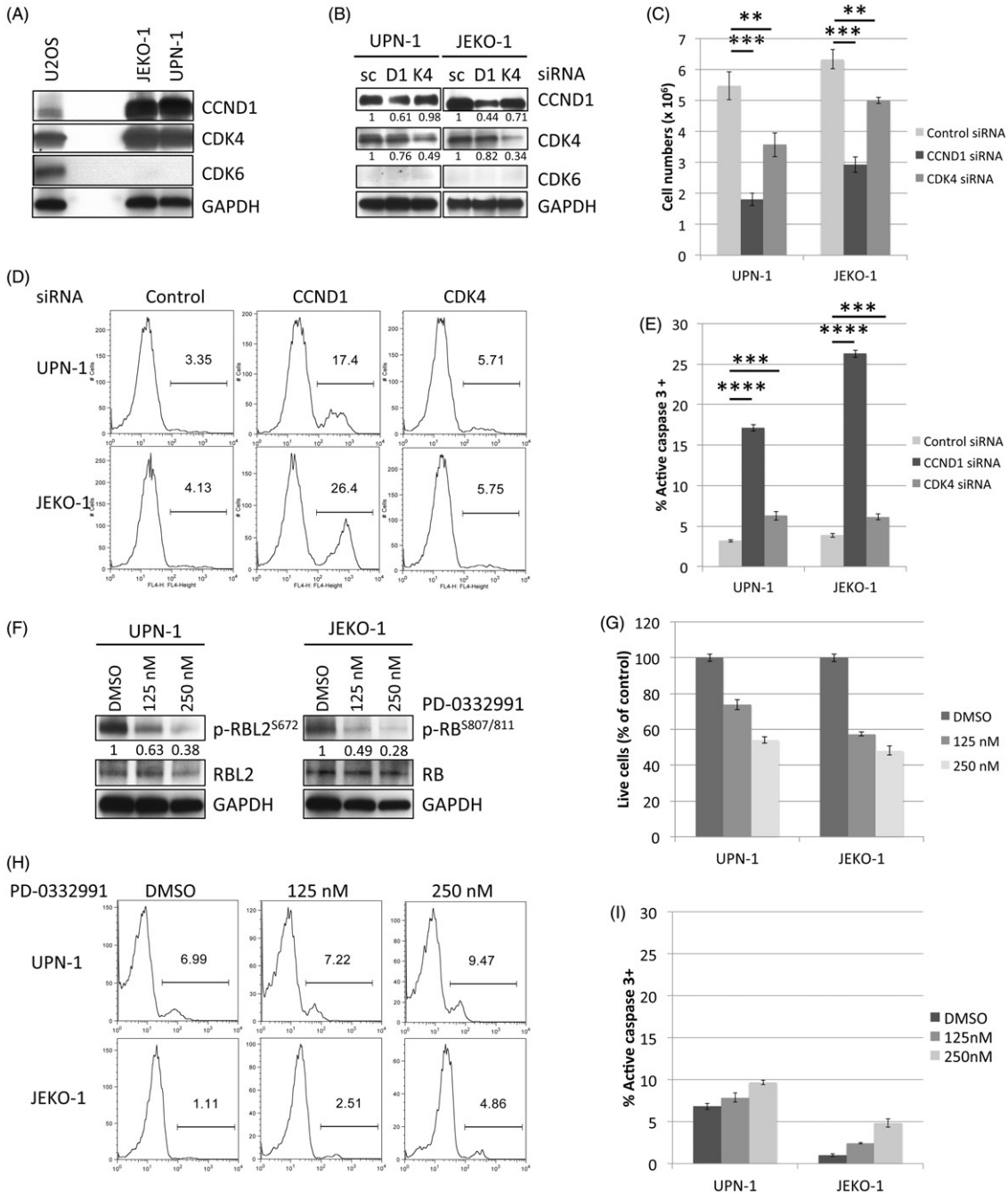

cells were then determined by monitoring the fractions of eGFP positive cells over time using flow cytometry. Compared to controls, CCND1 shRNA significantly reduced the viability of both UPN-1 and JEKO-1 cells in a time-dependent fashion (Figure 1J). Because CCND1 depletion is toxic in the MCL lines used in our study, we generated a stable UPN-1 cell line that conditionally expresses CCND1 shRNA, using a doxycycline (Dox)-inducible retroviral expression system.[24] To validate that the toxicity of the CCND1 shRNA was not due to an off-target effect, we demonstrated that a cDNA vector encoding wild-type CCND1 was able to rescue apoptosis induced by a 3′-UTR-directed CCND1 shRNA (Figure 1K). We next compared the effects of CCND1 and CDK4 shRNA-mediated knockdown on proliferation and survival using stable UPN-1 cell lines that conditionally express CCND1 or CDK4 shRNA. To ensure similar CCND1 and CDK4 knockdown efficiencies, cells with similar expression levels of the co-expressed eGFP marker were sorted by flow cytometry to normalize shRNA expression (Supplementary Figure S2). As expected, shRNA-mediated depletion of CCND1 in UPN-1 cells led to more growth inhibition and apoptosis than depletion of CDK4 in multiple time points

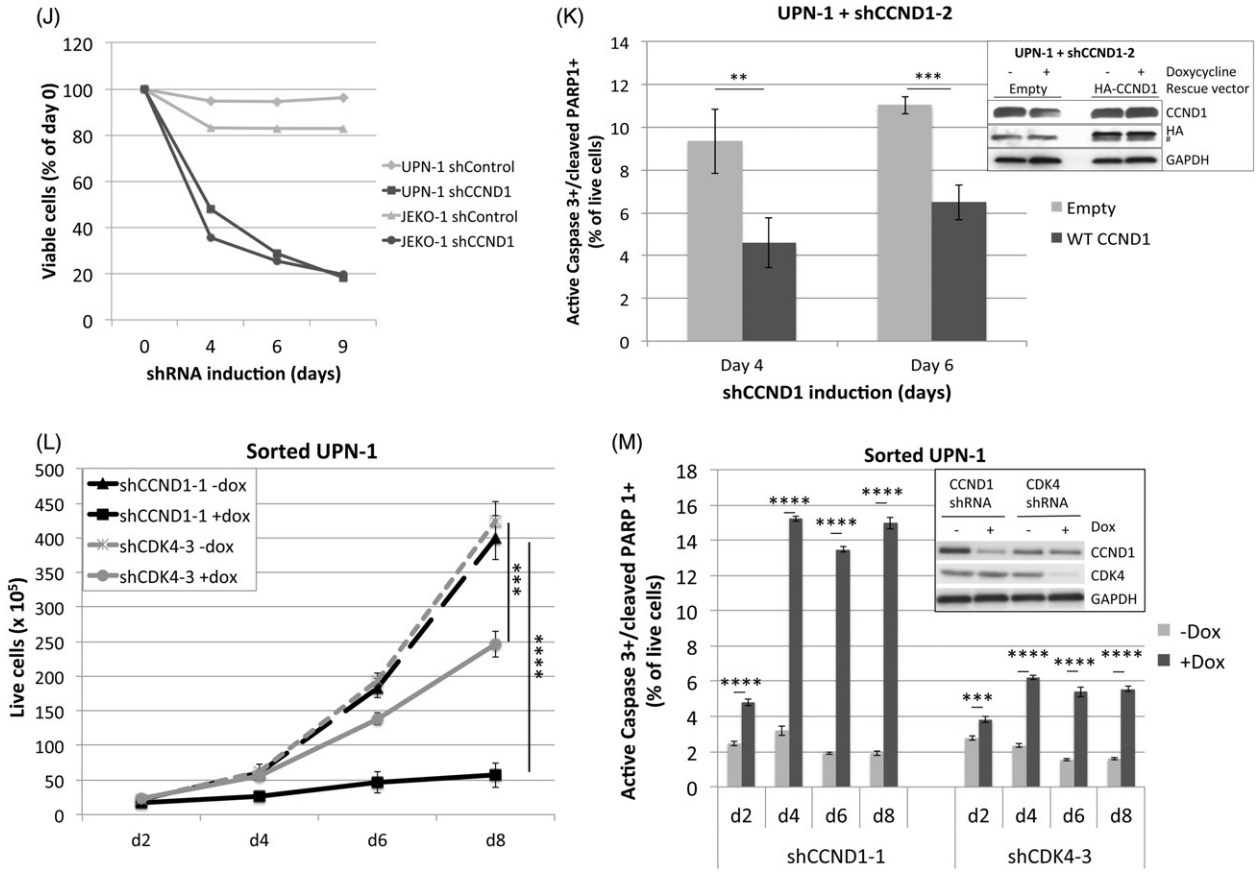

Figure 1. CCND1 is required for survival of MCL cells. (A) Immunoblot shows UPN-1 and JEKO-1 cells express little CDK6 with U2-OS cells as a positive control for CDK6 expression. (B) Immunoblot shows protein knockdown in indicated MCL cell lines on day 4 after transfection with scramble control (sc), CCND1 (D1), or CDK4 (K4) siRNA. Numbers below the bands are relative densitometric values between target proteins and GAPDH loading control, followed by normalization to the control siRNA for each protein. (C) Effects of siRNA knockdown on cell proliferation. Shown are the numbers of viable cells as determined by trypan blue exclusion on day 7 after transfection with indicated siRNA. (D) Detection of apoptosis in indicated cell lines 7 days after transfection with indicated siRNA. Shown are representative histograms of live cells stained with the active caspase-3 antibody followed by fluorescence-activated cell sorting (FACS) analysis. (E) Quantification of active caspase 3-positive cell fractions described in (D). (F). Immunoblot analysis of indicated cell lines 48 h after treatment with indicated doses of PD-0332991. Inhibition of CDK4/6 activity by PD-0332991 was shown by dephosphorylation of the CDK4/6 target protein RB or RBL2. RB was absent in UPN-1 cells and, therefore, RBL2 was analyzed. Relative densitometric values were calculated as described in (B). (G) Effects of PD-0332991 on cell proliferation. Shown are percentages of viable cells compared to DMSO-treated cells as determined by the Celltiter-Glo assay 7 days after treatment with indicated doses of PD-0332991. (H) Detection of apoptosis in indicated cell lines after 7-day treatment with PD-0332991 as described in (D). (I) Quantification of active caspase 3-positive cell fractions described in (H). (J) Toxicity of CCND1 shRNA in MCL cell lines. Shown are the normalized fractions (to day 0 values) of GFP^+, shRNA-expressing cells relative to GFP^-, shRNA-negative fractions at indicated times. (K) Rescue of CCND1 shRNA toxicity by cDNA complementation. UPN-1 cells were transduced with a doxycycline (dox)-inducible 3′-UTR-directed CCND1 shRNA (shCCND1-2) and a rescue vector constitutively expressing HA-tagged, wild-type (WT) CCND1 coding regions or an empty vector. Apoptotic cells were assessed as described in (D) at indicated times after shRNA induction and shown as percentages of active caspase 3/cleaved PARP-1-positive cells. Inset, immunoblot verifies CCND1 overexpression or knockdown 2 days after shRNA induction. #Nonspecific bands. (L) Effects of CCND1 or CDK4 depletion on cell growth. Shown are the means of live cell numbers of control or shRNA-induced cells as determined by trypan blue exclusion on indicated days. (M) Apoptosis in UPN-1 cells transduced with indicated shRNA was detected at indicated times after shRNA induction by staining with active caspase-3 and cleaved PARP-1 antibodies. Inset, immunoblot confirms protein knockdown 2 days after shRNA induction. Values in line graphs or bar graphs are the means of three independent experiments. Error bars, SD. ****$p < 0.0001$; ***$p < 0.001$; **$p < 0.01$ by a two-tailed Student's *t*-test.

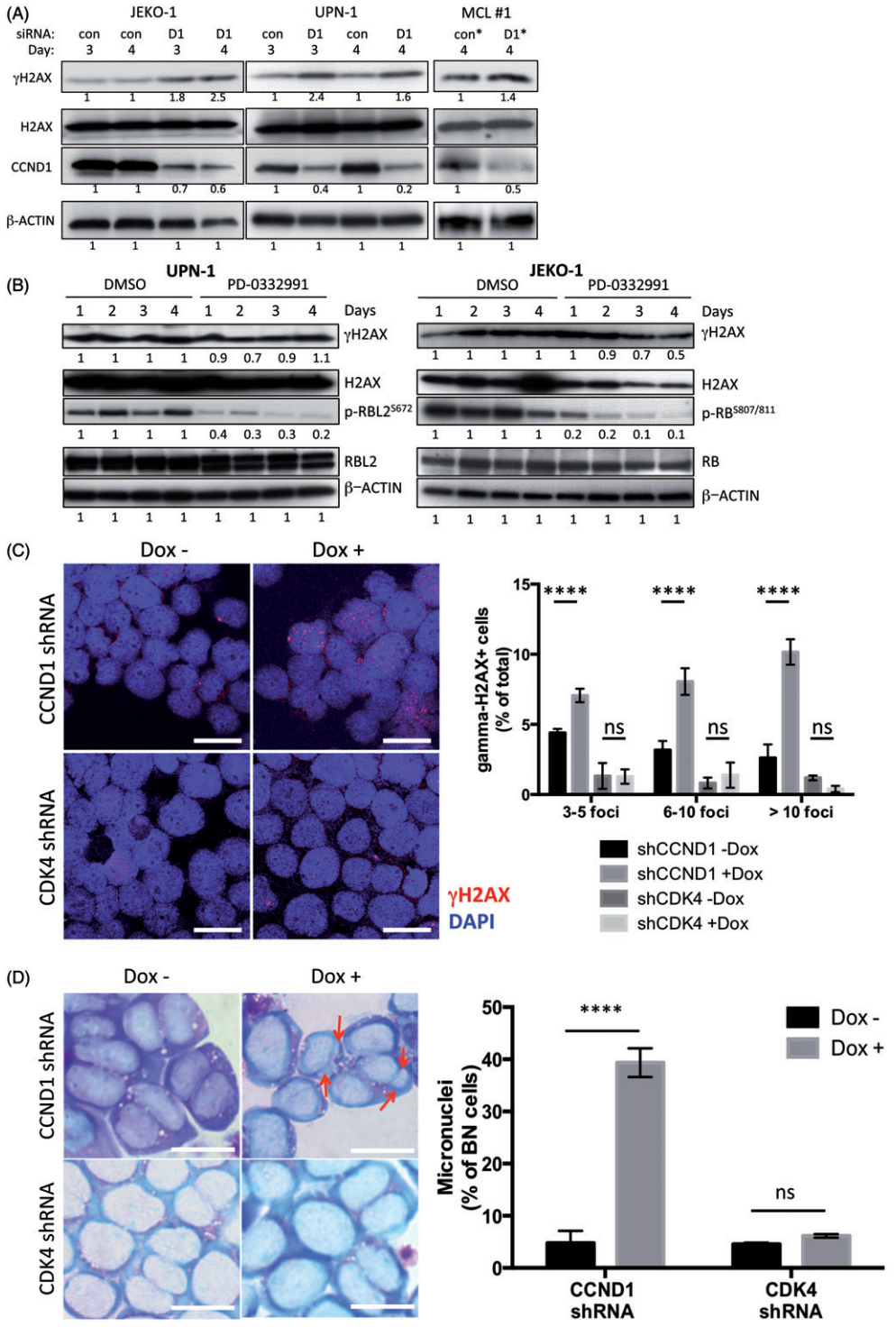

Figure 2. CCND1 is required for DNA stability in MCL cells. (A) CCND1 depletion induces γ-H2AX expression. Immunoblot analysis of indicated MCL cell lines on day three or four after transfection with control (con) or CCND1 (D1) siRNA. Primary MCL cells (MCL #1) with more than 95% of tumor content (see Supplementary Figure S4) were transduced with control or CCND1 shRNA-expressing lentivirus and analyzed by immunoblot on day 4 after transduction. Relative densitometric values were calculated as described in Figure 1B. (B) Effect of CDK4 inhibition on γ-H2AX expression. UPN-1 and JEKO-1 cells were treated with 250 nM of PD-0332991 for indicated times and analyzed by immunoblot. Relative densitometric values were calculated as described in Figure 1B. (C) CCND1 depletion induces DNA DSB foci. CCND1 or CDK4 shRNA-transduced UPN-1 cells were induced with Dox for four days. Shown are representative confocal immunofluorescence images of uninduced and induced cells stained with Alexa-Fluor 555-conjugated phospho-H2AX (S139) antibody (red) followed by nuclear staining with DAPI (blue). Scale bars, 20 μm. Bar graphs show the mean values of cell fractions that are positive for phospho-H2AX (γH2AX) foci from two independent experiments. Error bars, SEM. Foci of at least 1 μm in diameter were considered positive for γH2AX. On average, 500 cells from each group were counted. $^{****}p < 0.0001$ by a Chi-square test; ns, not significant. More γH2AX foci in uninduced CCND1 shRNA-transduced cells than in CDK4 shRNA-transduced cells indicate ''leakiness'' of the Dox inducible system in UPN-1 cells. (D) CCND1 depletion induces genomic instability. Representative bright-field images of uninduced or day-four induced UPN-1 cells treated with cytochalasin B followed by Giemsa nuclear staining. Scale bars, 20 μm. Bar graphs show the percentages of binucleated (BN) cells with micronucleus (MN) formation from two separate experiments. Error bars, SEM; $^{****}p < 0.0001$ by a two-sided Fisher's exact test. Approximately 200 binucleated (BN) cells from each group were counted.

starting on day 4 after Dox induction (Figure 1L and M). Altogether, we conclude that survival of UPN-1 and JEKO-1 cells is more dependent on CCND1 than on CDK4.

CCND1 is required for DNA stability in vitro *and in a xenograft model of MCL*

To determine whether apoptosis induced by CCND1 depletion was due to DNA damage, we evaluated DNA double-stranded break (DSB) formation by detecting histone H2AX phosphorylation on Ser139 (gamma-H2AX), an established DSB marker,[27] in UPN-1 and JEKO-1 cells transfected with CCND1 siRNA. Compared to controls, CCND1-depleted cells had increased gamma-H2AX expression on days 3 and 4 after siRNA (Figure 2A). In contrast, gamma-H2AX induction was not detected in these MCL lines treated with PD-0332991 (Figure 2B) or depleted of CDK4 (Supplementary Figure S3) for up to 4 days. Increased gamma-H2AX signals were also observed in primary MCL cells 4 days after transduction with CCND1 shRNA-expressing lentivirus (Figure 2A). The tumor content in this primary MCL sample was confirmed to have >95% of CD19 + CD5 + lymphoma cells (Supplementary Figure 4). As an alternative method of detecting DSBs, we used immunofluorescence to identify cells with nuclear gamma-H2AX foci. Using inducible knockdown UPN-1 cell lines generated above, we demonstrated that depletion of CCND1, but not CDK4, significantly increased the number of gamma-H2AX^{+} foci (Figure 2C), which were more frequent in the S and G2 phases of the cell cycle (Supplementary Figure S5). These data indicate that CCND1, but not CDK4, plays an important role in preventing DNA damage in MCL cells.

DNA damage after CCND1 depletion in MCL cells prompted us to evaluate genomic stability in these cells. Using a cytokinesis-block micronucleus assay [28] to detect nuclear damage during mitotic segregation, we observed that depletion of CCND1, but not CDK4, significantly increased micronucleus formation in UPN-1 cells (Figure 2D). Further cytogenetic analysis of chromosomal aberrations by metaphase karyotyping following CCND1 silencing in UPN-1 cells revealed chromosomal breaks, chromatid breaks and recurrent chromosomal gaps or constrictions that are associated with fragile sites (Supplementary Figure S6, Supplementary Table S2).

We next evaluated the *in vivo* relevance of CCND1 inactivation by engrafting CCND1 shRNA-expressing UPN-1 cells into immunodeficient NOD/SCID/IL2R-Gamma (NSG) mice. CCND1 depletion resulted in reduced growth (Figure 3A–C) and increased apoptosis, as detected by active caspase 3 immunofluorescence (Figure 3E), in the transplanted tumors. Increased accumulation of gamma-H2AX foci was also observed in CCND1-depleted, but not control, xenografts (Figure 3D). These findings are consistent with the *in vitro* effects of CCND1 depletion in UPN-1 cells on cell growth, apoptosis and DNA stability described above. Together, these data indicate that CCND1 is essential for maintaining DNA stability in MCL cells and specifically in the UPN-1 cells both in *in vitro* and *in vivo* conditions.

CCND1 depletion leads to defective DNA replication in UPN-1 cells

In the absence of induced DNA damage, DNA breakage often occurs during replication stress, a process when DNA synthesis becomes inefficient.[29] To determine whether DNA damage in CCND1-depleted UPN-1 cells were related to defects in DNA replication, the DNA combing assay [25] was used to assess replication initiation. In this assay, CCND1- or CDK4-depleted UPN-1 cells were pulse-labeled with the thymidine substitutes iododeoxyuridine (IdU) and chlorodeoxyuridine (CldU) for 20 and 40 min each. DNA fibers were extracted from cell lysates and spread on glass slides for immunofluorescence analysis using antibodies specific for IdU or CldU. Compared to uninduced or CDK4-depleted cells, CCND1-depleted cells showed a markedly reduced distance between replication origins, indicating increased frequency of origin firing (Figure 4). Thus, CCND1 may have an important role in DNA replication initiation and reduced CCND1 expression levels may result in unscheduled origin firing and replication stress-related DNA breakage.

CCND1 depletion sensitizes MCL cells to DNA replication inhibitors

We next determined whether CCND1 plays a role in the chemoresistance of MCL cells to the replication inhibitors hydroxyurea (HU) or cytarabine. To do so, we depleted CCND1 by siRNA in UPN-1 and JEKO-1 cell lines for 3 days. Equal numbers of siRNA-transfected cells were re-plated and treated with increasing concentrations of HU or cytarabine for 2 days followed by evaluation of apoptosis using Annexin V-based flow cytometry. Knockdown of target proteins in these experiments was confirmed by immunoblot analysis (Figure 5A and B insets). CCND1 depletion increased sensitivity of UPN-1 and JEKO-1 cells to HU

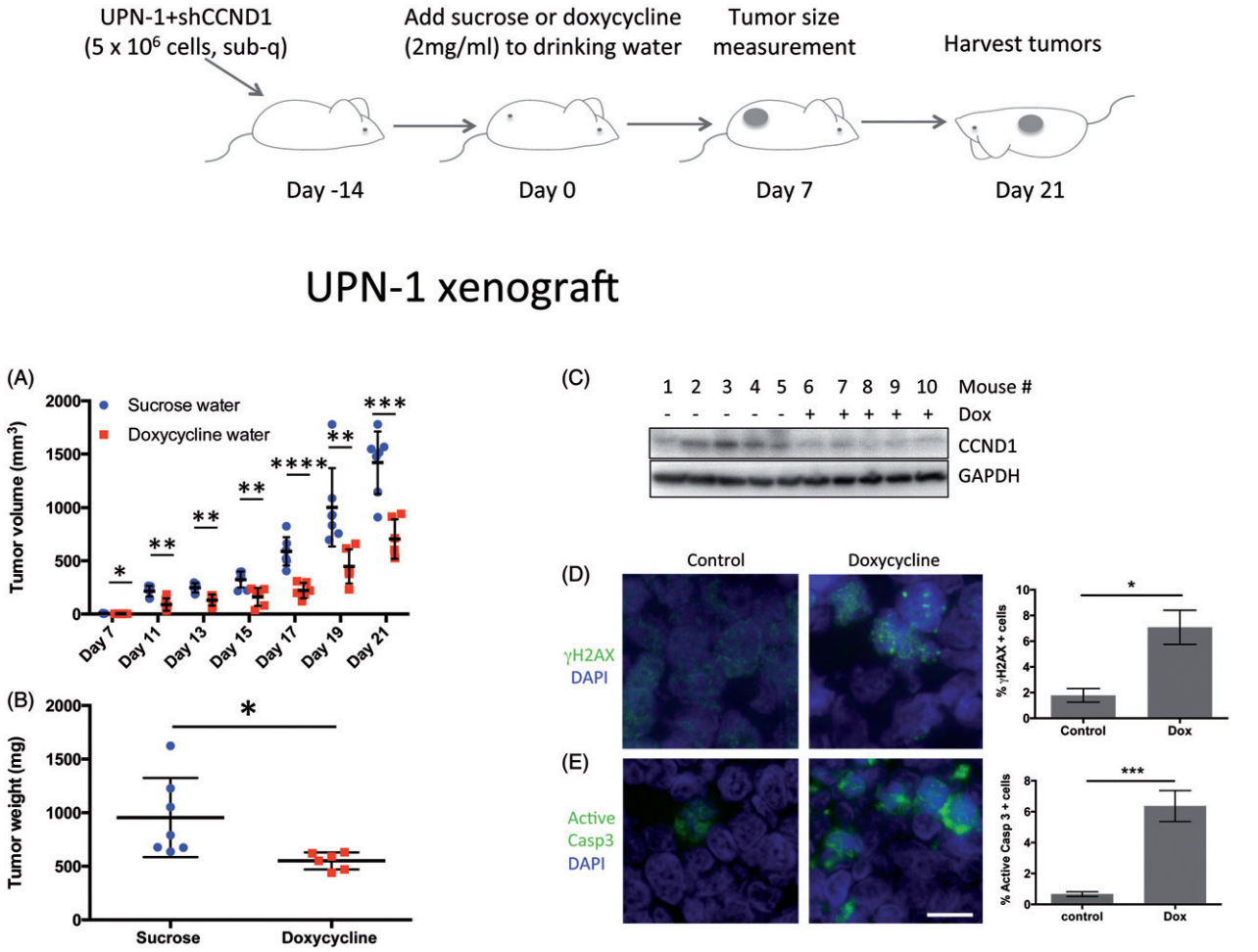

Figure 3. Effects of CCND1 depletion in a xenograft model of MCL. Five millions of CCND1 shRNA-transduced UPN-1 cells were injected subcutaneously into NSG mice and shRNA expression was induced by adding Dox to mouse drinking water. (A) Shown are the means of tumor volumes ($n = 7$). Error bars, SEM. (B) Shown are the means of tumor weights. Error bars, SD. (C) Lysates of MCL tumors harvested from control or Dox-induced mice on day 21 were immunoblotted with indicated antibodies. (D and E) Representative immunofluorescence images of tumor sections from control and Dox-induced groups were stained with indicated antibodies followed by fluorescently labeled secondary antibody and nuclear staining with DAPI. Scale bars, 10 μm. Bar graphs show the percentages of γH2AX+ or active caspase 3+ cells from control ($n = 3$) or Dox-induced ($n = 3$) xenografts. Foci with at least 1 μm in diameter were considered positive for γH2AX. At least 500 DAPI-positive cells were counted in non-overlapping fields of immunofluorescence images. Error bars, SD; ***$p < 0.001$; *$p < 0.05$ by a two-tailed Student's t-test.

(Figure 5A and B) or cytarabine (Figure 5C and D) dose-dependently. Using the inducible CCND1 knockdown UPN-1 cell line, we confirmed that induced CCND1 shRNA sensitized UPN-1 cells to HU or to another replication inhibitor aphidicolin (Figure 5E). Enhanced chemosensitivity of UPN-1 and JEKO-1 cells after CCND1 depletion was not due to CDK4 inactivation, as CDK4 depletion produced results similar to control knockdown cells (Figure 5A–D). In addition, pharmacologic inhibition of CDK4 using PD-0332991 increased resistance of these cells to HU (Figure 5F and G). These results indicate that CCND1, but not CDK4, is required for resistance of MCL cells to DNA replication inhibitors.

Effects of CCND1 depletion on the cell cycle of MCL cells

Because CCND1 primarily regulates cell-cycle progression through CDK4, increased chemosensitization in MCL cells after CCND1 depletion led us to examine the effect of loss of CCND1 on the cell cycle. Control or CCND1-depleted UPN-1 and JEKO-1 cells were labeled with bromodeoxyuridine (BrdU) and propidium iodide (PI), and the cell cycle was analyzed by flow cytometry. The CDK4 inhibitor PD-0332991 was also used in parallel experiments to compare with the effects of CCND1 depletion. Silencing of CCND1 in both UPN-1 and JEKO-1 cells was confirmed by qPCR (Figure 6A). While

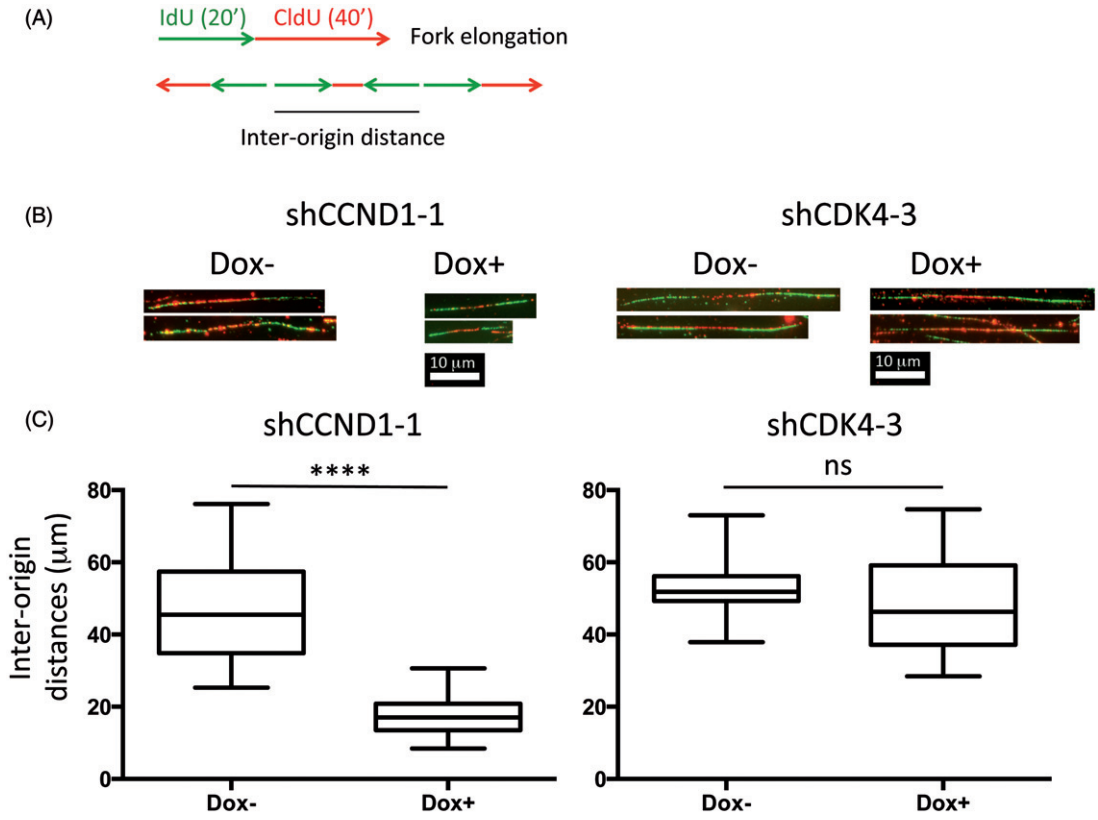

Figure 4. CCND1 depletion increases replication initiation frequency in UPN-1 cells. CCND1 or CDK4 shRNA-transduced UPN-1 cells were induced with Dox for four days and sequentially pulse-labeled with IdU and CIdU, as illustrated in the diagram (A). (B) DNA fibers from labeled cells were spread on glass slides and incorporated IdU and CIdU were detected by immunofluorescence. Shown are representative fluorescence images of labeled DNA fibers. (C) Inter-origin distances as illustrated in (A) and shown in (B) were measured in micrometers and quantified by boxplots, with bars contained in boxplots representing median values. Scale bars, 10 µm; ****$p < 0.0001$. ns: not significant. p values are from the two-tailed Mann-Whitney test for 100–200 scorable tracks on average per sample.

depletion of CCND1 or inhibition of CDK4 induced cell cycle arrest in both cell lines, more G1 arrest was observed in CDK4-inhibited cells (60–80%) than in CCND1-depleted cells (~50%) (Figure 6B and C). A strong induction of G1 arrest by CDK4 inhibition was consistent with the chemo-protective effect of PD-0332991, which prevented cells from entering the S phase where they were more sensitive to HU (Figure 5F and G). In contrast, weaker G1 arrest induced by CCND1 depletion sensitized cells to HU or cytarabine (Figure 5A–E). These data indicate a functional difference between CCND1 and CDK4 signaling with respect to chemosensitivity and suggest a CDK4-independent role of CCND1, which becomes essential when cells encounter replication inhibitors.

Discussion

The present study demonstrated that CCND1 is essential for the maintenance of established MCL tumor cell lines and uncovered a new role for CCND1 in preserving genomic stability during DNA replication in MCL cells. There are conflicting reports on the role of CCND1 in the survival of MCL cells. Klier et al. [30] showed that silencing of CCND1 in the MCL lines GRANTA-519, JEKO-1, and Z-138 for up to 7 days caused growth arrest but not cell death. In contrast, Weinstein et al. [31] detected apoptosis in the GRANTA-519 and JEKO-1 lines 8 days after CCND1 siRNA transfection. In agreement with the study of Weinstein et al.,[31] our data indicate that CCND1 is essential in JEKO-1 (and UPN-1) cells. Apoptosis in JEKO-1 cells after CCND1 depletion was detected both in the Weinstein et al. [31] and the present study but not in the study by Klier et al.[30] This discrepancy is probably due to the use of more sensitive apoptotic markers like Annexin V by Weinstein et al. [31] or active caspase 3/cleaved PARP 1 in our study, whereas Klier et al. [30] assessed apoptosis by quantifying the sub-diploid populations.

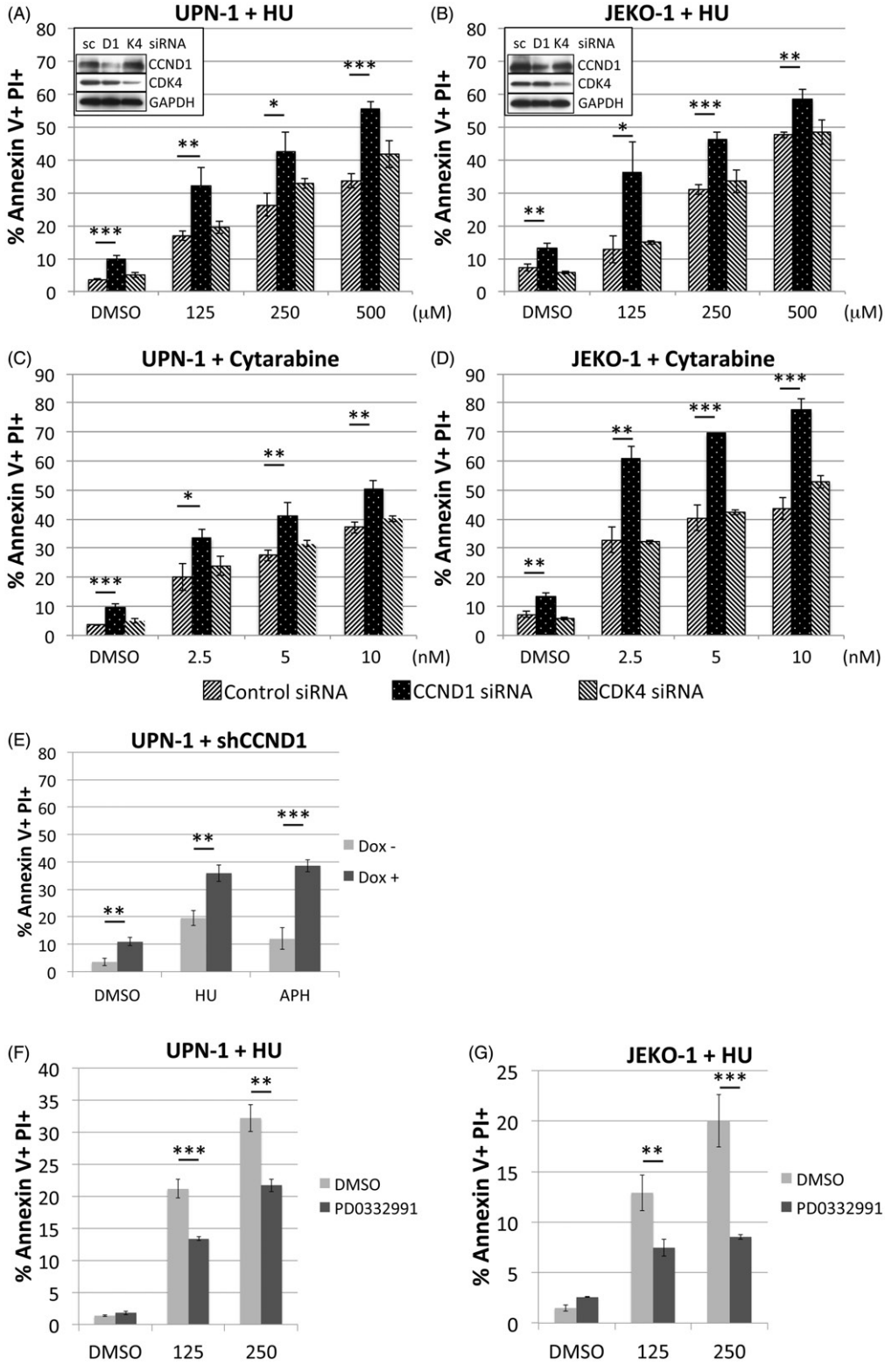

Figure 5. CCND1 depletion sensitizes MCL cells to DNA replication inhibitors. (A–D) MCL lines were transfected with siRNA against CCND1 (D1) or CDK4 (K4) or a control siRNA on day zero and again on day two (see Materials and Methods). On day three, 1.5×10^5 live cells were counted and re-plated, followed by addition of HU (A and B) or cytarabine (C and D) at indicated doses. Apoptosis was assessed by Annexin V/PI staining on day five. Shown are percentages of Annexin V+/PI+ cells. Inset, confirmation of protein knockdown three days after siRNA transfection by immunoblotting with indicated antibodies. (E) CCND1 shRNA sensitizes UPN-1 cells to DNA replication inhibitors. CCND1 shRNA-transduced UPN-1 cells were induced with Dox for four days followed by treatment with HU (0.25 mM) or aphidicolin (APH, 1000 nM) for two days and analyzed for apoptosis by Annexin V/PI staining. (F and G) CDK4 inhibition increases chemoresistance in MCL cells to HU. UPN-1 or JEKO-1 cells were treated with indicated doses of HU in combination with DMSO or 250 nM of PD-0332991 for 2 days and analyzed for apoptosis by Annexin V/PI staining. Bar graphs show means of three independent experiments. Error bars, SD. ***$p < 0.001$, **$p < 0.01$, *$p < 0.05$ by a two-tailed Student s *t*-test.

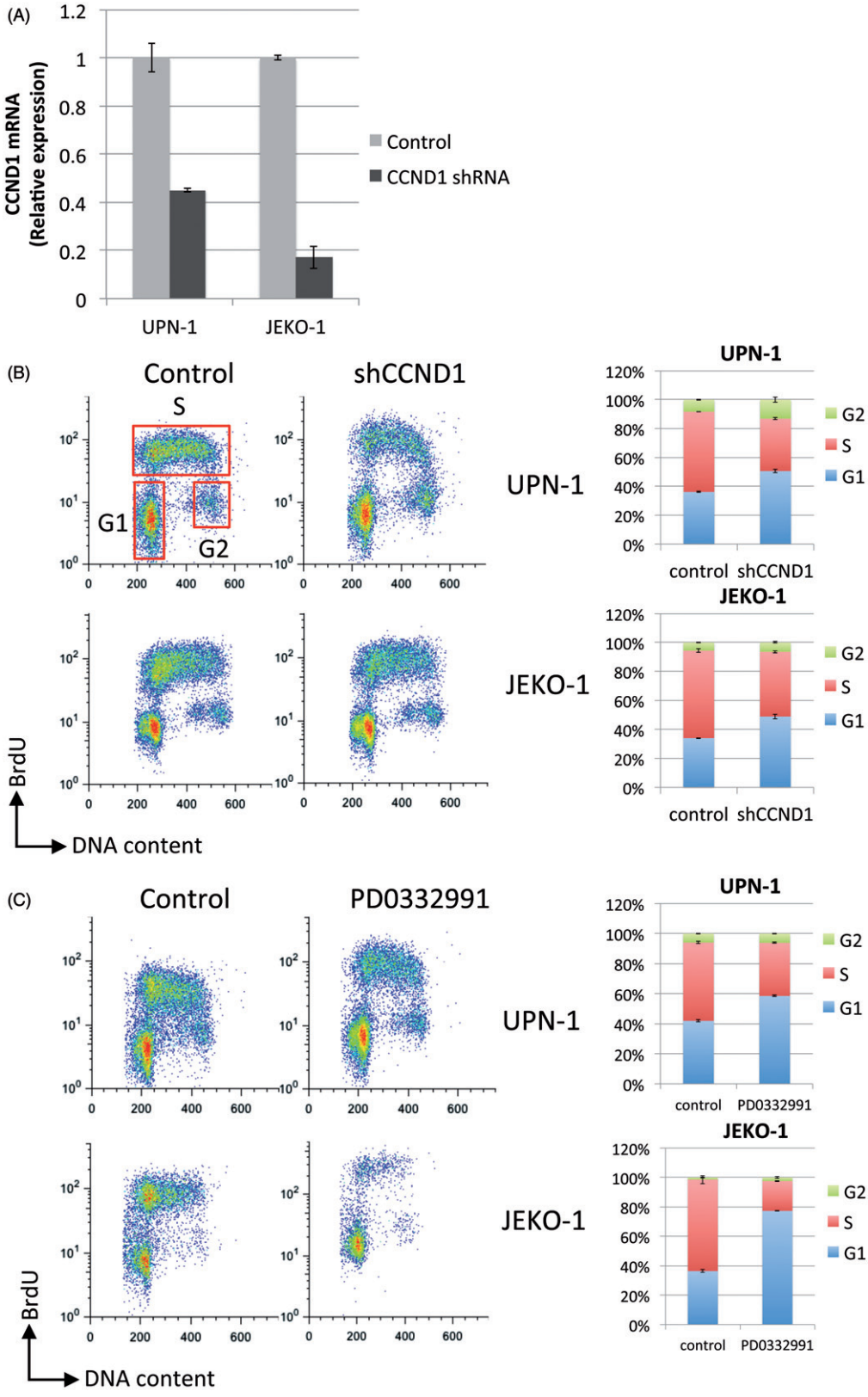

Figure 6. Effects of CCND1 depletion on the cell cycle. (A) Verification of CCND1 knockdown. Control or CCND1-depleted UPN-1 or JEKO-1 cells were analyzed for relative CCND1 mRNA expression by qPCR after 4 days of shRNA induction. Shown are the means of three independent experiments. Error bars, SD. (B) Cell cycle profiles of MCL cells after CCND1 depletion. Four days after CCND1 depletion, cells were BrdU labeled for 30 min followed by FACS analysis. Shown are representative FACS plots of control or CCND1 depleted UPN-1 or JEKO-1 cells. Stacked column graphs show percentages of cells in each cell cycle phase, as defined by the drawn gates. Values are the means from three independent experiments. Error bars, SD. (C) Cell cycle profiles of MCL cells after CDK4 inhibition. Indicated cells were treated with PD0332991 (250 nM) for 4 days and were labeled with BrdU as described in (B). Shown are representative FACS plots of control or treated UPN-1 or JEKO-1 cells. Stacked column graphs were generated as decribed in (B). Values are the means from three independent experiments. Error bars, SD.

We found that CCND1 depletion resulted in increased origin firing, leading to replication stress and DNA DSB. However, it is unclear how CCND1 plays a protective role in preventing DNA damage during replication in MCL cells. In a comprehensive proteomics study of CCND1-overexpressing human cancers, including one MCL line (Granta-519), Jirawatnotai et al. [32] demonstrated direct binding between CCND1 and the DNA repair protein RAD51 in the context of radiation-induced DNA damage. As RAD51 can also be recruited to the stalled replication forks independently of DNA breakage,[33,34] it would be of future interest to investigate whether CCND1 and RAD51 interaction is required to maintain genome stability during unperturbed replication in MCL.

Because CCND1 depletion is toxic in the MCL lines used in the present study, detailed studies of its function require a conditional knockdown system. By generating Dox-inducible knockdown cell lines in UPN-1 cells, we uncovered a previously unrecognized role for CCND1 in preserving genomic stability during DNA replication. This genome protective function of CCND1 is thus relevant to the resistance of MCL to chemotherapeutic agents. These data were, however, limited to the inducible knockdown system generated in UPN-1 cells. Multiple attempts to generate inducible CCND1 shRNA in JEKO-1 cells have been proven technically challenging, likely due to the inherent leakiness of the tetracycline inducible system in this cell line. Nonetheless, the roles of CCND1 in promoting survival and chemoresistance in JEKO-1 cells reported in this study are consistent with previous studies for this cell line.[21,31]

Aberrant CCND1 signaling is considered central to MCL pathogenesis and major efforts to target this pathway have been directed to its catalytic partner CDK4 using the highly specific inhibitor palbociclib (PD-0332991). Despite being a potent inhibitor of CDK4-RB signaling that can efficiently suppress tumor growth both *in vitro* and *in vivo*,[13–15] palbociclib induces little or very modest cell death in MCL, as demonstrated by others [15] and the present study. Our data indicate that the survival and chemoresistance of established human MCL lines are more dependent on CCND1 than on CDK4, suggesting CCND1 as a valid target in MCL. However, these cell line results were confirmed by only limited data on primary MCL cells (see Figure 2A) due to technical challenges in genetic manipulation of primary cells. Currently, there are no small-molecule inhibitors of CCND1 under clinical development, but pharmacologic agents that indirectly reduce CCND1 levels have been reported (see review in [35]). These agents will be helpful to confirm our cell line observations in primary MCL cells. Of interest, recent MCL treatment advances using ibrutinib, a Bruton's tyrosine kinase inhibitor, have produced durable responses in MCL patients.[36] Further studies by Ma et al. [37] to characterize MCL cells with different sensitivity to ibrutinib showed that this drug can down-regulate CCND1 levels in certain MCL cell lines. Our findings on the essential role of CCND1 in the survival and maintaining genomic stability of MCL cells are therefore highly relevant to future efforts to improve the efficacy of this emerging therapy.

In summary, this study has demonstrated a role for CCND1 in the survival and chemoresistance of MCL cells. CCND1 plays these essential roles likely through involvement in DNA replication to minimize DNA damage. These findings, thus, have important implications for understanding and treating the chemoresistance of aggressive MCL.

Acknowledgements

We thank Drs Louis M. Staudt and Yandan Yang for MCL cell lines and the Tet-repressor expressing UPN-1 cells, and Dr Jeremy Stark for feedback and technical advice. We also thank Dr Ravi Bhatia for helpful discussions. This work was supported in part by the National Cancer Institute of the National Institute of Health [grant number P30CA033572].

Potential conflict of interest: Disclosure forms provided by the authors are available with the full text of this article at http://dx.doi.org/10.1080/10428194.2016.1198958.

References

[1] Jares P, Colomer D, Campo E. Genetic and molecular pathogenesis of mantle cell lymphoma: perspectives for new targeted therapeutics. Nat Rev Cancer. 2007;7:750–762.

[2] Perez-Galan P, Dreyling M, Wiestner A. Mantle cell lymphoma: biology, pathogenesis, and the molecular basis of treatment in the genomic era. Blood. 2011;117:26–38.

[3] Raffeld M, Jaffe ES. bcl-1, t(11;14), and mantle cell-derived lymphomas. Blood. 1991;78:259–263.

[4] Sherr CJ. Mammalian G1 cyclins. Cell. 1993;73:1059–1065.

[5] Hatakeyama M, Brill JA, Fink GR, et al. Collaboration of G1 cyclins in the functional inactivation of the retinoblastoma protein. Genes Dev. 1994;8:1759–1771.

[6] Calbo J, Parreno M, Sotillo E, et al. G1 cyclin/cyclin-dependent kinase-coordinated phosphorylation of endogenous pocket proteins differentially regulates their interactions with E2F4 and E2F1 and gene expression. J Biol Chem. 2002;277:50263–50274.

[7] Sherr CJ, Roberts JM. CDK inhibitors: positive and negative regulators of G1-phase progression. Genes Dev. 1999;13:1501–1512.
[8] Wlodarska I, Dierickx D, Vanhentenrijk V, et al. Translocations targeting CCND2, CCND3, and MYCN do occur in t(11;14)-negative mantle cell lymphomas. Blood. 2008;111:5683–5690.
[9] Salaverria I, Royo C, Carvajal-Cuenca A, et al. CCND2 rearrangements are the most frequent genetic events in cyclin D1(-) mantle cell lymphoma. Blood. 2013;121:1394–1402.
[10] Sonoki T, Harder L, Horsman DE, et al. Cyclin D3 is a target gene of t(6;14)(p21.1;q32.3) of mature B-cell malignancies. Blood. 2001;98:2837–2844.
[11] Kouroukis CT, Belch A, Crump M, et al. Flavopiridol in untreated or relapsed mantle-cell lymphoma: results of a phase II study of the National Cancer Institute of Canada Clinical Trials Group. J Clin Oncol. 2003;21:1740–1745.
[12] Lin TS, Blum KA, Fischer DB, et al. Flavopiridol, fludarabine, and rituximab in mantle cell lymphoma and indolent B-cell lymphoproliferative disorders. J Clin Oncol. 2010;28:418–423.
[13] Fry DW, Harvey PJ, Keller PR, et al. Specific inhibition of cyclin-dependent kinase 4/6 by PD 0332991 and associated antitumor activity in human tumor xenografts. Mol Cancer Ther. 2004;3:1427–1438.
[14] Leonard JP, LaCasce AS, Smith MR, et al. Selective CDK4/6 inhibition with tumor responses by PD0332991 in patients with mantle cell lymphoma. Blood. 2012;119:4597–4607.
[15] Marzec M, Kasprzycka M, Lai R, et al. Mantle cell lymphoma cells express predominantly cyclin D1a isoform and are highly sensitive to selective inhibition of CDK4 kinase activity. Blood. 2006;108:1744–1750.
[16] Kornmann M, Danenberg KD, Arber N, et al. Inhibition of cyclin D1 expression in human pancreatic cancer cells is associated with increased chemosensitivity and decreased expression of multiple chemoresistance genes. Cancer Res. 1999;59:3505–3511.
[17] Biliran H, Jr.,Wang Y, Banerjee S, et al. Overexpression of cyclin D1 promotes tumor cell growth and confers resistance to cisplatin-mediated apoptosis in an elastase-myc transgene-expressing pancreatic tumor cell line. Clin Cancer Res. 2005;11:6075–6086.
[18] Noel EE, Yeste-Velasco M, Mao X, et al. The association of CCND1 overexpression and cisplatin resistance in testicular germ cell tumors and other cancers. Am J Pathol. 2010;176:2607–2615.
[19] Hashimoto T, Yanaihara N, Okamoto A, et al. Cyclin D1 predicts the prognosis of advanced serous ovarian cancer. Exp Ther Med. 2011;2:213–219.
[20] Rosenwald A, Wright G, Wiestner A, et al. The proliferation gene expression signature is a quantitative integrator of oncogenic events that predicts survival in mantle cell lymphoma. Cancer Cell. 2003;3:185–197.
[21] Tiemann K, Alluin JV, Honegger A, et al. Small interfering RNAs targeting cyclin D1 and cyclin D2 enhance the cytotoxicity of chemotherapeutic agents in mantle cell lymphoma cell lines. Leuk Lymphoma. 2011;52:2148–2154.
[22] M'Kacher R, Farace F, Bennaceur-Griscelli A, et al. Blastoid mantle cell lymphoma: evidence for nonrandom cytogenetic abnormalities additional to t(11;14) and generation of a mouse model. Cancer Genet Cytogenet. 2003;143:32–38.
[23] Amin HM, McDonnell TJ, Medeiros LJ, et al. Characterization of 4 mantle cell lymphoma cell lines. Arch Pathol Lab Med. 2003;127:424–431.
[24] Ngo VN, Davis RE, Lamy L, et al. A loss-of-function RNA interference screen for molecular targets in cancer. Nature. 2006;441:106–110.
[25] Frum RA, Deb S, Deb SP. Use of the DNA fiber spreading technique to detect the effects of mutant p53 on DNA replication. Methods Mol Biol. 2013;962:147–155.
[26] Pinyol M, Bea S, Pla L, et al. Inactivation of RB1 in mantle-cell lymphoma detected by nonsense-mediated mRNA decay pathway inhibition and microarray analysis. Blood. 2007;109:5422–5429.
[27] Rogakou EP, Pilch DR, Orr AH, et al. DNA double-stranded breaks induce histone H2AX phosphorylation on serine 139. J Biol Chem. 1998;273:5858–5868.
[28] Fenech M. Cytokinesis-block micronucleus cytome assay. Nat Protoc. 2007;2:1084–1104.
[29] Osborn AJ, Elledge SJ, Zou L. Checking on the fork: the DNA-replication stress-response pathway. Trends Cell Biol. 2002;12:509–516.
[30] Klier M, Anastasov N, Hermann A, et al. Specific lentiviral shRNA-mediated knockdown of cyclin D1 in mantle cell lymphoma has minimal effects on cell survival and reveals a regulatory circuit with cyclin D2. Leukemia. 2008;22:2097–2105.
[31] Weinstein S, Emmanuel R, Jacobi AM, et al. RNA inhibition highlights cyclin D1 as a potential therapeutic target for mantle cell lymphoma. PLoS One. 2012;7:e43343
[32] Jirawatnotai S, Hu Y, Michowski W, et al. A function for cyclin D1 in DNA repair uncovered by protein interactome analyses in human cancers. Nature. 2011;474:230–234.
[33] Petermann E, Orta ML, Issaeva N, et al. Hydroxyurea-stalled replication forks become progressively inactivated and require two different RAD51-mediated pathways for restart and repair. Mol Cell. 2010;37:492–502.
[34] Hashimoto Y, Ray Chaudhuri A, Lopes M, et al. Rad51 protects nascent DNA from Mre11-dependent degradation and promotes continuous DNA synthesis. Nat Struct Mol Biol. 2010;17:1305–1311.
[35] Alao JP. The regulation of cyclin D1 degradation: roles in cancer development and the potential for therapeutic invention. Mol Cancer. 2007;6:24
[36] Wang ML, Rule S, Martin P, et al. Targeting BTK with ibrutinib in relapsed or refractory mantle-cell lymphoma. N Engl J Med. 2013;369:507–516.
[37] Ma J, Lu P, Guo A, et al. Characterization of ibrutinib-sensitive and -resistant mantle lymphoma cells. Br J Haematol. 2014;166:849–861.

blood®
Regular Article

LYMPHOID NEOPLASIA

Regulation of SOX11 expression through CCND1 and STAT3 in mantle cell lymphoma

Atish Mohanty,[1] Natalie Sandoval,[1] An Phan,[1] Thang V. Nguyen,[2] Robert W. Chen,[3] Elizabeth Budde,[3] Matthew Mei,[3] Leslie Popplewell,[3] Lan V. Pham,[4] Larry W. Kwak,[5] Dennis D. Weisenburger,[6] Steven T. Rosen,[7] Wing C. Chan,[6] Markus Müschen,[1] and Vu N. Ngo[1,6]

[1]Department of Systems Biology, Beckman Research Institute, City of Hope, Monrovia, CA; [2]Division of Biology and Biological Engineering, California Institute of Technology, Pasadena, CA; [3]Department of Hematology and Hematopoietic Cell Transplantation, City of Hope Medical Center, Duarte, CA; [4]Department of Hematopathology, The University of Texas MD Anderson Cancer Center, Houston, TX; [5]Toni Stephenson Lymphoma Center, City of Hope Comprehensive Cancer Center, Duarte, CA; [6]Department of Pathology, City of Hope Medical Center, Duarte, CA; and [7]Beckman Research Institute, City of Hope, Duarte, CA

KEY POINTS

- CCND1 binds to and reduces recruitment of HDAC1 and HDAC2 to the *SOX11* promoter, causing increased histone acetylation and *SOX11* transcription.
- STAT3 represses *SOX11* transcription by interacting directly with the *SOX11* gene promoter and enhancer.

The neural transcription factor SOX11 is usually highly expressed in typical mantle cell lymphoma (MCL), but it is absent in the more indolent form of MCL. Despite being an important diagnostic marker for this hard-to-treat malignancy, the mechanisms of aberrant SOX11 expression are largely unknown. Herein, we describe 2 modes of SOX11 regulation by the cell-cycle regulator cyclin D1 (CCND1) and the signal transducer and activator of transcription 3 (STAT3). We found that ectopic expression of CCND1 in multiple human MCL cell lines resulted in increased SOX11 transcription, which correlated with increased acetylated histones H3K9 and H3K14 (H3K9/14Ac). Increased H3K9/14Ac and SOX11 expression was also observed after histone deacetylase 1 (HDAC1) or HDAC2 was depleted by RNA interference or inhibited by the HDAC inhibitor vorinostat. Mechanistically, we showed that CCND1 interacted with and sequestered HDAC1 and HDAC2 from the *SOX11* locus, leading to SOX11 upregulation. Interestingly, our data revealed a potential inverse relationship between phosphorylated Y705 STAT3 and SOX11 expression in MCL cell lines, primary tumors, and patient-derived xenografts. Functionally, inactivation of STAT3 by inhibiting the upstream Janus kinase (JAK) 1 or JAK2 or by STAT3 knockdown was found to increase SOX11 expression, whereas interleukin-21 (IL-21)–induced STAT3 activation or overexpression of the constitutively active form of STAT3 decreased SOX11 expression. In addition, targeting SOX11 directly by RNA interference or indirectly by IL-21 treatment induced toxicity in SOX11$^+$ MCL cells. Collectively, we demonstrate the involvement of CCND1 and STAT3 in the regulation of SOX11 expression, providing new insights and therapeutic implications in MCL. (*Blood*. 2019;00(00):1-13)

Introduction

The high-mobility group neural transcription factor SOX11 is predominantly expressed in the developing brain and has critical roles in neurogenesis and embryonic development.[1-4] Although SOX11 is not expressed in normal B cells and does not seem to play a role in lymphopoiesis, its aberrant expression has been found in several lymphoproliferative diseases, including mantle cell lymphoma (MCL),[5-7] Burkitt lymphoma,[8] and B- and T-cell lymphoblastic leukemias.[7,8] SOX11 is also overexpressed in several types of solid tumors, including ovarian carcinoma,[9,10] basal-like breast carcinoma,[11,12] glioma,[13] medulloblastoma,[14] and prostate cancer.[15] In MCL, SOX11 is highly expressed in most classical cases with nodal presentation but is notably absent in indolent leukemic cases that display an IGVH-mutated phenotype.[16]

The role of SOX11 in MCL is incompletely understood. Previous studies have identified several direct targets of SOX11 in MCL, including DBN1, SETMAR, HIG2, and WNT signaling.[17,18] Subsequent studies have revealed that SOX11 is essential for MCL xenograft growth in vivo and directly mediates transcription of the B-cell transcription factor PAX5 and thus is thought to promote lymphomagenesis through deregulated B-cell differentiation.[19] SOX11 also mediates the expression of platelet-derived growth factor α,[20] C-X-C motif chemokine receptor 4, and focal adhesion kinase,[21] which promote angiogenesis, tumor-cell migration, and metastasis, respectively. Despite conflicting results regarding its prognostic value,[6,16,22] SOX11 is an established diagnostic marker for MCL.[7] In breast cancer, SOX11 is essential for proliferation and expression of a gene signature characteristic of aggressive basal-like breast cancer.[12]

Given the important biology of SOX11, several studies have investigated the mechanism of aberrant SOX11 expression. Gustavsson et al[23] demonstrated that although SOX11 is important

in developing neurons, its expression is virtually absent in other tissues because of promoter hypermethylation. Studies by Vegliante et al[24] showed that SOX11 expression in embryonic stem cells and some B-cell lymphomas was associated with unmethylated DNA and active histones H3K9/14Ac and H3K4me3. SOX11 can be induced in MCL and breast cancer cell lines after treatment with the histone deacetylase (HDAC) inhibitor vorinostat (also known as SAHA) or trichostatin A, suggesting that HDACs might participate in the regulation of SOX11 expression.[24,25] More recently, an elegant integrative analysis of the epigenome in primary MCL uncovered a distant regulatory element 675 kb downstream from the *SOX11* gene that seems to influence transcriptional activity at the *SOX11* promoter.[26] Using the circularized chromosome conformation capture sequencing method to detect long-range chromatin interactions, Queirós et al[26] demonstrated that this distant enhancer has 3-dimensional contact with the *SOX11* gene promoter, but how it affects SOX11 expression remains to be determined.

In this study, we investigated 2 potential mechanisms of SOX11 expression. By ectopically expressing CCND1 in human MCL cell lines, we demonstrate that CCND1 mediates SOX11 expression through interaction with HDAC1 and HDAC2 at the *SOX11* locus. In addition, using genetic and pharmacological inhibition, we show that the signal transducer and activator of transcription 3 (STAT3) binds to the *SOX11* promoter and enhancer, and functions as a transcriptional repressor. These findings demonstrate 2 distinct modes of SOX11 regulation and may have implications for the treatment of MCL.

Materials and methods

Cell lines and culture conditions

Human MCL lines Z-138, JEKO-1, UPN-1, and SP-53 were kindly provided by Dr Louis Staudt. GRANTA-519, JVM-2, MINO, and MAVER-1 cells were obtained from the American Type Culture Collection (Manassas, VA). MCL lines Z-138, JEKO-1, GRANTA-519, and UPN-1 were authenticated by short tandem repeat DNA profiling (American Type Culture Collection; supplemental Table 1). Other cell lines were not authenticated. Cells were cultured in RPMI 1640 medium, except GRANTA-519, which was cultured in Dulbecco's modified Eagle medium (Life Technologies, Grand Island, NY), supplemented with 10% fetal bovine serum, 100 IU/mL of penicillin, and 100 μg/mL of streptomycin, in a humidified incubator at 37°C with 5% carbon dioxide.

Primary MCL samples and PDXs

Primary cells were obtained from the tumor bank of the Pathology Department of City of Hope as deidentified samples after approval by the institutional review board and prepared as previously described.[27] Briefly, frozen cells were thawed in a 37°C water bath, washed in RPMI 1640 medium, and cultured in RPMI 1640 medium supplemented with 20% fetal bovine serum and 200 Kunits/mL of DNAse I (Sigma, St. Louis, MO) for 15 minutes in a 37°C carbon dioxide incubator followed by washing. Cells were recovered overnight in a carbon dioxide incubator before experiments. MCL patient–derived xenografts (PDXs) were obtained from the public repository of xenografts (ProXe[28]; supplemental Table 2). Samples were transplanted into sublethally irradiated NOD.Cg-Prkdc^{scid}Il2rg^{tm1Wjl}/SzJ mice (The Jackson Laboratory, Bar Harbor, ME) through tail vein injection. Lymphoma xenografts were frozen in aliquots and subsequently thawed and cultured in RPMI 1640 medium supplemented with 20% fetal bovine serum, 100 IU/mL of penicillin, and 100 μg/mL of streptomycin in a humidified incubator at 37°C with 5% carbon dioxide.

cDNA expression vectors

The retroviral expression vector pBMN-CCND1-HA-IRES-Hygro, encoding carboxy-terminus hemaglutinin (HA)–tagged wild-type (WT) or mutant CCND1, was previously constructed.[27] HDAC-HA constructs were a kind gift from Dr. Yue Xiong (University of North Carolina, Chapel Hill), as previously described.[29] FLAG-tagged SOX11 expression vector was constructed by cloning the polymerase chain reaction (PCR)–generated SOX11 products from a Z-138–derived complementary DNA (cDNA) template into the pBMN-IRES-Hygro vector (a gift from Gary Nolan) at *Bam*HI and *Xho*I restriction sites. FLAG-SOX11 PCR products were generated using the following primer pairs: 5′TAGTAGGGATCCGCCGCCACCATGGACTACAAAGACGATGACGACAAGGTGCAGCAGGCGGAGAGCTTG and 5′CTACTACTCGAGTCAATATGTGAACACCAGGTCGGAGAA. The final SOX11 construct was confirmed by DNA sequencing. The lentiviral STAT3 constitutive active construct EF.STAT3C.Ubc.GFP was a gift from Linzhao Cheng (Addgene plasmid #24983), and its retroviral subclone was a gift from Lixin Rui.

RNA interference reagents

CCND1 and HDAC1 short hairpin RNA (shRNA) constructs and sequences were obtained from a previously generated shRNA library.[30] STAT3 shRNA (#840) pKLO construct was kindly provided by Anna Scuto as previously reported.[31] SOX11 shRNA (#454) and HDAC2 shRNA (#1678) pKLO constructs were obtained from Sigma (Sigma, St. Louis, MO). RNAi sequences are listed in supplemental Table 3. A DNA insert encoding a fusion puromycin N-acetyl-transferase–green fluorescence protein was cloned into the SOX11 shRNA pKLO vector at the *Bam*HI and *Kpn*I restriction sites to produce a green fluorescence protein–coexpressing vector.

Quantitative real-time PCR

Quantitative real-time PCR (qPCR) reactions were performed using RT^2 SYBR Green qPCR Master Mix (Qiagen, Valencia, CA) or Taqman Universal PCR Master Mix (Thermo Fisher Scientific, Waltham, MA) and analyzed by the StepOnePlus Real-Time PCR System (Life Technologies, Grand Island, NY). Because SOX11 is encoded by an intronless gene, in addition to DNAse treatment before cDNA synthesis, a poly-A–specific primer for SOX11[32] was used to minimize amplification of potential genomic DNA (gDNA) contamination. As a negative control, mock cDNA synthesis without addition of reverse transcriptase was also prepared to verify the presence of contaminating gDNA. We demonstrated that the cycle threshold (Ct) values for the poly-A–specific SOX11 primer in reverse transcription (RT)–positive cDNA samples were consistently >10 cycles fewer than those in mock cDNA samples (Ct, 24 vs 39; supplemental Table 4). Additional primers that can amplify SOX11 or glyceraldehyde-3-phosphate dehydrogenase (GAPDH) from gDNA also yielded similarly large differences in Ct values between RT$^+$ and mock cDNA samples (Ct, 25 vs 36 and 23 vs 39, respectively; supplemental Table 4). These results confirm the validity of our messenger RNA (mRNA) assessment using either SOX11 primer. Primer sequences for SOX11 and GAPDH are shown in

supplemental Table 5. Taqman probes for SOX11 (Hs00848583_s1), STAT3 (Hs00374280_m1), HDAC1 (Hs02621185_s1), and GAPDH (Hs02786624_g1) were purchased from Thermo Fisher. Relative mRNA expression was normalized to GAPDH signals and calculated using the ΔΔCt method.

Immunoblot and immunoprecipitation analyses

Cells were lysed in the presence of protease inhibitor cocktail (Sigma, St. Louis, MO) and Halt phosphatase inhibitor cocktail (Pierce Biotechnology, Rockford, IL) for 30 minutes. Lysates were cleared by centrifugation, and protein concentrations were determined by BCA protein assay (Pierce Biotechnology, Rockford, IL). Twenty micrograms of lysates per lane were separated by 4% to 15% sodium dodecyl sulfate polyacrylamide gel electrophoresis and immobilized on the nitrocellulose membranes (ThermoFisher, Waltham, MA) for immunoblotting. Immunoblot signals were developed by a chemiluminescent detection method (Pierce Biotechnology, Rockford, IL) and captured by standard autoradiographic films. Immunoprecipitation details are provided in supplemental Methods.

Chromatin immunoprecipitation

Chromatin immunoprecipitation was performed using the ChIP Assay Kit (Millipore, Temecula, CA) according to manufacturer's instructions. Details are described in supplemental Methods.

Statistical analyses

A 2-tailed Student *t* test or linear regression analysis was performed for comparison between 2 groups using Prism (version 6.0b; GraphPad Software, La Jolla, CA). *P* values $<.05$ were considered statistically significant.

Additional detailed method descriptions are available in supplemental Materials.

Results

CCND1 upregulates SOX11 expression in human MCL cell lines

To determine whether CCND1 induces SOX11, HA-tagged CCND1 was ectopically expressed in the human MCL lines Z-138, JEKO-1, and GRANTA-519. The recurrent mutation CCND1 Y44D, which affects phosphorylation-dependent proteolysis and results in increased protein levels,[27] was also expressed in Z-138 and JEKO-1 cells. Compared with empty vector controls, both WT and mutant CCND1 increased protein expression levels of SOX11 in these cell lines by immunoblot analysis (Figure 1A; supplemental Figure 1A). To ensure the specificity of the SOX11 antibody used in the current study, depletion or overexpression of SOX11 was carried out in MCL cell lines, and specific loss or increase in SOX11 expression was confirmed by immunoblot analysis (supplemental Figure 2A-B). We next used RT-PCR assays to determine whether CCND1 mediated SOX11 transcription. Because SOX11 is encoded by an intronless gene, we used an mRNA-specific RT-PCR assay (see "Materials and methods") and demonstrated that overexpression of WT or mutant CCND1 increased SOX11 mRNA levels in these cell lines (Figure 1B; supplemental Figure 1B).

To determine whether CCND1 is required for SOX11 expression, we depleted CCND1 in MCL cells using an shRNA validated in a previous study.[33] CCND1 depletion in both Z-138 and JEKO-1 cells resulted in reduced SOX11 protein levels (Figure 1C), in addition to decreased cell viability (Figure 1D) similar to that previously observed in JEKO-1 cells.[33] Depletion of SOX11 also resulted in reduced cell viability in Z-138, JEKO-1, and an additional MCL line, MINO (Figure 1E). We next determined whether SOX11 upregulation was due to altered protein stability by treating CCND1-HA–expressing Z-138 cells with CHX and assessing SOX11 protein turnover by immunoblot analysis. In this experiment, WT and mutant CCND1 samples consistently expressed more SOX11 than empty vector controls before CHX treatment (Figure 1F). However, the rate of SOX11 protein turnover in WT and mutant CCND1 samples was comparable to that of controls after 3 hours in CHX (Figure 1F). This result excluded increased protein stability as a mechanism of increased SOX11 expression. Together, these data suggest a role for CCND1 in the regulation of SOX11 expression in MCL cell lines.

CCND1 affects histone modification at the *SOX11* locus

Because SOX11 transcription is associated with histone acetylation,[24,25] we performed chromatin immunoprecipitation (ChIP) and qPCR assays to examine whether CCND1 influences histone modification at the *SOX11* locus. To determine the chromatin regions on the *SOX11* gene that are likely reactive to the active histone mark H3K9/14Ac antibody, we searched for H3K9Ac ChIP signals in SOX11-expressing cells in the ENCODE database and identified 2 potential DNA regions for PCR amplification (amplicons; Figure 2A). ChIP-qPCR experiments were carried out in Z-138 and JEKO-1 cells that overexpress CCND1 using a previously validated H3K9/14Ac antibody and PCR primers for the 2 amplicons.[24] Compared with empty vector controls, overexpression of CCND1 significantly increased H3K9/14Ac signals in both cell lines (Figure 2B-E). Enrichment of H3K9/14Ac at the *SOX11* locus was also observed in Z-138 cells treated with HDAC inhibitor SAHA (Figure 2F). In addition, SOX11 expression was positively correlated with H3K9/14Ac levels after treatment with SAHA in Z-138 cells (Figure 2G). Therefore, these data indicate that CCND1 mediates SOX11 expression through histone acetylation at the *SOX11* locus.

CCND1 interacts with HDAC1 and HDAC2

The effects of CCND1 overexpression and HDAC inhibition on histone acetylation of the *SOX11* locus led us to examine whether CCND1 physically associates with members of the HDAC family to mediate SOX11 transcription. We coexpressed individual HDACs with CCND1 in HEK-293T cells and analyzed potential interactions using coimmunoprecipitation. Figure 3A shows that CCND1 strongly interacts with HDAC1, HDAC2, and to a lesser extent HDAC3, but not with other HDAC members. Validation of this interaction in Z-138 cells or in primary MCL samples by immunoprecipitation with CCND1 or HDAC1 antibody also showed CCND1 in the complex with HDAC1 and HDAC2 (Figure 3B). In addition, shRNA-mediated depletion of HDAC1 from Z-138, JEKO-1 (Figure 3C; supplemental Figure 3A), or GRANTA-519 (supplemental Figure 3B-C) cells resulted in increased SOX11 mRNA and protein levels, further confirming the role of HDAC1 in modulating SOX11 expression. Increased SOX11 expression was also observed when HDAC2 was depleted in Z-138 and JEKO-1 cells (Figure 3D). Together,

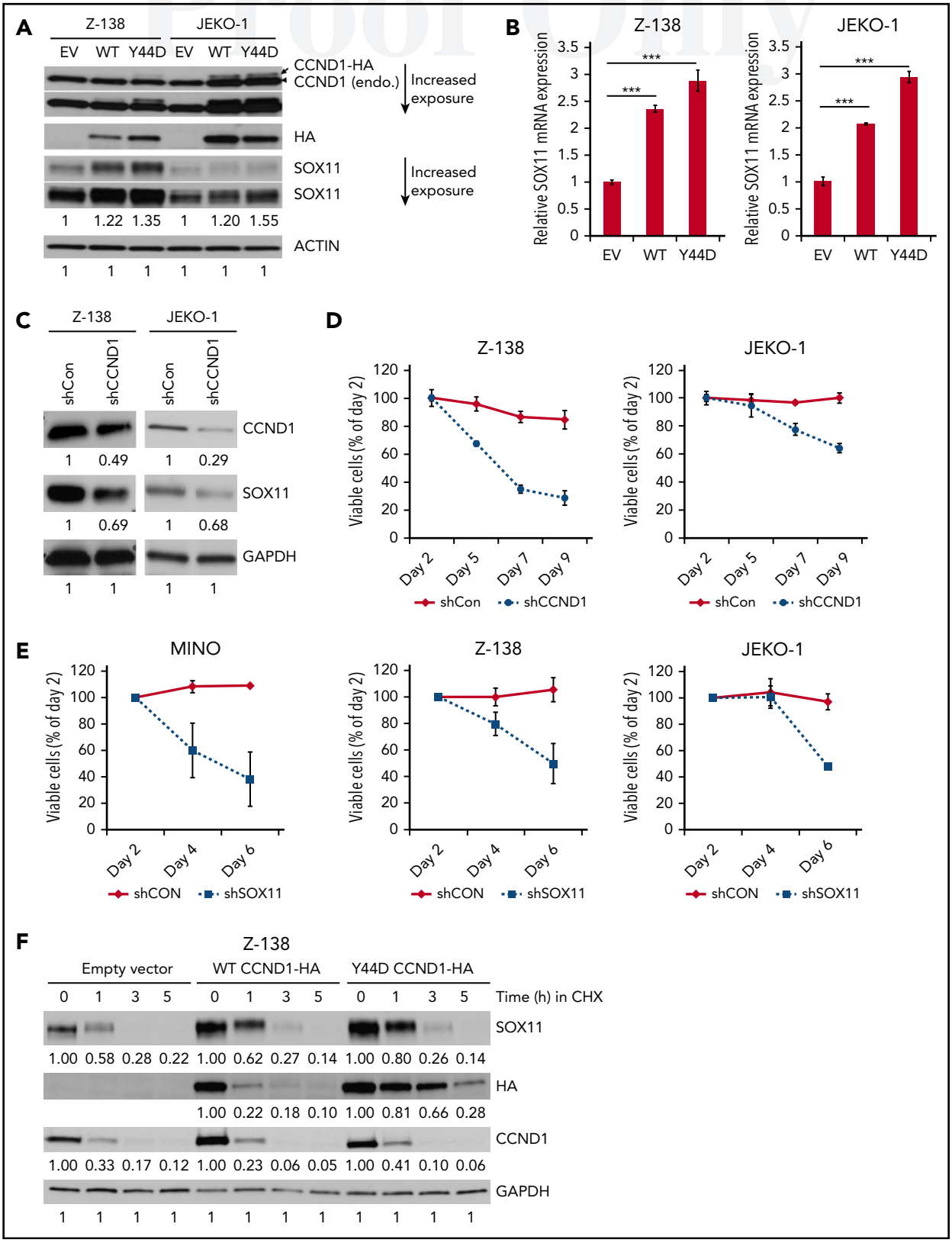

Figure 1. CCND1 upregulates SOX11 expression. (A) Immunoblot analysis of Z-138 and JEKO-1 cells stably transduced with empty vector (EV), WT, or Y44D mutant CCND1-HA constructs. Cell lysates (30 μg per lane) were separated by sodium dodecyl sulfate polyacrylamide gel electrophoresis gel and immunoblotted with indicated antibodies. Arrow indicates a mobility shift of the CCND1-HA protein. Arrowhead indicates endogenous CCND1. (B) qPCR analysis of SOX11 mRNA expression. Cell lines generated as described in panel A, and mRNAs were harvested for SOX11 qPCR. Shown are the means of mRNA expression levels after normalization to GAPDH signals from 4 independent amplification experiments. Error bars, standard deviation (supplemental Figure 1A-B). (C) CCND1 is required for SOX11 expression. Z-138 and JEKO-1 cells were stably transduced with control or CCND1 shRNA, and protein expression was analyzed by immunoblotting with indicated antibodies 2 days after transduction.

these results indicate that interaction of CCND1 with HDAC1 and HDAC2 plays a role in mediating SOX11 expression.

Reduced chromatin recruitment of HDAC1 in CCND1-overexpressing cells

We next asked whether CCND1 affected recruitment of HDAC1 at the *SOX11* locus. ChIP-qPCR assays were performed in CCND1-overexpressing Z-138 cells using anti-HDAC1 antibody and PCR primers located near the *SOX11* transcription start site. HDAC1 ChIP signals were significantly reduced in CCND1-expressing cells as compared with empty vector controls (Figure 4A). As an alternative approach, cell fractionation was used to assess the distribution of HDAC1 and HDAC2 within cellular compartments. Protein extracts from soluble cytoplasmic and nuclear fractions, as well as from insoluble nuclear fractions, from equal numbers of control and CCND1-overexpressing Z-138 cells were evaluated by immunoblot analysis. Nuclear proteins histone H3 and LAMIN A and C were used as markers for the nuclear fractions. We found that both HDAC1 and HDAC2 resided predominantly in the insoluble nuclear fraction in the empty vector controls. However, in cells with CCND1 overexpression, there was increased accumulation of HDAC1 and HDAC2 in the soluble nuclear fraction (Figure 4B). Similar increase of HDAC1 and HDAC2 protein levels in the soluble nuclear fraction was also observed in GRANTA-519 cells that overexpressed CCND1 (supplemental Figure 4). Taken together, these results indicate that CCND1 overexpression results in redistribution of HDAC1 and HDAC2 from the chromatin environment, including the chromatin of the *SOX11* gene.

STAT3 negatively regulates SOX11 expression

To further confirm the positive role of CCND1 in regulating SOX11 expression, we transduced CCND1-expressing lentivirus into the SOX11$^-$ MCL cell line JVM-2. Surprisingly, compared with an increase in SOX11 levels in JEKO-1 cells, ectopically expressed CCND1 did not induce SOX11 in JVM-2 cells (Figure 5A). Analysis of publicly available gene expression data from SOX11$^+$ and SOX11$^-$ MCL cases[34] also revealed no correlation between SOX11 and CCND1 (Figure 5B). However, a positive correlation between CCND1 and SOX11 was observed in SOX11$^+$ cases, although it was not statistically significant because of a small sample size (n = 15; supplemental Figure 5A). Analysis of relevant public data from another study,[16] in which SOX11 positivity was identified in 13 cases, also showed a positive correlation between CCND1 and SOX11, although again not statistically significant (supplemental Figure 5B).

These observations prompted us to investigate additional mechanisms of SOX11 regulation. Because SOX11$^-$ MCL cases typically have plasmacytic differentiation,[16,35] we hypothesized that SOX11 transcription might be negatively regulated during B-cell differentiation. To identify the molecules potentially involved in this process, we analyzed transcription factors that bind to the *SOX11* locus, including the recently identified *SOX11* enhancer,[26] using ChIP sequencing data from the ENCODE project.[36] Among *SOX11* locus–bound factors, STAT3 was chosen for further study because of its role in B-cell differentiation.[37] Interestingly, expression of SOX11 and the active phosphorylated Y705 (pY705) STAT3 were inversely correlated in MCL cell lines (except JEKO-1; Figure 5C), in primary MCL samples (except samples #11 and #15; Figure 5D), and in MCL PDXs (Figure 5D). To determine whether SOX11 is negatively regulated by activated STAT3, we treated JEKO-1, GRANTA-519, MAVER-1, and JVM-2 cells, which express high pY705 STAT3 levels, with AZD1480, an inhibitor of the upstream kinases JAK1 and JAK2.[38] Immunoblot analysis showed that AZD1480 effectively blocked STAT3 phosphorylation and resulted in increased SOX11 mRNA and protein levels in JEKO-1, GRANTA-519, and MAVER-1 cells (Figure 5E-F), but not in JVM-2 cells (supplemental Figure 6A). Similar increases in SOX11 expression were also observed in GRANTA-519 cells after treatment with another STAT3 inhibitor, JAK inhibitor I (MilliporeSigma, Burlington, MA; supplemental Figure 6B). AZD1480-induced upregulation of SOX11 was mediated by STAT3 inhibition, because depletion of STAT3 also led to increased SOX11 mRNA and protein expression in both JEKO-1 and GRANTA-519 cells (Figure 5G-H).

In line with the repressive role of STAT3, interleukin-21 (IL-21) induced STAT3 activation[39] in MINO, SP-53, Z-138 (Figure 6A-B), and MCL PDX models (Figure 6C) or ectopic expression of a constitutively active form of STAT3[40] in Z-138 cells (supplemental Figure 7) resulted in reduced SOX11 expression. Interestingly, IL-21 also reduced viability of MCL lines (MINO, SP-53, and Z-138) or PDX models (#5 and #7) with low or negative STAT3 activity (Figure 6D-E), whereas it had little effect on MCL cells with high pY705 STAT3 expression (JEKO-1, MAVER-1, and GRANTA-519; supplemental Figure 8). Because depletion of SOX11 also reduced cell viability in MINO, Z-138, and JEKO-1 cells (Figure 1E), we depleted SOX11 from the remaining MCL lines and determined their survival. We found that SOX11 depletion had little effect on the viability of GRANTA-519 cells and slightly increased cell growth in MAVER-1 cells (supplemental Figure 9A-B). Data from SP-53 cells were not available because of the sensitivity of this cell line under our lentiviral transduction conditions. Therefore, similar to IL-21 treatment, SOX11 depletion is toxic in MINO and Z-138 cells, whereas it has little effect in GRANTA-519 and MAVER-1 cells. JEKO-1 cells seem to be an exception, because they are resistant to IL-21 but sensitive to SOX11 depletion.

We next determined whether STAT3 was recruited directly to the *SOX11* gene by performing ChIP-qPCR experiments with an anti-pY705 STAT3 antibody in JEKO-1 cells. Because STAT3 phosphorylation is required for DNA binding[41] and this phosphorylation is efficiently inhibited by AZD1480, we used AZD1480-treated JEKO-1 cells as a negative control for the

Figure 1 (continued) (D) Effect of CCND1 knockdown on cell survival. Z-138 and JEKO-1 cells were stably transduced with control or CCND1 shRNA, and propidium iodide (PI)–negative (viable) cells were assessed by flow cytometry over time. Shown are the means of PI$^-$ fractions compared with day-2 samples from at least 2 independent experiments. (E) Effect of SOX11 knockdown on MCL survival. Indicated MCL cell lines were transduced with control or SOX11 shRNA lentiviral vector that coexpresses GFP. Shown are the means of GFP$^+$ fractions compared with day 2 from 2 independent experiments. (F) Z-138 cells expressing EV, WT, or Y44D CCND1-HA were treated with 10 μM of cycloheximide (CHX) for indicated times, and cell lysates were prepared for immunoblot analysis with indicated antibodies. Numbers below immunoblots are relative densitometric values of corresponding bands after normalization to ACTIN or GAPDH and respective control signals. ***$P < .001$ by 2-sided Student t test.

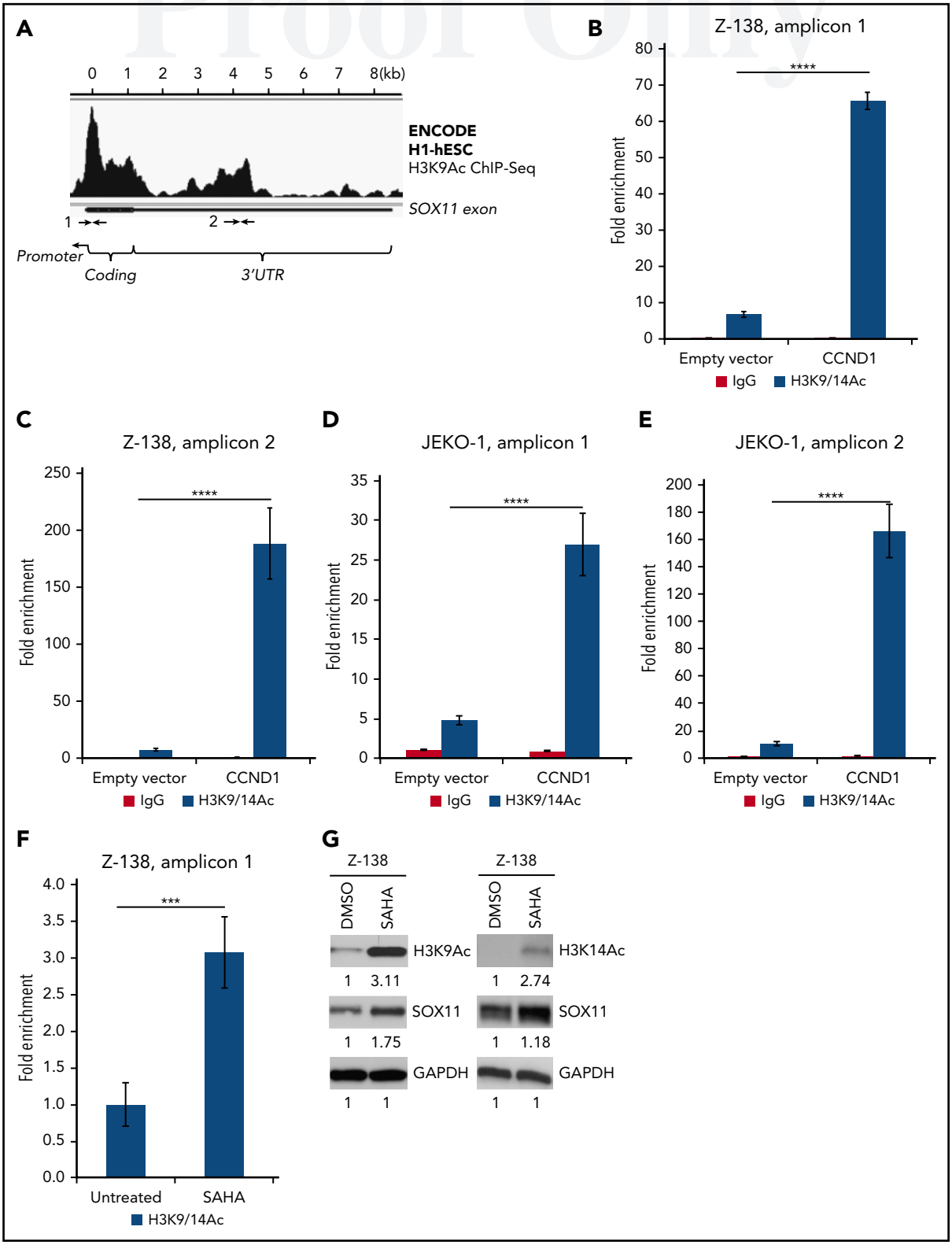

Figure 2. CCND1 affects histone modifications at the *SOX11* locus. (A) ENCODE H3K9Ac ChIP sequencing (seq) data for H1-hESC cells show *SOX11* gene regions that have positive ChIP peak signals. Arrows indicate regions where PCR primers were designed. (B-F) H3K9/14Ac chromatin immunoprecipitation assays for the *SOX11* gene from indicated cells stably transduced with empty vector or CCND1 (B-E) or treated with 1 μM of SAHA for 16 hours (F). Bar graphs show means of qPCR signals of DNA region 1 or 2 (amplicons 1 and 2) pulled down by the H3K9/14Ac antibody as fold enrichment relative to the background signals from the isotype control immunoglobulin G (IgG) antibody. Error bars, standard deviation. (G) Immunoblot analysis of Z-138 cells treated with 2 μM of SAHA for 3 h and immunoblotted with indicated antibodies. ***$P < .001$, ****$P < .0001$ by 2-sided Student *t* test. DMSO, dimethyl sulfoxide; UTR, untranslated region.

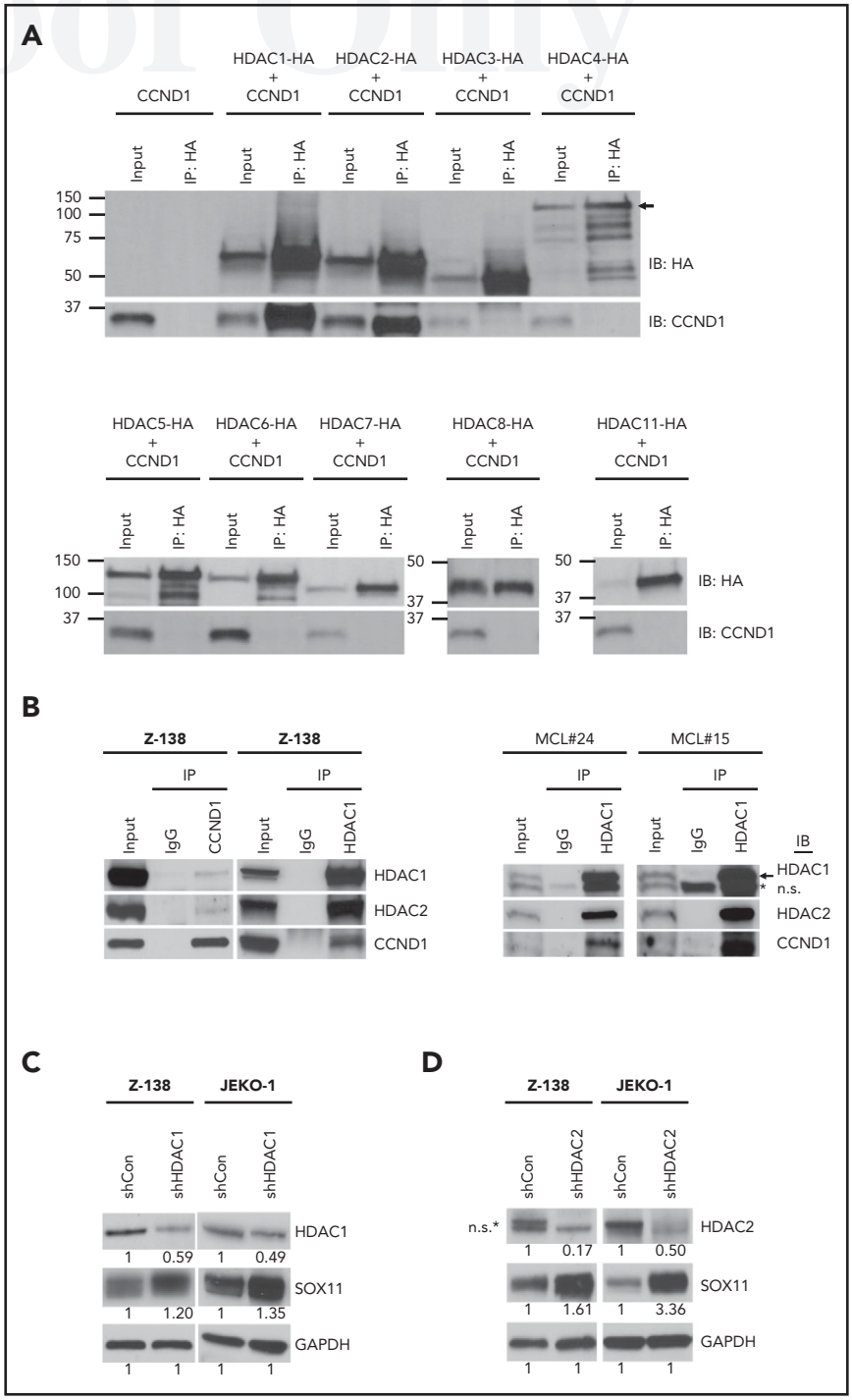

Figure 3. CCND1 interacts with HDAC1 and HDAC2. (A) HEK-293T cells were transiently cotransfected with untagged CCND1 and individual HA-tagged HDACs and immunoprecipitated (IP) with HA antibody followed by immunoblotting (IB) with indicated antibodies. Lysates before immunoprecipitation were used as input samples. Arrow indicates specific bands for HDAC4-HA. (B) Z-138 cells or primary MCL samples were immunoprecipitated with isotype control immunoglobulin G (IgG), CCND1, or HDAC1 antibody and immunoblotted with indicated antibodies. Lysates before immunoprecipitation were used as input samples. Arrow indicates specific HDAC1 staining. (C-D) Z-138 and JEKO-1 cells were stably transduced with control, HDAC1 (C), or HDAC2 (D) shRNA, and protein expression was analyzed by immunoblot analysis with indicated antibodies 3 days after transduction (~~supplemental Figure 3A-C~~). *Non-specific bands. n.s., ~~not significant~~.

Q:10

pY705 STAT3 ChIP-qPCR experiments. Figure 7A shows that pY705 STAT3 was specifically recruited to the *SOX11* gene and enhancer, and this recruitment was significantly impaired after AZD1480 treatment. Increased active histone H3K9/14Ac signals at the *SOX11* promoter and enhancer regions were also observed in AZD1480-treated MAVER-1 cells using H3K9/14Ac ChIP-qPCR (Figure 7B). Taken together, these findings indicate that STAT3 represses SOX11 transcription through recruitment of pY705 STAT3 to the *SOX11* locus and that manipulation of the STAT3-SOX11 axis directly through SOX11 or indirectly through STAT3 induces toxicity in SOX11$^+$ MCL cells.

Discussion

The current study reveals 2 distinct regulatory mechanisms of SOX11 expression in MCL, specifically through CCND1 and STAT3. By genetically manipulating CCND1 levels using ectopic expression and gene knockdown, we have demonstrated that CCND1 is sufficient and necessary for SOX11 expression in the MCL cell lines Z-138, JEKO-1 and GRANTA-519. SOX11 expression is also negatively regulated by the post–germinal center B-cell differentiation factor STAT3, which may link SOX11 regulation to specific stages of B-cell differentiation.

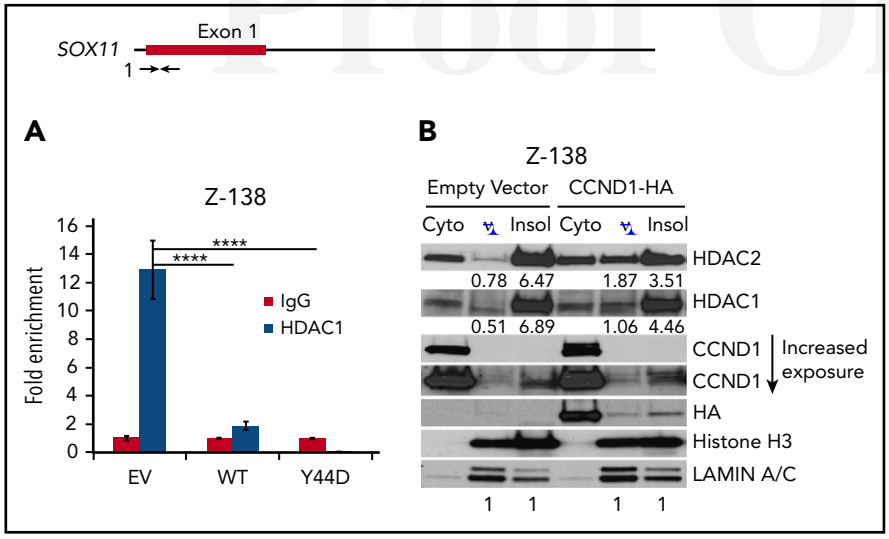

Figure 4. Reduced chromatin localization of HDAC1 in CCND1 overexpressing cells. (A) Chromatin immunoprecipitation assays for the *SOX11* gene from Z-138 cells stably transduced with empty vector (EV), WT, or mutant Y44D CCND1. Bar graphs show means of quantitative PCR signals of region 1 (amplicon 1) pulled down by the HDAC1 antibody as fold enrichment relative to the background signals from the isotype control immunoglobulin G (IgG) antibody. Error bars, standard deviation. (B) Cytosolic, soluble, and insoluble nuclear extracts were prepared as described in "Materials and methods" from Z-138 cells that stably expressed empty vector or WT CCND1-HA. The extracts were immunoblotted with indicated antibodies. LAMIN A/C and histone H3 were used to confirm nuclear fractions (~~supplemental Figure 4~~). ****$P < .0001$ by 2-sided Student *t* test. cyto, cytoplasmic; sol, soluble nuclear fraction; insol, insoluble nuclear fraction.

Q:11

In our proposed model, CCND1 interacts with and sequesters HDAC1 and HDAC2 from regulatory elements in the *SOX11* locus, leading to increased histone acetylation and *SOX11* transcription (Figure 7C). The ability of CCND1 to associate with transcriptional regulators and affect gene transcription is well recognized.[42] Fu et al[43] demonstrated that CCND1 preferentially associates with HDAC1, HDAC2, HDAC3, and HDAC5 and recruits HDAC1 to the *PPAR-γ* promoter to repress its transcription. We found that CCND1 consistently binds to HDAC1 and HDAC2 and, to a lesser extent, HDAC3, but not other HDAC members (Figure 3A). In contrast to transcriptional repression as a consequence of HDAC1 recruitment to the gene promoter as reported by Fu et al,[43] we have shown that elevated CCND1 levels in MCL cells result in reduced HDAC1 recruitment at the *SOX11* promoter and subsequent increased gene transcription. Mechanisms of gene expression through HDAC1 relocation from transcriptional regulators have been described. For example, Di et al[44] reported that treatment with estrogen or the glycolysis inhibitor 2-deoxyglucose in the breast cancer cell line MCF-7 caused eviction of HDAC1 from a corepressor complex, leading to increased histone acetylation at the *BRCA1* promoter and *BRCA1* transcription. In another study focusing on developing neurons, expression of Lmo4 led to displacement of Hdac1 from the transcriptional repressor complex NuRD, resulting in derepression of the Ctip2 locus.[45] Together, these observations support the removal of HDAC1 from regulatory elements as a common mechanism and indicate that diverse signals can mediate this process depending on the cellular context. In line with this notion, we speculate that in addition to CCND1, other abnormalities that interfere with HDAC1 function may also contribute to SOX11 expression. Characterization of new mutations, particularly those affecting HDAC1-interacting proteins, may provide further insight into the mechanisms of deregulated SOX11 expression.

Although our data favor CCND1-mediated HDAC1 sequestration as the mechanism of SOX11 upregulation, it is possible that CCND1 may influence SOX11 transcription by affecting enzymes that maintain the dynamic histone acetylation/deacetylation equilibrium, such as the histone acetyl-transferases EP300, PCAF, and GCN5. Indeed, CCND1 has been shown to physically associate with EP300[46] and PCAF[47] and regulate gene expression. Furthermore, through its cyclin-dependent kinase (CDK) partners CDK4 and CDK6, CCND1 elicits transcriptional changes by phosphorylating and activating GCN5.[48] In the current study, we found that treating MCL cell lines with the EP300 inhibitor C646 strongly downregulated SOX11 expression (supplemental Figure 10), consistent with involvement of EP300 in regulating SOX11 expression. These observations warrant additional studies into the molecular interactions between CCND1 or the CCND1/CDK4 complex and transcriptional regulators at the *SOX11* promoter.

Although ectopic expression of CCND1 can induce SOX11 expression in multiple MCL lines, SOX11 is not expressed in a subset of t(11;14)$^+$ MCL cases[16] or in any t(11;14)$^+$ multiple myeloma (MM) cases.[49] These observations suggest that SOX11 expression is regulated by additional factors and/or cellular contexts. To investigate additional mechanisms of SOX11 expression, we turned to a recent study profiling the methylome of MCL. In that study, Queirós et al[26] found a potential SOX11 regulatory element 675 kb downstream of the *SOX11* gene that was hypomethylated and associated with the active enhancer mark H3K27ac in SOX11$^+$, but not in SOX11$^-$, MCL cells. We then examined the transcription factors that are associated with this putative enhancer, as previously reported by the ENCODE project.[36] Among factors that bind to this enhancer, we focused on STAT3 as a potential repressor of SOX11, because STAT3 is important for post–germinal center B-cell differentiation,[37] a commonly recognized phenotype of SOX11$^-$ MCL.[16,19] Indeed, our data revealed that STAT3 is recruited to both *SOX11* gene and enhancer loci and functions as a transcriptional repressor in multiple MCL lines, including JEKO-1, GRANTA-519, and MAVER-1. Our findings are consistent with previous reports that showed constitutively active STAT3 in a majority (70%) of indolent leukemic MCL cases,[50] which do not express SOX11.[16] As mentioned, t(11;14)$^+$ MM is another example of the inverse correlation of STAT3 activation and SOX11 expression, because a majority of MM cases show constitutive activation of STAT3.[51] Our data, however, do not exclude additional mechanisms of SOX11 regulation, because nonconcordant cases do exist, including JEKO-1, MCL #15 and MCL #24 (pY705 STAT3$^+$, SOX11$^+$), and MCL #11 (pY705 STAT3$^-$, SOX11$^-$). Similarly, although AZD1480 effectively reduced pY705 STAT3 levels in JVM-2 cells, little SOX11 induction was observed, implicating a repressive

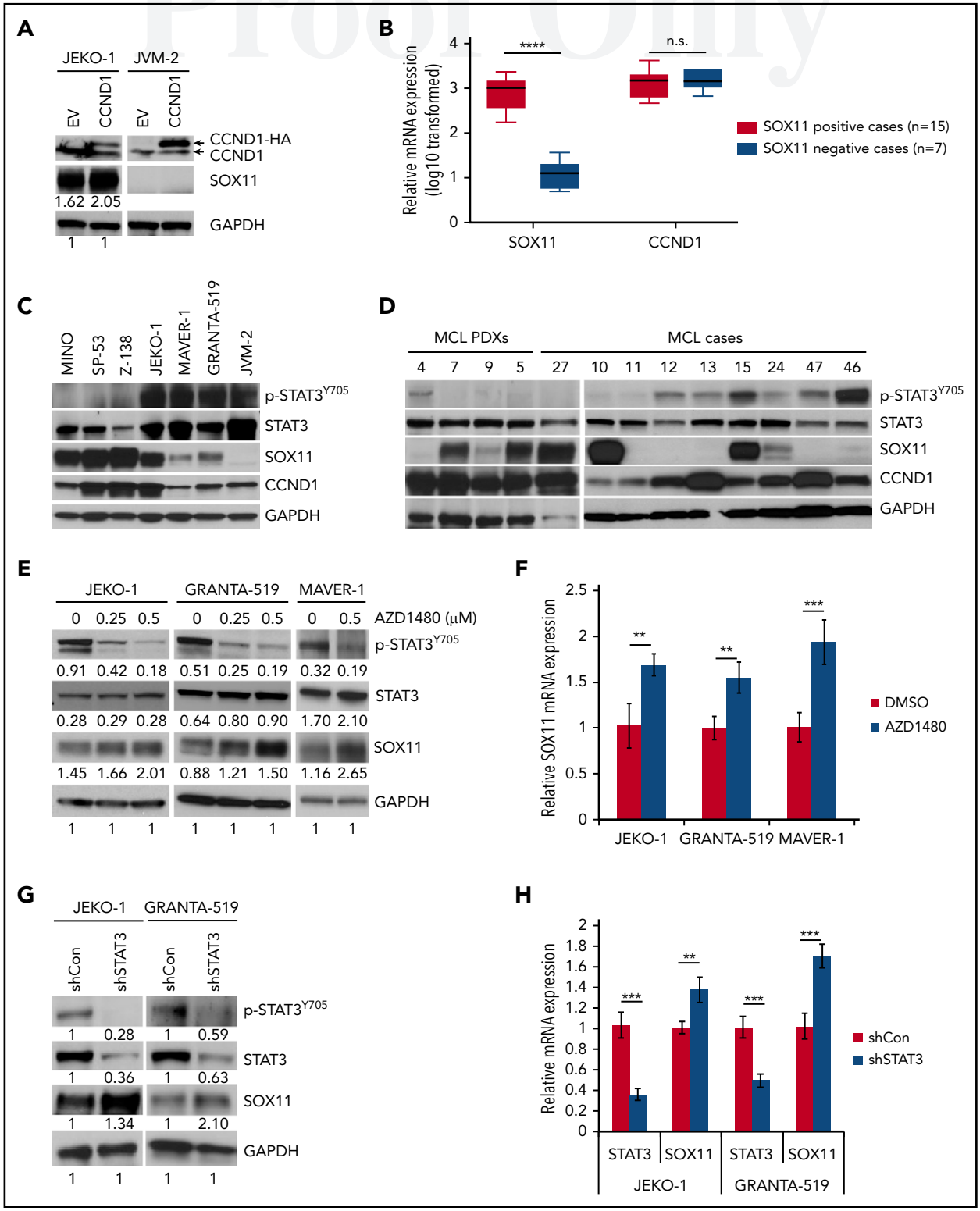

Figure 5. STAT3 negatively regulates SOX11 expression. (A) JEKO-1 and JVM-2 cells were transduced with empty vector (EV) or CCND1-HA, and cell lysates were immunoblotted with indicated antibodies. (B) Box plots of relative SOX11 and CCND1 mRNA expression in primary MCL cases. Gene expression data for SOX11 and CCND1 were obtained from GSE16455[34] (supplemental Table 6; ~~supplemental Figure 5A~~) and plotted using GraphPad Prism v7.0a. (C-D) Immunoblot analysis of MCL cell lines (C) or MCL PDXs and primary MCL cases (D) with indicated antibodies. (E) Indicated MCL cell lines were treated with indicated doses of the JAK1/2 inhibitor AZD1480 for 16 hours and immunoblotted with indicated antibodies (~~supplemental Figure 6A-B~~). (F) Indicated MCL cell lines were treated with AZD1480 as in panel E, and SOX11 mRNA was analyzed by qPCR. Shown are the means of mRNA expression levels after normalization to GAPDH signals from 4 independent amplification experiments. (G) JEKO-1 or GRANTA-519 cells were transduced with control or STAT3 shRNA, and protein lysates were prepared for immunoblot analysis with indicated antibodies. (H) Indicated MCL lines were treated with 500 nM of AZD1480 for 16 hours, and SOX11 mRNA was analyzed by qPCR. Bar graphs show the means of mRNA expression levels after normalization to GAPDH signals from 4 independent amplification experiments. Error bars, standard deviation. $^{**}P < .01$, $^{***}P < .001$, $^{****}P < .0001$ by 2-sided Student *t* test. n.s. non-significance.

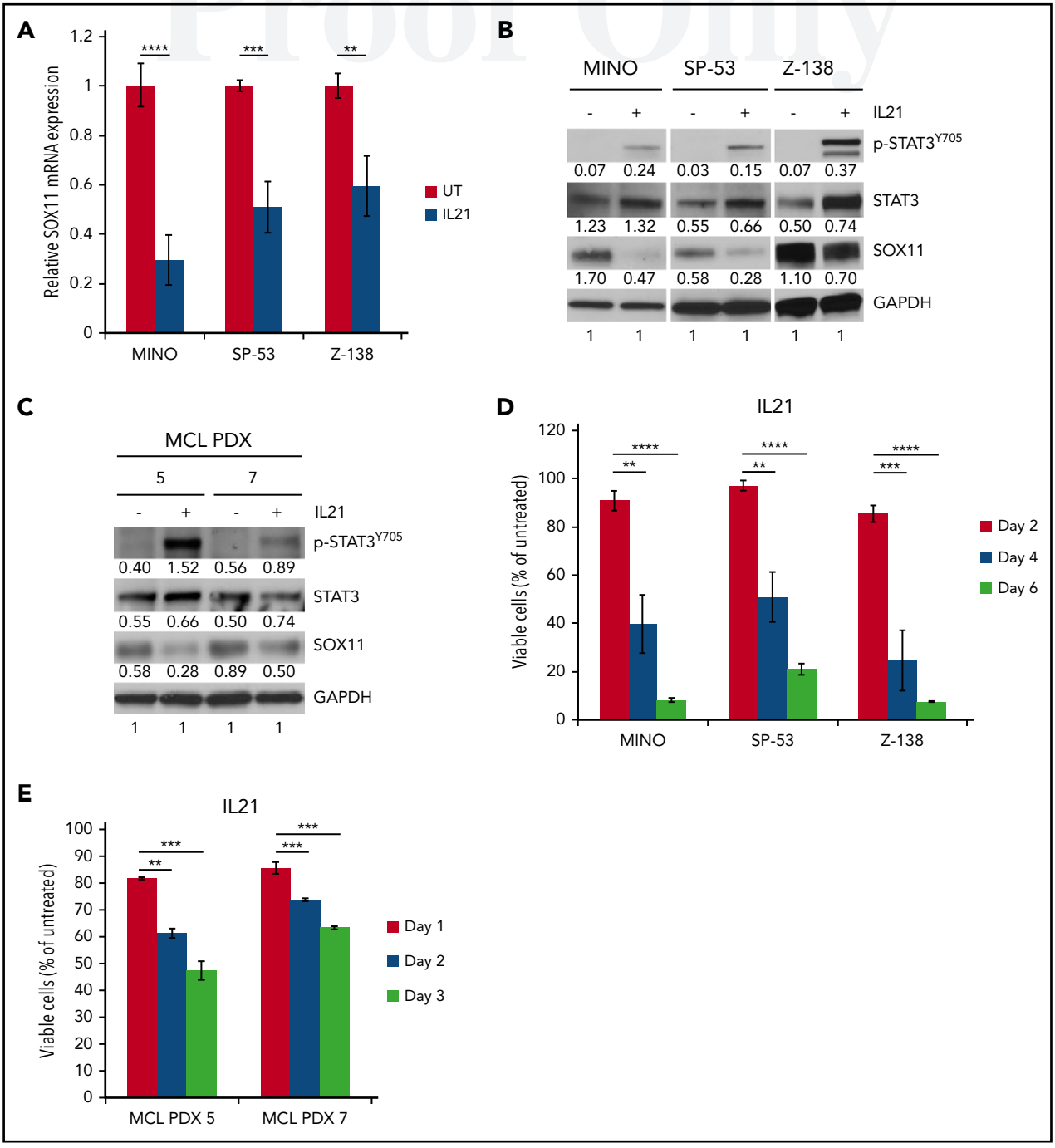

Figure 6. Effects of IL-21 on STAT3 activity, SOX11 expression, and cell viability in MCL cells. (A) Indicated MCL cell lines were treated with 50 ng/mL of IL-21 for 96 hours, and SOX11 mRNA was analyzed by qPCR. Shown are the means of mRNA expression levels after normalization to GAPDH signals from 4 independent amplification experiments. (B) Immunoblot analysis of indicated MCL cell lines treated as described in panel A. (C) Immunoblot analysis of MCL PDX models treated with 50 ng/mL of IL-21 for 72 hours. (D) Indicated MCL cell lines were treated with 50 ng/mL of IL-21, and viable cells (propidium iodide (PI) negative) were assessed by flow cytometry at indicated times. Shown are the means of PI^- fractions compared with untreated samples from at least 2 independent experiments. (E) MCL PDX cells were treated with IL-21, and viable cells were analyzed as in panel D for the indicated times. Shown are the means of PI^- fractions compared with untreated samples from at least 2 independent experiments. Error bars, standard deviation. $^{**}P < .01$, $^{***}P < .001$, $^{****}P < .0001$ by 2-sided Student *t* test.

mechanism other than pY705 STAT3 (supplemental Figure 6A). The Epstein-Barr virus–positive status of JVM-2 cells unlikely contributed to the lack of AZD1480-induced SOX11 expression, because Epstein-Barr virus–positive GRANTA-519 cells readily upregulated SOX11 expression after STAT3 inhibition (Figure 5E-F; supplemental Figure 6B). It is possible that mutations affecting SOX11 transcriptional machinery exist in MCL cells with little STAT3 activity. In support of this notion, many MCL tumors, including JVM-2 cells, were found to harbor frameshift mutations[52-54] that affect mixed-lineage leukemia genes *MLL2* and/or *MLL4*, which encode enzymes that methylate H3K4 and positively regulate gene transcription.[55] Confirmation of these mutations and elucidation of the underlying mechanisms that regulate SOX11 expression are therefore warranted. In addition, potential crosstalk between

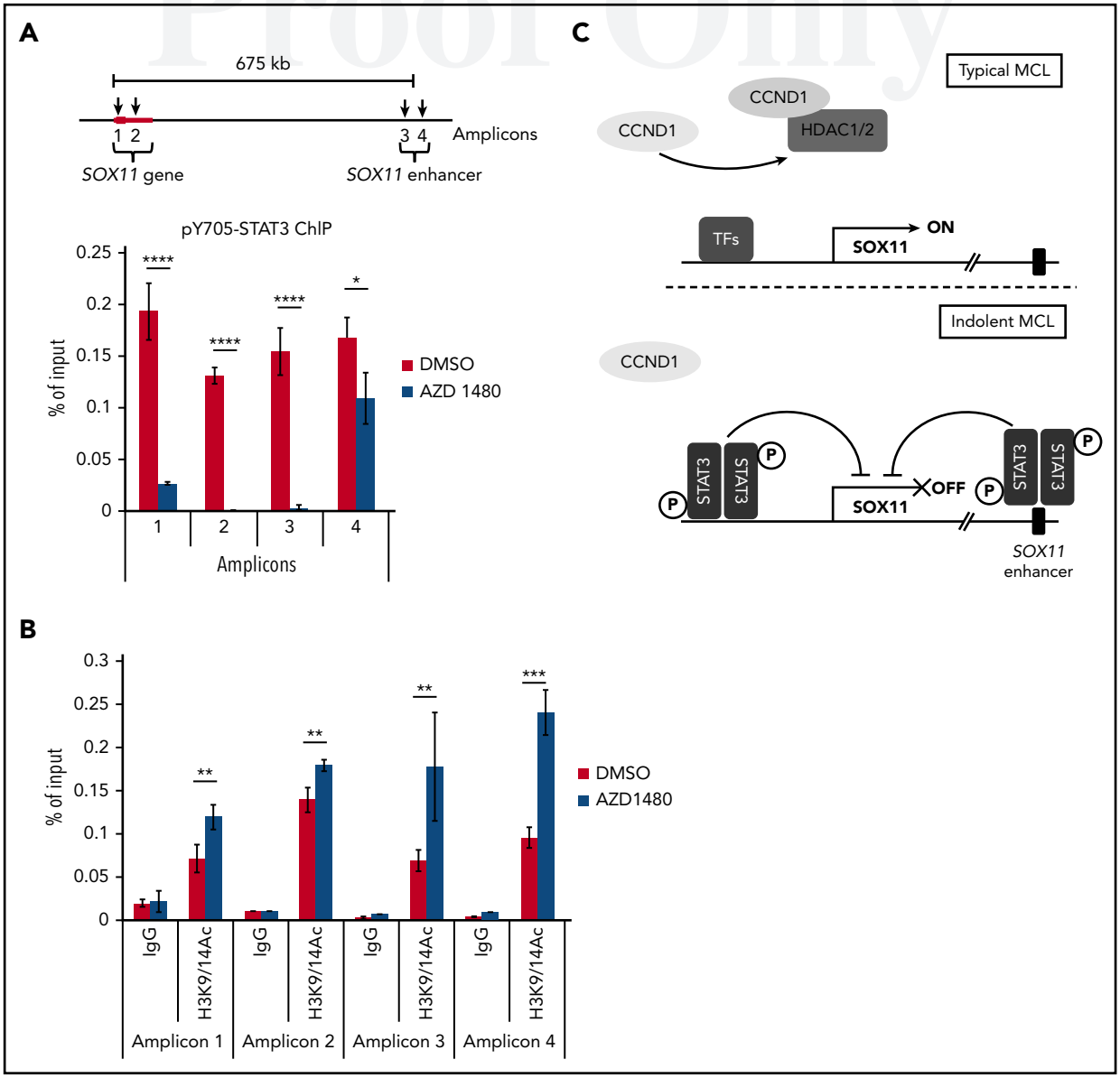

Figure 7. pY705 STAT3 is directly recruited to the *SOX11* gene. (A) Diagram of the *SOX11* gene and enhancer (not drawn to scale; top). Arrows indicate STAT3 binding sites. JEKO-1 cells were treated with 500 nM of AZD1480 or dimethyl sulfoxide (DMSO) for 16 hours, and chromatin immunoprecipitation assays were performed using the pY705 STAT3 antibody (bottom). (B) Chromatin immunoprecipitation assays using isotype immunoglobulin G (IgG) or H3K9/14Ac antibody for MAVER-1 cells treated with 500 nM of AZD1480 or DMSO for 16 hours. (A-B) Bar graphs show means of qPCR signals from 4 independent amplification experiments using primers to regions 1 to 4 (amplicons). Data are shown as percentage of total input chromatin DNA. Error bars, standard deviation. (C) Proposed model of SOX11 expression through distinct mechanisms mediated by CCND1 and STAT3 in typical or indolent form of MCL. *$P < .05$, **$P < .01$, ***$P < .001$, ****$P < .0001$ by 2-sided Student *t* test. TF, XXX.

Q:12

CCND1 and STAT3, which has been observed in other systems, may provide additional clues to understand SOX11 regulation. For example, overexpression of a constitutively active form of STAT3 in HEK-293T cells[56] or of a dominant-negative variant of STAT3 in mouse NIH-3T3 cells[57] directly activated or inhibited CCND1 promoter activity, respectively. Interestingly, CCND1 was also found to repress STAT3 activation in HepG2 cells.[58] Therefore, investigating how such crosstalk influences SOX11 expression in the context of MCL will be needed to further improve our understanding of complex SOX11 regulation.

Our findings have implications for a better understanding of the 2 clinically distinct MCL subtypes (ie, typical and indolent MCLs). We believe that the previously described post–germinal center phenotype of SOX11$^-$ indolent MCL[16,19] could be related to upregulated STAT3 activity. In contrast, MCLs that initially express high levels of CCND1 and SOX11 are likely prevented from plasmacytic differentiation, possibly because of SOX11-mediated PAX5 upregulation,[19] and thus have low STAT3 activity. Our data also have implications for the development of new treatment strategies for MCL. Although CCND1 and SOX11 are promising therapeutic targets, pharmacological inhibitors of these molecules are currently not available. In contrast, despite the availability of small-molecule inhibitors for HDAC1 and HDAC2 or STAT3 signaling, targeting these molecules would not be beneficial for MCL patients because of the undesired effect of increasing SOX11 levels. Indeed, clinical studies in MCL using vorinostat as a single agent have shown very modest activity to date. For example,

Kirschbaum et al[59] found that none of 9 MCL patients responded to vorinostat. Similarly, Ogura et al[60] showed that vorinostat had no effect on the overall survival of all 4 enrolled MCL patients. Although the efficacy of STAT3 inhibition remains unclear from 1 study with limited MCL patient enrollment,[61] the present study indicates that STAT3 may not be an ideal target in MCL because of its negative role in SOX11 regulation. Instead, our data advocate for additional studies that target the regulatory mechanisms of SOX11 to reduce SOX11 levels and potentially differentiate aggressive MCL tumors to an indolent phenotype. In support of this notion, we showed that IL-21, a potent plasma cell–inducing cytokine,[62] effectively upregulated STAT3 activity, leading to reduced SOX11 levels and viability in SOX11^{+} MCL cells. Our data are thus consistent with previous studies that showed IL-21–mediated toxicity in MCL through an STAT3-dependent mechanism.[63,64] However, IL-21 susceptibility seems limited to MCL cell lines with low or negative STAT3 activity, because pY705 STAT3^{high} MCL cells are resistant to IL-21 treatment. Thus, our results also reveal pY705 STAT3 as a potential biomarker for IL-21–based therapy.

In summary, we have demonstrated that CCND1 and STAT3 play key roles in regulating SOX11 expression. CCND1 binds to and reduces recruitment of HDAC1 and HDAC2 to the *SOX11* promoter, leading to increased histone acetylation and *SOX11* transcription. In contrast, STAT3 directly interacts with the *SOX11* gene locus and its enhancer and functions as a transcriptional repressor. These findings have implications for our understanding of SOX11 deregulation in MCL and may have therapeutic potential for MCL patients.

Acknowledgments

This work was supported in part by National Institutes of Health National Cancer Institute Cancer Center Support Grant P30CA033572 to the City of Hope, by the American Society of Hematology, by the Gabrielle's Angel Foundation for Cancer Research, and by Department of Defense Grant CA140945 (V.N.N.).

Authorship

Contribution: A.M. and V.N.N. designed the experiments; A.M., N.S., A.P., and V.N.N. performed the experiments; A.M., M. Mei, and V.N.N. analyzed data; T.V.N. provided essential research reagents; R.W.C., E.B., M. Mei, L.P., L.V.P., L.W.K., D.D.W., S.T.R., W.C.C., and M. Müschen provided and reviewed pathological data; D.D.W. edited the manuscript; and V.N.N. directed the research and wrote the manuscript. Q:8

Conflict-of-interest disclosure: The authors declare no competing financial interests.

ORCID profile: M.M., 0000-0002-1109-6955. Q:A2

Correspondence: Vu N. Ngo, Department of Systems Biology, Beckman Research Institute, City of Hope, 1218 South Fifth Ave, Monrovia, CA 91016; e-mail: vngo@coh.org.

Footnotes

Submitted 16 May 2018; accepted 30 November 2018. Prepublished online as *Blood* First Edition paper, 10 December 2018; DOI 10.1182/blood-2018-05-851667.

The publication costs of this article were defrayed in part by page charge payment. Therefore, and solely to indicate this fact, this article is hereby marked "advertisement" in accordance with 18 USC section 1734.

REFERENCES

1. Dy P, Penzo-Méndez A, Wang H, Pedraza CE, Macklin WB, Lefebvre V. The three SoxC proteins--Sox4, Sox11 and Sox12--exhibit overlapping expression patterns and molecular properties. *Nucleic Acids Res*. 2008;36(9):3101-3117.
2. Bergsland M, Werme M, Malewicz M, Perlmann T, Muhr J. The establishment of neuronal properties is controlled by Sox4 and Sox11. *Genes Dev*. 2006;20(24):3475-3486.
3. Bhattaram P, Penzo-Méndez A, Sock E, et al. Organogenesis relies on SoxC transcription factors for the survival of neural and mesenchymal progenitors. *Nat Commun*. 2010;1:9.
4. Sock E, Rettig SD, Enderich J, Bösl MR, Tamm ER, Wegner M. Gene targeting reveals a widespread role for the high-mobility-group transcription factor Sox11 in tissue remodeling. *Mol Cell Biol*. 2004;24(15):6635-6644.
5. Ek S, Dictor M, Jerkeman M, Jirström K, Borrebaeck CA. Nuclear expression of the non B-cell lineage Sox11 transcription factor identifies mantle cell lymphoma. *Blood*. 2008;111(2):800-805.
6. Wang X, Asplund AC, Porwit A, et al. The subcellular Sox11 distribution pattern identifies subsets of mantle cell lymphoma: correlation to overall survival. *Br J Haematol*. 2008;143(2):248-252.
7. Mozos A, Royo C, Hartmann E, et al. SOX11 expression is highly specific for mantle cell lymphoma and identifies the cyclin D1-negative subtype. *Haematologica*. 2009;94(11):1555-1562.
8. Dictor M, Ek S, Sundberg M, et al. Strong lymphoid nuclear expression of SOX11 transcription factor defines lymphoblastic neoplasms, mantle cell lymphoma and Burkitt's lymphoma. *Haematologica*. 2009;94(11):1563-1568.
9. Brennan DJ, Ek S, Doyle E, et al. The transcription factor Sox11 is a prognostic factor for improved recurrence-free survival in epithelial ovarian cancer. *Eur J Cancer*. 2009;45(8):1510-1517.
10. Sernbo S, Gustavsson E, Brennan DJ, et al. The tumour suppressor SOX11 is associated with improved survival among high grade epithelial ovarian cancers and is regulated by reversible promoter methylation. *BMC Cancer*. 2011;11:405.
11. Zvelebil M, Oliemuller E, Gao Q, et al. Embryonic mammary signature subsets are activated in Brca1-/- and basal-like breast cancers. *Breast Cancer Res*. 2013;15(2):R25.
12. Shepherd JH, Uray IP, Mazumdar A, et al. The SOX11 transcription factor is a critical regulator of basal-like breast cancer growth, invasion, and basal-like gene expression. *Oncotarget*. 2016;7(11):13106-13121.
13. Weigle B, Ebner R, Temme A, et al. Highly specific overexpression of the transcription factor SOX11 in human malignant gliomas. *Oncol Rep*. 2005;13(1):139-144.
14. Lee CJ, Appleby VJ, Orme AT, Chan WI, Scotting PJ. Differential expression of SOX4 and SOX11 in medulloblastoma. *J Neurooncol*. 2002;57(3):201-214.
15. Yao Z, Sun B, Hong Q, et al. The role of tumor suppressor gene SOX11 in prostate cancer. *Tumour Biol*. 2015;36(8):6133-6138.
16. Navarro A, Clot G, Royo C, et al. Molecular subsets of mantle cell lymphoma defined by the IGHV mutational status and SOX11 expression have distinct biologic and clinical features. *Cancer Res*. 2012;72(20):5307-5316.
17. Wang X, Björklund S, Wasik AM, et al. Gene expression profiling and chromatin immunoprecipitation identify DBN1, SETMAR and HIG2 as direct targets of SOX11 in mantle cell lymphoma. *PLoS One*. 2010;5(11):e14085.
18. Kuo PY, Leshchenko VV, Fazzari MJ, et al. High-resolution chromatin immunoprecipitation (ChIP) sequencing reveals novel binding targets and prognostic role for SOX11 in mantle cell lymphoma. *Oncogene*. 2015;34(10):1231-1240.
19. Vegliante MC, Palomero J, Pérez-Galán P, et al. SOX11 regulates PAX5 expression and blocks terminal B-cell differentiation in aggressive mantle cell lymphoma. *Blood*. 2013;121(12):2175-2185.
20. Palomero J, Vegliante MC, Rodríguez ML, et al. SOX11 promotes tumor angiogenesis through transcriptional regulation of PDGFA

in mantle cell lymphoma. *Blood*. 2014; 124(14):2235-2247.

21. Balsas P, Palomero J, Eguileor Á, et al. SOX11 promotes tumor protective microenvironment interactions through CXCR4 and FAK regulation in mantle cell lymphoma. *Blood*. 2017; 130(4):501-513.

22. Nygren L, Baumgartner Wennerholm S, Klimkowska M, Christensson B, Kimby E, Sander B. Prognostic role of SOX11 in a population-based cohort of mantle cell lymphoma. *Blood*. 2012;119(18):4215-4223.

23. Gustavsson E, Sernbo S, Andersson E, et al. SOX11 expression correlates to promoter methylation and regulates tumor growth in hematopoietic malignancies. *Mol Cancer*. 2010;9:187.

24. Vegliante MC, Royo C, Palomero J, et al. Epigenetic activation of SOX11 in lymphoid neoplasms by histone modifications. *PLoS One*. 2011;6(6):e21382.

25. Nordström L, Andersson E, Kuci V, et al. DNA methylation and histone modifications regulate SOX11 expression in lymphoid and solid cancer cells. *BMC Cancer*. 2015;15:273.

26. Queirós AC, Beekman R, Vilarrasa-Blasi R, et al. Decoding the DNA methylome of mantle cell lymphoma in the light of the entire B cell lineage. *Cancer Cell*. 2016;30(5):806-821.

27. Mohanty A, Sandoval N, Das M, et al. CCND1 mutations increase protein stability and promote ibrutinib resistance in mantle cell lymphoma. *Oncotarget*. 2016;7(45): 73558-73572.

28. Townsend EC, Murakami MA, Christodoulou A, et al. The public repository of xenografts enables discovery and randomized phase II-like trials in mice [published correction appears in Cancer Cell. 2016;30(1):183]. *Cancer Cell*. 2016;29(4):574-586.

Q:9

29. Lin HP, Cheng ZL, He RY, et al. Destabilization of fatty acid synthase by acetylation inhibits de novo lipogenesis and tumor cell growth. *Cancer Res*. 2016;76(23):6924-6936.

30. Ngo VN, Davis RE, Lamy L, et al. A loss-of-function RNA interference screen for molecular targets in cancer. *Nature*. 2006;441(7089): 106-110.

31. Scuto A, Kujawski M, Kowolik C, et al. STAT3 inhibition is a therapeutic strategy for ABC-like diffuse large B-cell lymphoma. *Cancer Res*. 2011;71(9):3182-3188.

32. Hamborg KH, Bentzen HH, Grubach L, Hokland P, Nyvold CG. A highly sensitive and specific qPCR assay for quantification of the biomarker SOX11 in mantle cell lymphoma. *Eur J Haematol*. 2012;89(5):385-394.

33. Mohanty S, Mohanty A, Sandoval N, et al. Cyclin D1 depletion induces DNA damage in mantle cell lymphoma lines. *Leuk Lymphoma*. 2017;58(3):676-688.

34. Fernàndez V, Salamero O, Espinet B, et al. Genomic and gene expression profiling defines indolent forms of mantle cell lymphoma. *Cancer Res*. 2010;70(4):1408-1418.

35. Pérez-Galán P, Mora-Jensen H, Weniger MA, et al. Bortezomib resistance in mantle cell lymphoma is associated with plasmacytic differentiation. Blood. 2011;117(2):542-552.

36. ENCODE Project Consortium. An integrated encyclopedia of DNA elements in the human genome. *Nature*. 2012;489(7414):57-74.

37. Avery DT, Deenick EK, Ma CS, et al. B cell-intrinsic signaling through IL-21 receptor and STAT3 is required for establishing long-lived antibody responses in humans. *J Exp Med*. 2010;207(1):155-171.

38. Hedvat M, Huszar D, Herrmann A, et al. The JAK2 inhibitor AZD1480 potently blocks Stat3 signaling and oncogenesis in solid tumors. *Cancer Cell*. 2009;16(6):487-497.

39. Zeng R, Spolski R, Casas E, Zhu W, Levy DE, Leonard WJ. The molecular basis of IL-21-mediated proliferation. *Blood*. 2007;109(10): 4135-4142.

40. Hillion J, Dhara S, Sumter TF, et al. The high-mobility group A1a/signal transducer and activator of transcription-3 axis: an achilles heel for hematopoietic malignancies? *Cancer Res*. 2008;68(24):10121-10127.

41. Levy DE, Darnell JE Jr. Stats: transcriptional control and biological impact. *Nat Rev Mol Cell Biol*. 2002;3(9):651-662.

42. Bienvenu F, Jirawatnotai S, Elias JE, et al. Transcriptional role of cyclin D1 in development revealed by a genetic-proteomic screen. *Nature*. 2010;463(7279):374-378.

43. Fu M, Rao M, Bouras T, et al. Cyclin D1 inhibits peroxisome proliferator-activated receptor gamma-mediated adipogenesis through histone deacetylase recruitment. *J Biol Chem*. 2005;280(17):16934-16941.

44. Di LJ, Fernandez AG, De Siervi A, Longo DL, Gardner K. Transcriptional regulation of BRCA1 expression by a metabolic switch. *Nat Struct Mol Biol*. 2010;17(12):1406-1413.

45. Harb K, Magrinelli E, Nicolas CS, et al. Area-specific development of distinct projection neuron subclasses is regulated by postnatal epigenetic modifications. *eLife*. 2016;5:e09531.

46. Fu M, Wang C, Rao M, et al. Cyclin D1 represses p300 transactivation through a cyclin-dependent kinase-independent mechanism. *J Biol Chem*. 2005;280(33): 29728-29742.

47. Reutens AT, Fu M, Wang C, et al. Cyclin D1 binds the androgen receptor and regulates hormone-dependent signaling in a p300/CBP-associated factor (P/CAF)-dependent manner. *Mol Endocrinol*. 2001;15(5):797-811.

48. Lee Y, Dominy JE, Choi YJ, et al. Cyclin D1-Cdk4 controls glucose metabolism independently of cell cycle progression. *Nature*. 2014;510(7506):547-551.

49. Chen YH, Gao J, Fan G, Peterson LC. Nuclear expression of sox11 is highly associated with mantle cell lymphoma but is independent of t(11;14)(q13;q32) in non-mantle cell B-cell neoplasms. *Mod Pathol*. 2010;23(1):105-112.

50. Baran-Marszak F, Boukhiar M, Harel S, et al. Constitutive and B-cell receptor-induced activation of STAT3 are important signaling pathways targeted by bortezomib in leukemic mantle cell lymphoma. *Haematologica*. 2010; 95(11):1865-1872.

51. Catlett-Falcone R, Landowski TH, Oshiro MM, et al. Constitutive activation of Stat3 signaling confers resistance to apoptosis in human U266 myeloma cells. *Immunity*. 1999;10(1):105-115.

52. Rahal R, Frick M, Romero R, et al. Pharmacological and genomic profiling identifies NF-κB-targeted treatment strategies for mantle cell lymphoma. *Nat Med*. 2014;20(1):87-92.

53. Beà S, Valdés-Mas R, Navarro A, et al. Landscape of somatic mutations and clonal evolution in mantle cell lymphoma. *Proc Natl Acad Sci USA*. 2013;110(45):18250-18255.

54. Zhang J, Jima D, Moffitt AB, et al. The genomic landscape of mantle cell lymphoma is related to the epigenetically determined chromatin state of normal B cells. *Blood*. 2014; 123(19):2988-2996.

55. Shilatifard A. The COMPASS family of histone H3K4 methylases: mechanisms of regulation in development and disease pathogenesis. *Annu Rev Biochem*. 2012;81:65-95.

56. Bromberg JF, Wrzeszczynska MH, Devgan G, et al. Stat3 as an oncogene. *Cell*. 1999;98(3): 295-303.

57. Sinibaldi D, Wharton W, Turkson J, Bowman T, Pledger WJ, Jove R. Induction of p21WAF1/CIP1 and cyclin D1 expression by the Src oncoprotein in mouse fibroblasts: role of activated STAT3 signaling. *Oncogene*. 2000; 19(48):5419-5427.

58. Bienvenu F, Gascan H, Coqueret O. Cyclin D1 represses STAT3 activation through a Cdk4-independent mechanism. *J Biol Chem*. 2001; 276(20):16840-16847.

59. Kirschbaum M, Frankel P, Popplewell L, et al. Phase II study of vorinostat for treatment of relapsed or refractory indolent non-Hodgkin's lymphoma and mantle cell lymphoma. *J Clin Oncol*. 2011;29(9):1198-1203.

60. Ogura M, Ando K, Suzuki T, et al. A multicentre phase II study of vorinostat in patients with relapsed or refractory indolent B-cell non-Hodgkin lymphoma and mantle cell lymphoma. *Br J Haematol*. 2014;165(6):768-776.

61. Hong D, Kurzrock R, Kim Y, et al. AZD9150, a next-generation antisense oligonucleotide inhibitor of STAT3 with early evidence of clinical activity in lymphoma and lung cancer. *Sci Transl Med*. 2015;7(314):314ra185.

62. Ettinger R, Sims GP, Fairhurst AM, et al. IL-21 induces differentiation of human naive and memory B cells into antibody-secreting plasma cells. *J Immunol*. 2005;175(12):7867-7879.

63. Gelebart P, Zak Z, Anand M, Dien-Bard J, Amin HM, Lai R. Interleukin-21 effectively induces apoptosis in mantle cell lymphoma through a STAT1-dependent mechanism. *Leukemia*. 2009;23(10):1836-1846.

64. Bhatt S, Matthews J, Parvin S, et al. Direct and immune-mediated cytotoxicity of interleukin-21 contributes to antitumor effects in mantle cell lymphoma. *Blood*. 2015; 126(13):1555-1564.